Inferred musculature and kinematics of the forelimb in a lambeosaurine hadrosaurid dinosaur

by

Samantha Marie Hamilton

A thesis submitted in partial fulfillment of the requirements for the degree of

Master of Science

In

Systematics and Evolution

Department of Biological Sciences

University of Alberta

Abstract

Hadrosaurid dinosaurs are largely considered to be facultatively bipedal. However, a distinct lack of well-described hadrosaurid postcranial material in the literature makes comparative analysis of hadrosaurid biomechanics difficult. A newly recovered lambeosaurine (crested) hadrosaurid from the Oldman Formation of southern Alberta presents an ideal specimen for comparative biomechanical analysis due to the high level of preservation of its pectoral girdle, forelimbs, manus, and sternal plates. Here, the osteology of the forelimb and pectoral girdle of TMP2015.044.0036 is described in detail and its morphology is compared with other known ornithopods. The musculature of the pectoral girdle and forelimb of TMP2015.044.0036 is inferred based on phylogenetic bracketing. Finally, the range of motion is assessed for the shoulder, elbow, and wrist of TMP2015.044.0036, and this inferred range of motion is used to plot muscle trajectories of the shoulder musculature onto a three-dimensional computational model of the articulated pectoral girdle and forelimb of TMP2015.044.0036. This model is used to estimate moment arms for these muscles. Findings suggest that TMP2015.044.0036 habitually utilized its forelimbs in quadrupedal locomotion, as evidenced by a rigid pectoral region, a pillar-like manus, cartilaginous carpals, and hoof-like unguals for distal phalanges. Limited range of motion of the shoulder, elbow, and manus suggest that movement was limited to anterior-posterior swing which is corroborated by very well-developed muscles involved in humeral protraction and retraction, namely M. pectoralis, M. supracoracoideus and M. coracobrachialis, and a lack of well-developed humeral adduction-abduction musculature. This study lends support to the hypothesis that hadrosaurids represent principally quadrupedal animals.

Acknowledgments

It takes a village to raise a thesis, or at least, makes it an incredibly rewarding experience. I was certainly fortunate to have a community of incredibly intelligent and supportive mentors, colleagues, and friends to whom I owe a great deal of gratitude. I will forever be especially thankful to my supervisor, Corwin Sullivan, for providing me with the opportunity to be one of the founding members of his lab. The last few years have been the most exciting and rewarding of my life, not to mention the knowledge and experiences I would never have had the privilege of acquiring without Corwin's confidence in me and unrelenting support. Likewise, I must extend my thanks to my committee advisor David Evans, for trusting me with my beautiful research specimen collected by his team and for providing incredibly helpful feedback throughout my project. David's enthusiasm for this project greatly inspired my research.

I was extremely lucky to be a part of the University of Alberta Laboratory for Vertebrate Palaeontology community. As someone who came to the lab new to the field of palaeontology, I had a lot to learn and luckily for me, I had a wonderful team of people who were more than willing to share their wisdom. Thank you so very much to Clive Coy, Howard Gibbins, and Robin Sissons for helping me with specimens, sharing ideas, and training me in fossil preparation and field techniques. Thank you to Eva Koppelhus and Phil Currie for sharing your space and equipment, for including me in field excursions, and for sharing their knowledge and ideas with me throughout my studies. To my fellow graduate (and former graduate) students: Rebekah Vice, Yan-Yin Wang, Michael Hudgins, Mark Powers, Gregory Funston, Matthew Rhodes, Aaron Dyer, Annie McIntosh, and Bray Holland. Your friendship, patience, and guidance are what got me through these last few difficult years. Without you, I would not have had the confidence to become the researcher I am today.

For access to collections, I must thank Braden Barr of the University of Alberta comparative anatomy collections, Brandon Strilisky and Heather Feeney of the Royal Tyrrell Museum, and the wonderful collections staff at the Canadian Museum of Nature. I also thank the Dinosaur Research Institute and University of Albert Department of Biological Sciences for funding travel expenses. This research was funded partly by an NSERC Discovery Grant (RGPIN-2017-06246) and endowment funds, both awarded to my supervisor Corwin Sullivan.

Lastly, I thank my family and friends for their support and assistance throughout this project. I would be remiss if I did not specifically thank Margaret Cross for her enthusiasm, encouragement, and friendship. Margaret was by my side, literally, for much of my project. Her constant support made even the hardest days worthwhile. I thank Freya and Milo for bringing such joy to my life everyday. Finally, I owe much of who I am and what I have accomplished to my incredible husband, Taryn Huszar. You are my inspiration, my loudest voice of encouragement, and my greatest support.

Table of Contents

List of Tables

List of Figures

List of institutional Abbreviations

AEHM, Amur Natural History Museum, Blagoveschensk, Russia

AMNH, American Museum of Natural History, New York City, New York, USA

CMN, Canadian Museum of Nature, Ottawa, Ontario, Canada

CUST, Changchun University of Science and Technology, Changchun, Jilin, China

IRSNB, Institut Royal des Sciences Naturelles de Belgique, Brusels, Belgium

LACM, Natural History Museum of Los Angeles County, Los Angeles, California, USA

MOR, Museum of the Rockies, Bozeman, Montana, USA

NMC, Canadian Museum of Nature (formerly the National Museum of Canada), Ottawa, Ontario

PMU, Museum of Evolution, Uppsala University, Uppsala, Sweden

ROM, Royal Ontario Museum, Toronto, Ontario, Canada

SBDE, Sino-Belgian Dinosaur Expedition

TMP, Royall Tyrrell Museum of Palaeontology, Drumheller, Alberta, Canada

List of Anatomical Abbreviations

ap, acromion process

b., M. biceps brachii

br., M. brachialis

c.delt., M. deltoideus clavicularis

cbr., M. coracobrachialis

cf, coracoid facet

cp, cranial process

csc., M costocoracoideus

DII, digit II

DIIPII, digit II phalanx II

DIIPIII, digit II phalanx III

DIII, digit III

DIIIPI, digit III phalanx I

DIIIPII, digit III phalanx II

DIV, digit IV

DIVPI, digit IV phalanx I

DIVPII, digit IV phalanx II

DIVPIII, digit IV phalanx III

DV, digit V

dr, deltoid ridge

e.c.r., M. extensor carpi radialis

e.c.u., M. extensor carpi ulnaris

f.c.r., M. flexor carpi radialis

f.c.u., M. flexor carpi ulnaris

gf, glenoid facet

gfs, glenoid fossa

h.tr., M. triceps (humeral head)

ld., M. latissimus dorsi

lev.s., M. levator scapulae

lp, lateral process

MIII, metacarpal III

MIV, metacarpal IV

op, olecranon process

p., M. pectoralis

p.c., M. palmaris communis

pvb, proximoventral buttress

r, radius

rhomb., M. rhomboideus

s.delt., M. deltoideus scapularis

s.tr.,M. triceps (scapular head)

sb, scapular blade

sbs., M. subscapularis

sc., M. supracoracoideus

ser.p., M. serratus profundus

ser.s., M. serratus superficialis

sh.a., M. scapulohumeralis anterior

sh.p., M. scapulohumeralis posterior

sn, sapular neck

t.maj., M. teres major

tr., M. triceps

trap., M. trapezius

u, ulna

Chapter 1. General Introduction

An animal's posture, or range of potential postures, is fundamental to its ecology and behavior. In fact, bipedalism, in which movement is driven by the hindlimbs alone, has several potential advantages over a quadrupedal gait (movement using both the hindlimbs and forelimbs). These include superior ability to fight off predators and competitors (Carrier 2011), enhanced thermoregulation (Wheeler 1991), an improved visual range (Ravey 1978), and higher cursorial efficiency (Persons and Currie 2017). Ornithischians present an interesting case in the evolution of posture, as basal members of each major group of ornithischians (Ornithopoda, Thyreophora, and Marginocephalia (Sereno 1986; Butler et al. 2008; Maidment et al. 2014b)) were bipedal, but secondary quadrupedalism later arose at least once in each group (Dodson et al. 2004; Horner et al. 2004; Norman et al. 2004; Maidment and Barrett 2012; Maidment et al. 2014b). Indeed, Maidment et al. (2014b) postulate that within Ornithopoda, facultative quadrupedality arose separately several times (Norman 1980; Wright 1999; Carpenter and Wilson 2008; Maidment and Barrett, 2014). Hadrosaurid ornithischians are often regarded as an example of a secondarily quadrupedal lineage, but their posture has proved contentious. When first described by scientists, these animals were first assumed to be primarily aquatic organisms, utilizing their manus in paddling through water (Leidy 1858; Cope 1883; Colbert 1951). Shortly after, it was generally agreed that the evidence for aquatic habits was insufficient (Ostrom 1964), hadrosaurids came to be accepted as terrestrial bipeds (Ostrom 1964; Galton 1970; Maryańska and Osmólska 1984). Today, current evidence suggests that most hadrosaurids were largely quadrupedal, and possibly facultatively bipedal, but that the forelimbs were involved in locomotion to some extent (Carrano 2001; Hornet at al. 2004; Evans 2007; Sellers et al. 2009; Maidment et al. 2014b; Maidment and Barrett 2014). Furthermore, some authors have suggested

that based on limb-bone scaling and trackways, hadrosaurids may have been predominantly quadrupedal (Dilkes 2000; Lockley and Wright 2001; Maidment et al. 2014b). In any case, the fact that hadrosaurids have shifted their mode of locomotion from bipedalism to quadrupedalism and vice versa more than any other group of organisms (Maidment et al. 2014b; Maidment and Barrett 2014) provides a unique opportunity to study the mechanical evolution of both bipedalism and quadrupedalism. Yet, the mechanics of locomotion within Hadrosauridae remains poorly understood, and the posture of many hadrosaurid species remains controversial. Our present understanding suggests that posture varied among species, and even across ontogenetic stages within individual species (Dilkes 2000). Continuing uncertainty on this point complicates attempts to reconstruct the evolution of posture in dinosaurs overall and hinders investigations of hadrosaurid behavior and ecology.

It has been proposed that the forelimb in at least some dinosaur lineages displayed bipedal features before the hindlimb in the context of a shift from quadrupedalism to bipedalism (Maidment and Barrett 2014), and there is indeed a current trend in the literature towards using the structure and proportions of the forelimb to draw biomechanical inferences in various groups (Dilkes 2000; Carpenter and Wilson 2008; Baier and Gatesy 2013; Otero et al. 2017). Although the skulls of many ornithischian dinosaurs are very well studied (e.g. Weishampel and Jensen 1979; Brink et al. 2011; Bramble et al. 2017; Gates et al. 2021) information on the rest of the skeleton is relatively scarce in the scientific literature. This creates difficulties for researchers who wish to gather data for any kind of comparative study of the biomechanics or morphometrics of the postcranium across multiple ornithischian taxa. Given the potential informativeness of hadrosaurid forelimb material, in particular, there is a clear need for greater attention to this portion of the hadrosaurid skeleton in the scientific literature. My hope is that

this thesis will serve as an example of the amount of detailed information, both written and illustrated, that should be provided as a matter of standard practice when describing the frequently disregarded postcranial osteology of ornithischian taxa.

This study will test the hypothesis that hadrosaurid species can be placed on a spectrum ranging from facultative to obligate quadrupeds (Maidment and Barrett 2014). I will also assess the idea that these animals represent a transitional stage within the evolution of bipedalism to quadrupedalism (Carrano 2001). Support for these hypotheses would favour the idea that hadrosaurids are a reasonable model for studying the evolution of bipedalism from a functional perspective. The objectives of this study are to inform on the posture of hadrosaurids and investigate what use they might have made of their forelimbs. This is vital for understanding not only their palaeobiology, but also their role in Mesozoic ecosystems. Hadrosaurid fossils have a global distribution and are especially common in the Upper Cretaceous deposits of western North America. Furthermore, hadrosaurids were ecologically important in the Mesozoic, comprising over 80% of recovered material found in some North American fossil assemblages (Cullen and Evans 2016). Additionally, the popularity of these animals with the public, and their frequent reconstructions in such media as films and video games, imply that a clear resolution to the question of hadrosaurid posture would be of interest to laypeople and the creative community, as well as to scientists.

The functional morphology of the forelimb may hold the key to determining whether hadrosaurids were predominantly bipedal or quadrupedal. A recently recovered partial lambeosaurine (crested) hadrosaurid skeleton (TMP2015.044.0036) from the Oldman Formation of southern Alberta, lends itself particularly well to this type of study, as it includes a complete set of remarkably preserved forelimbs and its pectoral girdle with sternal plates.

TMP2015.044.0036 remains taxonomically indeterminate at the species level, but its completeness and close association of recovered elements make this specimen ideal for biomechanical analysis. The forelimbs, pectoral girdle, and sternal plates of TMP2015.044.0036 are thoroughly described in this thesis and compared with other known ornithopod taxa. The musculature of TMP2015.044.0036 is reconstructed based on phylogenetic bracketing, and the inferred myology combined with osteological ranges of motion are used to generate moment arm plots to infer how the forelimbs may have been used. This is presented in the hope that providing realistic, quantitative constraints on the movement of one well-preserved individual will lend insight into what actions lambeosaurine hadrosaurids were adapted to execute, and what ecological significance their functional capabilities may have had in the context of North American Mesozoic ecosystems.

Chapter 2. Osteological description of the forelimb, pectoral girdle, and sternum of a lambeosaurine hadrosaurid from the Oldman Formation (Alberta, Canada).

2.1 Introduction

Hadrosaurid dinosaurs were integral to Mesozoic ecosystems as evidenced by the global distribution of recovered remains and the number of new species being described each year. In North America, hadrosaurid material comprises over 80% of the elements recovered from some Cretaceous fossil assemblages (Cullen and Evans 2016), which stands to reason; living hadrosaurids were massive, herbivorous animals that likely traveled in large herds (Currie 1983; Lockley et al. 1983), making them an extremely important source of sustenance for hunting carnivores, scavengers, and decomposers. Though the cranial anatomy of hadrosaurids is reasonably well understood, descriptions of the postcranial anatomy of hadrosaurids are scarce in the scientific literature, and studies of hadrosaurid postcranial functional morphology even more so. Well-defined models of theropod movement, posture, musculature, and range of motion are readily available in the literature (e.g., Gatesy and Middleton 1997; Carrano and Hutchinson 2002; Senter and Robins 2005; Gatesy et al. 2009; Hutchinson et al. 2011; Bates and Schachner 2012; White et al. 2015; Senter and Sullivan 2019). However, even the posture of hadrosaurids remains widely uncertain. Hadrosaurid postcranial remains are frequently left undescribed, and often uncollected. Unsurprisingly, this makes identification and comparative anatomy of hadrosaurid taxa extremely difficult and functional morphological studies such as computer modelling nearly impossible. This issue pervades into museum and institution collections (Senter 2012), which often contain many ornithopod postcranial elements identified only as "Hadrosauridae" and very little material identified to the species level.

This chapter presents an in-depth description and illustration of the osteology of the pectoral girdle, forelimb, and manus of a newly recovered lambeosaurine hadrosaurid partial skeleton (TMP2015.044.0036). This material is compared to other hadrosauroid specimens and taxonomic groups to present taxonomically significant morphological variations in hadrosaurid forelimb and pectoral girdle material.

2.2 Fossil Material

A partial, articulated skeleton of a hadrosaurid (TMP2015.044.0036) was recently recovered from the Upper Cretaceous Oldman Formation of southern Alberta, Canada. The specimen comprises a possible skull fragment, several teeth, ribs, and tendons, both sternal plates, the right scapula and coracoid, both humeri, ulnae, and radii, and both complete manus. TMP2015.044.0036 also includes a hip block which remains unprepared, as this study focuses on the forelimb and pectoral girdle only. TMP2015.044.0036 has been identified as a sub-adult based on the comparatively small size of the skeleton and its limb bone proportions. TMP2015.044.0036 has been attributed to Lambeosaurinae indet. based on several osteological features characteristic of lambeosaurine hadrosaurids, such as a forearm longer than the humerus, a deltopectoral crest that extends more than halfway down the humeral shaft, a robust ischium, and a short metacarpus (see Evans 2007; Brett-Surman and Wagner 2007; Prieto-Márquez 2008; Prieto-Márquez 2010; Evans and Reisz 2010).

Absence of any complete cranial material in TMP2015.04.0036 makes this specimen difficult to identify to the genus level, though some information can be interpreted based on stratigraphic association. The Oldman Formation belongs to the Campanian Belly River Group

which, from oldest to youngest, is composed of the Foremost, Oldman, and Dinosaur Park Formations (Eberth and Hamblin 1993; Cullen and Evans 2005; Eberth 2005). This group is very well studied from a palaeontological perspective, the Oldman and Dinosaur Park Formations being some of the most well-sampled Cretaceous deposits in the world, allowing for well established biostratigraphy of dinosaur groups (Currie and Russell 2005; Ryan and Evans 2005; Evans et al. 2009; Mallon et al. 2012; Eberth et al. 2013; Cullen and Evans 2016; Fowler 2017). From the Oldman Formation, three genera of lambeosaurine have been suggested: *Parasaurolophus*, *Corythosaurus,*and *Lambeosaurus* (Dodson 1975; Evans and Ryan 2005). A biostratigraphic assessment of *Parasaurolophus* by Evans et al. (2009) constrained all known genuine occurrences of *Parasaurolophus* between 76.5 and 75.3 million years ago (see also Eberth and Hamblin 1993; Sullivan and Williamson 1999; Eberth 2005). Thus, the temporal range of *Parasaurolophus* seems to lie strictly within the lower half of the Dinosaur Park Formation with no published material recovered from the underlying Oldman Formation (Evans et al. 2009). Though genuine *Parasaurolophus* material is generally scarce, this geologic constraint suggests that TMP2015.044.0036 is likely not a representative of *Parasaurolophus*. Regardless of this, the rounded deltopectoral crest of TMP2015.044.0036 and the more extreme constriction and elongation of the scapular neck compared to the angular deltopectoral crest and short scapular neck of *Parasaurolophus* provides some indication that TMP2015.044.0036 is morphologically more similar to *Corythosaurus* and *Lambeosaurus* at least in the anatomy of the shoulder girdle and forelimb. Further osteological comparison is discussed below, though TMP2015.044.0036 likely represents a juvenile to sub-adult member of one of the aforementioned genera.

The skeleton of TMP2015.044.0036 is partially articulated and incomplete. The pectoral girdle, sternal plates, forelimb and manus are preserved in articulation and the posture in which they are preserved is one that could have been adopted in life. There is only minor post-mortem damage to the bones and no large-scale deformation due to burial. The surface texture remains intact on most elements, preserving muscle and tendon scarring and cartilaginous attachment zones. For these reasons TMP2015.044.0036 makes an excellent specimen for comprehensive osteological description. This chapter describes in detail the right scapula and coracoid, the sternal plates, the left humerus, both sets of antebrachial bones, and both complete manus. Anatomical orientation is assumed as the initial resting phase of a hypothetical step cycle for a quadrupedal animal where the scapular blade lies on the lateral aspect of the trunk, perpendicular to the ribs, and the forelimb is oriented vertically with the proximal end of the humerus housed in the glenoid dorsally and the antebrachium and manus extending ventrally. Comparison with other hadrosaurid material was accomplished through a combination of literature review of published hadrosauroid forelimb and pectoral girdle elements (e.g., Sternberg 1935; Lull and Wright 1942; Ostrom 1963; Galton 1970; Hu et al. 1973; Maryańska and Osmólska 1984; Rasmussen 1998a; Rasmussen 1998b; Dilkes 2000; Egi and Weishampel 2002; Norman 2002; Brett-Surman and Wagner 2007; Evans 2007; Evans and Reisz 2007; Carpenter and Wilson 2008; Prieto-Márquez 2008; Cuthbertson and Holmes 2010; Prieto-Márquez 2010; Prieto-Márquez and Norell 2010; Senter 2012; Prieto-Márquez 2014; Campione 2014; Poole 2015) and firsthand observations of hadrosaurid forelimb elements from the galleries and collections of the University of Alberta Laboratory for Vertebrate Palaeontology (Edmonton, Alberta), the Royal Tyrrell Museum of Palaeontology (Drumheller, Alberta), the Canadian Museum of Nature (Ottawa, Ontario), and the Royal Ontario Museum (Toronto, Ontario).

2.3 Osteological Description

2.3.1 Pectoral girdle

Scapula

The complete right scapula (Fig. 1) is preserved in TMP2015.044.0036. The scapula measures 847 mm from the coracoid facet to the distal end (Table 1A). Overall, its shape is elongate but slightly curved dorsoventrally. At the proximal end, there are two facets. The more dorsally situated of the two, with which the coracoid articulates anteriorly, is directed anteriorly and is basically triangular in shape, and is wider than tall, and has a rounded ventral apex and indented dorsal margin. The coracoid facet has a thin concavity running antero-medially along its centre and a deep rugose texture to the bone that indicates a cartilaginous covering was present in life. The glenoid facet (Prieto-Márquez 2014) is ventral to the coracoid facet and is a larger, rugose, concave surface that, combined with the glenoid facet of the coracoid, creates a wide strip with a ventrally concave curvature that houses the head of the humerus ventrally. Dorsal to the coracoid facet is the acromion process, a rounded projection that is flattened dorsoventrally. The acromion process projects dorsally as in *Corythosaurus intermedius* (CMN 9704) and *Charonosaurus jiayinensis* (CUST JII1398) (Prieto-Márquez 2008), though it is not as posteriorly oriented as in *Iguanodon atherfieldensis* (IRSNB 1551), *Parasaurolophus walkeri* (ROM 768), or *Tanius sinensis* (PMU R241) (Prieto-Márquez 2008). This is different from *Saurolophus angustirostris*, in which the acromion process curves ventrally (Mariańska and Osmólska 1984). The dorsal surface of the acromion process bears rugose scarring for muscle attachment. The proximoventral buttress is the ventralmost surface of the anterior end of the scapula, located on the ventral edge of the glenoid facet. The proximoventral buttress is broad and ventrally directed with some scarring of the bone surface for muscle attachment. Just posterior to the acromion process, the scapula

narrows to form a laterally compressed neck that is 97 mm wide dorsoventrally and ovoid in cross section. The high degree of constriction at the scapular neck is like that seen in *Lambeosaurus* and *Parasaurolophus* (Ostrom 1963; Evans and Reisz 2007).

In lateral view, the scapular blade is strongly curved so that the anterior end is directed downward anteriorly at roughly a 150^{o} angle from the horizontal posterior edge of the scapular blde, creating a slight dorsally projecting hump just posterior to the scapular neck, and a larger ventral concavity on the ventral edge of the scapular blade itself. This downward projecting anterior portion that is comprised of the scapular neck and articular head makes up roughly one third of the length of the entire scapula. This curve and this elongated anterior portion seem to be highly variable among hadrosaurids. *Edmontosaurus regalis* (Campione 2014), *Brachylophosaurus canadensis* (Cuthbertson and Holmes 2010), *Maiasaura peeblesorum* (Dilkes 2000), and *Saurolophus* (Maryańska and Osmólska 1984) possess this anterior curvature to their scapulae, but the ventrally projecting anterior end is only about a fifth the entire length of the scapula in all individuals. In the case of *Edmontosaurus* (previously *Anatosaurus*) (Lull and Wright 1943), the angle between the scapular head and blade is much smaller (about 100^{o}) but the anterior portion is of a similar proportion to *Edmontosaurus*. The long, ventrally projecting anterior portion of the scapula in TMP2015.044.0036 is likely a characteristic feature of lambeosaurines since this condition is also present in *Lambeosaurus magnicristatus* (Evans and Reisz 2007), *Corythosaurus intermedius* (ROM 845) (Prieto-Márquez 2008), and *Parasaurolophus cyrtocristatus* (Ostrom 1963). Brett-Surman and Wagner (2007), note that the scapula of hadrosaurine dinosaurs is long anteroposteriorly and low dorsoventrally, giving an elongated appearance to the scapula. *Lambeosaurus* is unique in its scapular morphology in that they have a ratio of anteroposterior length to dorsoventral height that is large like the

hadrosaurine morph, raising the possibility that TMP2015.044.0036 could possibly belong to the genus *Lambeosaurus* for this character alone.

Posterior to the scapular neck, the width of the scapula increases gradually into the scapular blade, which reaches a maximum dorsoventral width of 157 mm. The distal portion of the scapular blade is considerably dorsoventrally wider than the proximal region of the scapula reaching the point of maximum dorsoventral width slightly anterior to the posterior end of the scapula. This distal dorsoventrally wide body of the scapula is a feature of "sauroloph" and other hadrosaurines, and lambeosaurines (Prieto-Márquez 2008). At the location of the dorsoventral expansion of the scapular blade, there is an antero-medial thinning which begins as an abrupt decrease in mediolateral width posterior to the scapular neck, then gradually diminishes to about five millimetres of mediolateral width at the distal end of the scapular blade. The mediolateral thickness is a few millimeters greater on the dorsal edge than it is on the ventral edge, in contrast to *Saurolophus angustirostris* whose scapular blade has a markedly greater curve ventrally (Maryańska and Osmólska 1984). The scapular blades of lambeosaurines tend to be shorter antero-posteriorly and wider dorsoventrally than those of saurolophines (Brett-Surman and Wagner 2007), but *Lambeosaurus* (ROM 1218) is an exception to this (Evans and Reisz 2007), having a long and relatively dorsoventrally short scapula. TMP2015.044.0036 more closely resembles hadrosaurines in this way, with a dorsoventral width of the blade and scapular neck similar to that of *Lambeosaurus* and *Corythosaurus*, but with an antero-posterior length even greater than *Lambeosaurus.* As in most other hadrosaurids (Maryańska and Osmólska 1984; Prieto-Márquez 2008) the distal half of the scapular blade is convex medially. The deltoid ridge runs along the centre of the lateral surface of the scapular blade anteroposteriorly, and terminates at the scapular neck. The deltoid ridge is a raised surface for muscle attachment that is laterally

convex with a distinct ventral margin, very similar to the condition in *Edmontosaurus regalis* (Campione 2014). There is some damage below the deltoid ridge of TMP2015.033.0036 that may overaccentuate the concavity below the deltoid ridge. The posterior margin of the scapular blade is dorsoventrally straight, giving the distal end a rectangular shape as in most hadrosaurids. The corners of the distal end of the scapular blade are slightly damaged in TMP2015.044.0036, but appear rounded as in *Edmontosaurus regalis* (Campione 2014), rather than sharply perpendicular as in *Brachylophosaurus canadensis* and *Lambeosaurus magnacristatus* (Evans and Reisz 2007; Cuthbertson and Holmes 2010).

Coracoid

The right coracoid of TMP2015.044.0036 (Fig. 2) is extremely well preserved. There is some minor distortion due to damage post-burial, but the overall shape is consistent with that seen in other hadrosaurids, namely *Edmontosaurus regalis* (CMN 2289), and lambeosaurines (Prieto-Márquez 2008; Campione 2014) in that the coracoid is anteroposteriorly longer than it is tall dorsoventrally at its centre. It is posteriorly mediolaterally broad at the articular facets, and thinner but still quite tall at the anterior margin between the proximoventral buttress and the ventral process. Iguanodontians and other early forms of hadrosauroid, in contrast, tend to have rounded plate-like coracoids in lateral view (Brett-Surman and Wagner 2007; Norman 2002; Carpenter and Wilson 2008; Prieto-Márquez 2008).

The coracoid of TMP2015.044.0036 is 170 mm long antero-posteriorly (Table 1A) and attaches via the scapular facet to the scapula's anteriorly facing coracoid facet. The scapular facet mirrors the coracoid facet in being a posteriorly oriented, upside-down kidney bean shape

with a long concavity along its centre and a rugose texture for cartilage attachment. The glenoid facet also mirrors the glenoid facet of the scapula, and is a large, posteroventrally oriented concavity that creates the glenoid fossa (shoulder joint) that houses the humeral head when combined with the glenoid facet of the scapula. The glenoid facet also has a strong rugosity for cartilage attachment. As in most hadrosaurids, the glenoid facet and scapular facets laterally meet at an angle greater than 115°, and in fact, in TMP2015.044.0036 these facets meet at an angle of ~150°, much larger than in *Edmontosaurus regalis* and *Brachylophosaurus canadensis* (Prieto-Márquez 2008; Cuthbertson and Holmes 2010; Campione 2014). The coracoid foramen is an almond-shaped hole that passes mediolaterally through the centre of the coracoid. Anteriorly, the coracoid thins antero-medially to form the subtriangular ventral process, an anteromedially oriented, dorsoventrally long projection of bone that encompasses the entire length of the coracoid and extends to form a ventrally oriented point. The anterior edge of the ventral process has a rugose surface along its approximately inch thick surface for cartilage attachment. At the anterodorsal corner of the coracoid is the bicipital tubercle. This tubercle is an anteriorly directed bulge with a large convex surface. As in *Saurolophus angustirostris* (Maryańska and Osmólska 1984), this knob-like structure would have accommodated the origin of the biceps tendon.

2.3.2. Sternum

Sternal Plate

The sternal plates of TMP2015.044.0036 (Fig. 3) are extremely well-preserved and are in presumed natural midline contact. The plates are unfused but have only a couple millimeters of space between them anteriorly. A diamond-shaped gap interrupts the line of articulation between the two plates, which are also separated anteriorly and posteriorly by shallow notches edged with unfinished bone. A similar sized gap is present in *Corythosaurus* (CMN 1947) and at least juvenile *Lambeosaurus lambei* (AMNH 5340) (Prieto-Márquez 2008), though in the latter taxon the gap has rounded rather than being diamond-shaped. Considerably smaller gaps are also visible in *Brachylophosaurus canadensis* (MOR 1071; UCMP 130139) and a separate specimen of *Corythosaurus* (ROM 1947) (Prieto-Márquez 2008). The medially located body of each sternal plate has a kidney bean shape, where the concave sides are directed medially. The condition is most similar to the shape of the main plates of *Corythosaurus* and *Lambeosaurus* (Prieto-Márquez 2008). In ventral view, the posterior (lower) portion of the main plate is approximately 47 mm wide (Table 1B) and is smooth, flat, and thin dorsoventrally. This thinness is maintained up to its contact with the opposing plate where it terminates in a strongly rounded posterior edge (the bottom of the kidney bean). The anterior portion of the main plate is twice as wide in anterior view as the posterior portion, being approximately 80 mm wide mediolaterally, and is thin medially (a few millimeters) and thicker laterally (about a centimeter). There is a natural, sudden increase in dorsoventral width a few centimeters from the anterior edge, which reaches a maximum dorsoventral thickness of 60 mm. The anterior end is flat and angled anteromedially. The anterior surface is highly rugose for cartilaginous attachment.

The sternal plates resemble those of other hadrosaurids in bearing long posterolateral processes, which contribute approximately two thirds of the length of each element. In TMP20105.044.0036 these processes extend posterolaterally from the central portions of the lateral edges of the main plates, and maintain an approximately constant height and width until they reach their posterolateral articular ends. The shafts of the posterolateral processes of TMP2015.044.0036 are slightly curved inward medially creating a large, rounded chest region. The ratio of length of the posterolateral processes to the width of the scapular blades themselves seems to be fairly consistent across hadrosaurine and lambeosaurine taxa (Brett-Surman 1989), but it is unclear if this medial curvature is unique to TMP2015.044.0036, as most prepared sternals are described as having straight processes (Norman 1980; Brett-Surman 1989; Prieto-Márquez 2014).

The articular ends expand very slightly antero-posteriorly but otherwise retain the shape of the posterolateral processes, and end in a straight perpendicular edge. It is unclear if there are one or two articular facets on the posterior articular surfaces. In anterior view, there is wide angle of 110^0 between the two plates, which is assumed to mostly be the natural anatomy of the pectoral region, however there is a difference of several degrees from the median between the two sides, the right sternal plate having a wider angle between the sagittal plane and the posterolateral process than that of the left. The angle between the posterolateral processes is variable among ornithopod taxa and is much wider in TMP2015.044.0036 than in at least some other hadrosaurids, including *Edmontosaurus* (Osborn 1912; Campione 2014; Prieto-Márquez 2014).

2.3.3 Forelimb

Humerus

Although field notes indicate that both humeri of TMP2016.044.0036 were preserved and collected, only the left humerus was prepared at the time of this description. The left humerus (Fig. 4) is very well preserved with only minor damage to the proximal articular head and the apex of the deltopectoral crest. The overall shape of the humerus of TMP2015.044.0036 is like that of *Edmontosaurus* (Campione 2014; Prieto-Márquez 2014), though somewhat broader mediolaterally. It is known that lambeosaurines tend to have anteroposteriorly broader humeri especially at the deltopectoral crest compared to those of hadrosaurines, however, this feature varies considerably through ontogeny and cannot be confidently used as an indication of taxonomic placement (Dilkes 2000; Egi and Weishampel 2002). The humerus of TMP2015.044.0036 is relatively long and with a posterior edge that is much straighter compared to *Parasaurolophus cyrtocristatus* and *Brachylophosaurus canadensis* (NMC 8893) (Ostrom 1963; Cuthbertson and Holmes 2010).

From proximal to distal ends, the humerus is 480 mm long (Table 1C), a size consistent with a juvenile to sub-adult individual (Egi and Weishampel 2002). The proximal, articular head is divided into three projections that make the humeral head roughly the shape of an equilateral triangle, each end with a laterally projecting condyle that is roughened for muscle attachment. The anteriormost of these projections is in line with the deltopectoral crest and is the insertion for the deltoideus scapularis muscle. The posterolaterally directed condyle is the insertion for the coracobrachialis, and the posteromedial condyle is the insertion for the scapulohumeralis posterior and subscapularis muscles. The proximal head in its entirety is slightly curved posteriorly and articulates with the coracoid and scapula via the glenoid fossa. The deltopectoral

crest is large and highly developed in TMP2015.044.0036 and runs along the proximal 50% of the lateral margin of the anterior face of the humerus. The deltopectoral crest is 18 mm wide proximally and ends at a peak in anteroposterior width with a maximum width of 77 mm and a slight medial concavity just posterior to the anterior edge, which is rounded. The deltopectoral crest is concave medially and has a rugose texture along the anterior edge for insertion of the deltoideus clavicularis and scapula-humeralis anterior muscles. The anterior margin of the deltopectoral crest is medially deflected, a feature present in *Brachylophosaurus* (NMC 8893) and *Parasaurolophus* (Ostrom 1963; Cuthbertson and Holmes 2010). The deltopectoral crest is also distinctly different than that of *Maiasaura* peeblesorum, whose humerus bears an antero-posteriorly thin deltopectoral crest (Dilkes 2000). At the termination of the deltopectoral crest, the shaft of the humerus is cylindrical and splits into two large condyles at the distal end with strong grooves dividing the margins of the two for the last 150 mm of the humeral shaft on both the anterior and posterior sides. The radial condyle is the more lateral of the two and articulates with the radius distally. The ulnar condyle, which articulates with the ulna, is medially positioned and is a few millimetres longer than the radial condyle. Both condyles are rounded and are directed anteriorly, unlike *Edmontosaurus regalis* and *Brachylophosaurus canadensis* for which the distal articular condyles are deflected slightly medially (Cuthbertson and Holmes 2010; Campione 2014; Prieto-Márquez 2014). There is a very clear sinuous line along the circumference of both condyles that marks the edge of the cartilaginous cap of the distal end of the humerus.

Radius

Both left (Fig. 5) and right (Fig. 6, 7) radii and ulnae of TMP2016.044.0036 were collected and prepared. However, the right radius (Fig. 6) and ulna (Fig. 7) were much better preserved, being fractured, and separated transversely along the mid-to-proximal portion of the shaft before excavation but with otherwise only minor damage to the bones. The left radius and ulna were not separable during preparation, having somewhat fused together at their contact along their mediolateral lengths, and strongly bent cranially at their distal-most portion. The left radius and ulna were also crushed downward at their proximal ends, resulting in the distalmost portion of the radial and ulnar heads being fractured and forced downward onto the proximal-most portion of their shafts. For these reasons, this study will focus only on the right radius and ulna.

The radius is slightly expanded mediolaterally at the distal and proximal ends (Table 1C). The distal end is relatively flat and thin antero-posteriorly, indeed likely thinner than in the living animal due to slight compression during burial. The thin proximal end widens mediolaterally slightly before constricting into the radial shaft, which is circular in cross section. This shaft reaches its minimum circumference at the centre of the shaft, then expands mediolaterally once more towards the proximal end. There is a medial expansion along the proximal third of the radius that contacts the ulna laterally. This expansion borders a concavity on the proximal head that accommodates the ulna laterally. In dorsal view, the proximal radial head is roughly circular, with the concavity for the ulna giving the head a slightly crescent shape medially.

Ulna

Consistent with other hadrosaurids, the ulna (Fig. 5, 7) is the longest bone in the forelimb (Evans and Reisz 2007; Campione 2014), making the zeugopodium longer than the stylopodium (Table 1C) as is typical for lambeosaurines (Evans and Reisz 2007). Distally, the ulna resembles the distal end of the radius in being relatively flat mediolaterally and having a roughly rectangular distal end. The distal end of the right ulna of TMP2016.044.0036 is slightly crushed antero-posteriorly, making the posterior surface of the distal half veined with fractures. Like the radius, the ulna is thinnest in its midshaft region which is circular in cross section. A triangular divot forms on the distal-most portion of the mid-shaft on the anterior surface of the ulna, expanding to a large, triangular shaped concavity on the proximal end that articulates with the radius. This large trough terminates at the proximal end in the lateral process laterally, and the cranial process, antero-medially so that these processed define the boundaries of the trough. There is a 90-degree angle between these two processes. The olecranon process projects anterolaterally at approximately 90 degrees from the cranial process, and 180 degrees from the lateral process. The olecranon process articulates with the posterior distal end of the humerus. This process is the dorsal-most reaching point of the ulna, extending approximately 5 cm past the terminal points of the lateral and cranial processes. There is a second longitudinal trough along the shaft of the ulna between the olecranon process and the lateral process, though it is shallower than the one between the lateral and cranial processes, and only extends to the middle ulnar shaft. The three proximal processes give the proximal surface of the ulna a T-shape, with concavities between the lateral and cranial processes, and the cranial and olecranon processes. There is no concavity between the lateral and olecranon processes.

2.3.4 Manus

Carpals

No carpals are preserved in TMP2016.044.0036, though there is a distinct gap preserved between the radius and ulna and metacarpals of the left side. This gap is believed to be a true representation of the space that would accommodate the carpals and not due to effects of burial since the surrounding bones do not appear damaged or displaced post-burial. The right side does not preserve a similar spacing between the ulna and radius and metacarpals but does show damage to the radius and ulna consistent with post-burial distally- directed force which could explain why the right side shows no gap while the left side does.

Metacarpals

Metacarpal II (Fig. 8, 28, 29) is a long and slender bone, compressed antero-posteriorly. Proximally, it is mediolaterally wide, forming a rounded but blocky proximal end that would have articulated with the carpals (carpals were not preserved in TMP2016.044.0036). The shaft maintains its width distally (Table 1D), to a slight constriction just before the distal end, where it then curves slightly laterally against metacarpal III. The distal surface is roughly rectangular and articulates with the first phalanx of digit II. Before separation of the manus, metacarpal II articulated with metacarpal III along the lateral edge of metacarpal II, covering a large portion of the postero-medial edge of metacarpal III.

Metacarpal III (Fig. 9, 10, 28, 29) is the longest of the metacarpals (Table 1D). Like metacarpal II it is long and slender, though it is compressed mediolaterally. The proximal end is small and circular, with a slight pinching at the posterior margin. The shaft is roughly rectangular

in cross section, especially at the distal end, where there are visible right angles on the bone surface on the anterior, posterior, medial, and lateral corners. The distal surface is rectangular, and the anterior edge is a few millimeters longer than the posterior edge, and the medial and lateral edges are slightly concave to accommodate metacarpal II medially and metacarpal IV laterally. Metacarpal III is situated anterior to metacarpals II and IV, giving the manus a columnar shape when articulated, metacarpal III forming the anterior most portion of this cylinder. The proximal edge is not in line with those of metacarpals II and IV, but begins a few centimetres distally, and its distal end terminated a few centimeters past metacarpal IV and about 10 cm past metacarpal II distally. At the distal end of metacarpal III, phalanx I of digit II articulates with metacarpal III medially where metacarpal II terminates, and projects past metacarpal III about 1 cm distally.

Metacarpal IV (Fig. 9, 11, 28, 29) is nearly the same length as metacarpal III (Table 1D). Proximally, metacarpal IV is much wider anteromedially than metacarpal III due to a large antero-posterior compression. This compression causes the proximal articular surface of metacarpal IV to be thin a thin and long oval, the mediolateral width almost double the anteroposterior width. Metacarpal IV becomes more rectangular in cross section along the shaft of the bone, maintaining its dimensions until a slight mediolateral expansion at the distal end. The distal articular surface is rectangular, though much smaller than the distal end of metacarpal III, and articulates with the first phalanx of digit III. The whole anteromedial edge of metacarpal IV is in close contact with the posterolateral surface of metacarpal III. Metacarpal V sits on the proximal-most posterior surface of metacarpal IV.

Metacarpal V (Fig. 12, 28, 29) is the shortest of the metacarpals (Table 1D), being reduced to at least half the length of the other metacarpals. It is elongated proximodistally like

the condition in *Bactrosaurus* johnsoni (SBDE 95E) and unlike *Maiasaura peeblesorum* (ROM 44770) (Dilkes 2000; Prieto-Márquez 2008). It also has the most unique shape of the metacarpals, being triangular in anterior and posterior views. It is not compressed antero-posteriorly like the other metacarpals but does have a wide articular surface proximally that is angled so that the medial end of the articular surface reaches higher up the manus than the lateral edge. The proximal articular surface is also concave and highly rugose, presumably for attachment to cartilaginous carpals. The anterior edge of the proximal surface has a semi-circular concavity where it attached to metacarpal IV. The proximal anterior surface is concave to accommodate its articulation on the posterior surface of metacarpal IV. The medial posterior surface of metacarpal V is also slightly concave, forming a smooth divet in the surface. The bone pinches distally so that the distal articular surface is much smaller than the proximal end and is round and convex in shape with a small posteriorly projecting point on the postero-medial edge created by the divet on the posterior surface.

Phalanges

Phalanx I of digit II (Fig. 13, 28. 29) buttresses the metacarpal column medially by its contact with metacarpal III along the lateral edge of phalanx I. Phalanx I is mediolaterally compressed and flares anteroposteriorly at both proximal and distal ends (Table 1D). The proximal articular surface is semi-circular with a flat laterally to articulate with metacarpal II. The distal end of phalanx I has prominent points anteriorly and posteriorly, though the anterior process is more slender and farther projecting than the posterior one. The proximal articular surface is oval-shaped with a slight posterolateral concavity appearing on both right and left phalanx I of digit II.

Phalanx II of digit II (Fig. 14, 15, 28, 29) is a small, triangular bone. In anterior view it is flat and shaped somewhat like an equilateral triangle, tapering to a narrow point medially (Table 1D). Anteriorly, this triangular surface is flat, but the proximal and distal surfaces of the bone meet at a thin edge posteriorly, so that the anterior surface is considerably broader than the posterior surface. The medial tapering combined with the comparatively narrow posterior potion causes phalanx III of digit II to be directed medially, toward the midline of the body.

Phalanx III of digit II (Fig. 14, 16, 28, 29) is about twice as long dorsoventrally as it is anteroposteriorly (Table 1D). Proximally, the articular surface is round and slightly concave to accommodate phalanx II. The anterior surface of digit II phalanx III is convex and smooth, nearly cylindrical in cross section proximally, but flattens distally and becomes broader mediolaterally to form a semicircular distal end. The phalanx tapers towards the distal end, which has an anteroposterior thickness of only a few mm. The posterior surface reflects the shape of the anterior surface but is flat rather than convexly shaped. The posterior surface would have contacted the ground, accounting for the mediolaterally wide distal end that would diffuse the weight applied to the unguals by the forelimb. There are a few large pits on the posterior surface of the distal end of the phalanx to accommodate blood vessels to the digit. Phalanx III of digit II is directed medially towards the midline of the body when articulated with its respective phalanges.

Phalanx I of digit III (Fig. 17, 19, 28, 29) is approximately square in anterior or posterior view, and is twice as wide mediolaterally as it is anteroposteriorly (Table 1D), expanded mediolaterally as in *Parasaurolophus walker* (ROM 768) and unlike *Corythosaurus intermedius* (ROM 845) and *Maiasaura peeblesorum* (ROM 44770) (Dilkes 2000; Prieto-Márquez 2008). The centre of the bone is constricted and roughly ellipsoid in cross section, while the proximal

and distal end flare outward. This flaring is most pronounced at the distal end of phalanx I where there is a well-developed lip medially and laterally that is deflected slightly dorsally. The proximal articular surface is flat, while the distal articular surface is cocave and bowed mediolaterally to accommodate phalanx II. This gives the distal end a saddle shape in anterior and posterior views. The ventral surface bears some minor pitting and one large foramen in the centre for a circulatory canal. When articulated, the distal end of phalanx I of digit III is side by side with the distal end of the first phalanx of digit IV.

Phalanx II of digit III (Fig. 18, 20, 28, 29) is triangular in anterior and posterior views, with a wide lateral base and medial apex (Table 1D). The lateral half of the anterior and almost entire posterior sides are concave and saddle shaped. The proximal surface is broad, rectangular, flat, and smooth. The distal articular surface is also roughly rectangular but has a convex surface for articulation with phalanx III. The lateral margin of the distal side has a swelling, forming a lip that extends a few millimeters laterally. This lip dips steeply towards the medial tip, the angle shallowing about halfway along the articular surface.

The third phalanx of digit III (Fig. 21, 28, 29) is an ungual like that of digit II but is much shorter dorsoventrally (Table 1D). In anterior and posterior views, the overall shape of phalanx III is rectangular with a proximal end a few millimeters mediolaterally thinner than the distal end. The proximal edge is thick anteroposteriorly and steeply inclines to a thin distal edge. There is a small square notch on the medial and lateral sides about halfway down the length of the phalanx that forms a slight mediolateral constriction. The proximal articular surface is ovoid, anteroposteriorlly compressed, and slightly concave. The distal end of phalanx III is slightly rounded and all along the distal, medial, and lateral edges there is a series of small notches and projections (~ 1 mm) extending outward, giving these edges a sinuous appearance in anterior and

posterior views. The anterior surface is smooth and flat, while the posterior surface is convex and with a mottled texture. The distal end of the posterior surface is bordered with small foramina for vascular canals, and there are two or three larger foramina ~1 cm proximal to the distal edge on the posterior surface.

Phalanx one of digit IV (Fig. 17, 22, 28, 29) is the longest phalanx in the manus of TMP2015.044.0036 (Table 1D). The distal articular surface is broad and rectangular, with a large notch running mediolaterally to accommodate metacarpal IV. On either side of this notch are swellings, forming an anterior and posterior ridge on the proximal surface. In anterior and posterior views, phalanx I retains its rectangular shape, constricting slightly mediolaterally ~2 cm from the distal end, where it immediately flares mediolaterally to form a lipped edge on the medial and lateral sides, the lateral being the larger of the two. Between these raises edges is an antero-posteriorly oriented notch on the distal articular surface that articulated with phalanx II. The articular surfaces are otherwise smooth. There is a depression on the distal-most anterior surface as well as the distal-most lateral surface, giving the corner between the distal anterior and lateral edges a pinched appearance. The lateral surface is otherwise smooth and convex, while the medial surface is concave with a depression running dorsoventrally. This depression accommodates phalanx I of digit II distally and the distal-most portion of metacarpal II proximally. A small notch on metacarpal II suggests that phalanx I of digit III may slightly overlap the anterior surface of metacarpal II.

Phalanx II of digit IV (Fig. 18, 23, 28, 29) bears a strong resemblance to phalanx II of digit II (Table 1D). The proximal and distal articular surfaces are smooth and roughly rectangular. In anterior and posterior views, phalanx II is triangular and tapers to a point medially. This caused phalanx III to be slightly medially oriented, like digit II. There is a divet

that runs around the bone, from the medial-most edge of the anterior surface to the medial-most edge of the posterior surface, giving the bone a concave appearance.

Phalanx III of digit IV (Fig. 23, 24, 28, 29) is a very small bone (Table 1D). In anterior and posterior views it is rectangular to ovoid, and about three times wider mediolaterally than it is dorsoventrally. In proximal and distal views, phalanx III is anteroposteriorly thin, and mediolaterally wide. There is a thin notch running mediolaterally along the distal surface of phalanx III.

Phalanx I of digit V (Fig. 25, 28, 29) is rectangular in anterior and posterior views with a proximal end that is much wider mediolaterally (~1 cm greater) than the distal end (Table 1D). The proximal articular surface is very slightly concave and anteroposteriorly compressed so that the anterior portion of the proximal surface is convex, and the posterior surface is concave, giving the articular surface a kidney bean shape, this cross sectional shape is maintained throughout the length of the element. The anterior surface is smooth and convex, while the posterior surface is flat and textured with small, long pits, possibly for vascular tissues, muscle attachment, or because it rests upon the posterior surface of metacarpal IV. The distal articular surface is strongly convex and more circular than the proximal end. It is small, about half the mediolateral width of the proximal end.

Phalanx II of digit V (Fig. 26, 28, 29) is almost identical in shape to phalanx I of digit V, though phalanx II is much shorter dorsoventrally (Table 1D). Both proximal and distal articular surfaces are oval in shape, compressed anteroposteriorly, though the proximal surface is concave and the distal surface convex. Anteriorly, the element is covex, and smooth, with a wide proximal end and narrow distal end. At both proximal and distal edges there is a lip that protrudes slightly over the edge around the circumference of the bone. This lip is slightly more

pronounced and bulbous at the lateral edge of the distal end. Like phalanx I, the posterior surface is textures with small pitting but otherwise is flat.

Phalanx III of digit V (Fig. 27, 28, 29) is a very small bone (~2 cm long). It is twice as long anteroposteriorly than it is mediolaterally (Table 1D)0. In anterior and posterior views it is bullet-shaped, with a straight proximal edge, parallell medial and lateral sides, and a rounded distal end. The proximal end is oval, anteroposteriorly compressed and flat. The anterior and posterior surfaces are smooth, thought the posterior is flat while the anterior surface is convex.

2. 4 Discussion

Structure and articular relationships of the partially ossified sternum in TMP2015.044.0036

The sternum in most reptiles is a largely or entirely cartilaginous skeletal element that contacts the coracoids anteriorly and articulates with several pairs of usually cartilaginous sternal ribs (Kälin 1929; Sanders and Farmer 2012; Baier et al. 2018). Hadrosaurids and other derived iguanodontian dinosaurs are well known for their distinctive “hatchet-shaped” sternal ossifications, which comprise a pair of flat plates with elongate posterolateral processes (see Osborn 1912; Norman 1980; Dodson and Madsen Jr. 1981; Norman 1986; Forster 1990; Bultynck 1992; Wang et al. 2011; Wang et al. 2017; Prieto-Márquez 2014; Verdú et al. 2017). In many vertebrates the sternum contributes to the ventilatory movements of the ribcage during respiration and the structural bracing function of the shoulder girdle (Codd 2004; Schachner et al. 2009; Farmer 2015; Codd 2010). Published information on hadrosaurid sterna is limited to

brief descriptions of typically disarticulated sternal plates, since these bones are usually poorly preserved and seem to have easily become separated and displaced postmortem following decay of the sternum's cartilaginous portion. Hence, the elements are often missing from illustrations and museum mounts of hadrosaurid skeletons.

The level of ossification of the sternal plates varies among ornithopods, and some taxa show indications that the coracoids would have articulated with the anterior part of the sternum. In at least one known juvenile specimen of *Edmontosaurus* (LACM 23504), the sternal plates are fused together and elongated in the anterior direction, and appear to bear large anterolateral depressions that could have accommodated the coracoids. In the articulated *Edmontosaurus* AMNH 5060 the sterna are preserved well posterior to the coracoids, despite being anteriorly extended as in LACM 23504 (Brett-Surman 1989), but Osborn (1912) suggested this separation of the sterna from the coracoids was an unnatural condition caused by "insinking" of the chest region, which seems likely given that it is an unusual feature unique to this specimen.

Iguanodon shows a different pattern of reinforcement of the anterior part of the sternum, in that an irregular, mineralized "intersternal" element is consistently found anterior to the sternal plates and between the coracoids in articulated specimens (Norman 1980). Other hadrosauroids that do not show a mineralized element in this position presumably possessed a mass of cartilage attaching the sternum to the coracoids. The existence of the mineralized "intersternal" element in *Iguanodon* was interpreted by Norman (1980) as a structural response to stresses transmitted to the pectoral region by the forelimbs, and thus as an indicator of a quadrupedal gait. Following this logic, the lack of any apparent ossification between the coracoids of TMP2015.044.0036 raises the possibility that this hadrosaurid might have been bipedal. However, other features such as the presence of hoof-like unguals and the pillar-like configuration of the metacarpals suggest

the animal was in fact habitually quadrupedal. Absence of ossification between the coracoids might then indicate that the forelimb in TMP2015.044.0036 bore a smaller proportion of the weight of the body than in *Iguanodon*, or that the minimally ossified carpals in hadrosaurids (see below) acted as shock absorbers and reduced the transmission of locomotor impacts to the pectoral girdle. Testing these possibilities will require the careful construction of biomechanical models, in which the sternum will have to be incorporated as an integral component. Alternatively, a posterior, medial sternal gap morphologically comparable to that of TMP2015.044.0036 was observed in a sub-adult emu (*Dromaius novaehollandiae*, 27 kg male, 3 years of age), though this gap continues linearly posteriorly rather than being diamond-shaped like that of TMP2015.044.0036. The sternum is one of the last elements to completely ossify in ratites and is largely cartilaginous upon hatching (Maxwell and Larsson 2009). Indeed, the last portion of the sternum to ossify in ratites seems to be this posterior area which begins ossifying laterally and terminates centrally (Maxwell and Larsson 2009). Although neognaths do not display this same process of ossification, their sterna are highly modified to accommodate a large, fleshy M. pectoralis muscle for flight, while emus possess a ventrally flat sternum like those of hadrosaurids. This raises the possibility that since TMP2015.044.0036 is a juvenile to sub-adult individual, the sternum of hadrosaurids may terminate ossification of the medial sternal plates later in ontogeny. Embryonic hadrosaurid material seems to corroborate this hypothesis (Horner and Currie 1994) in displaying a comparatively greater medial gap in their plates than TMP2015.044.0036 and other non-juvenile hadrosaurid specimens (Brett-Suman 1989; Prieto-Márquez 2008). However, further study on the development of the sternum across Hadrosauridae would be necessary to explore this hypothesis and a lack of well-preserved sterna from various ontogenetic stages makes this difficult.

The lateral ends of the posterolateral processes would likely have articulated with the first two or three pairs of sternal ribs (Fig. 30), as has been suggested for other derived iguanodontians (e.g. Norman 1980). As evidenced by the lack of ossified elements recovered for hadrosaurids and the condition seen in extant crocodilians (e.g. Cong et al. 1998; Sanders and Farmer 2012; Baier et al. 2018), the sternal ribs would have been cartilaginous and it is possible that intermediate ribs may have also been present as in crocodilians. The anterior sternal ribs were presumably very short, given the small space that would have been available between the posterolateral processes and the vertebral ribs, and such reduction of the cartilaginous component of the anterior part of the ribcage would have resulted in greater rigidity in this area. By contrast, the unfinished notches between the sternal plates suggest that cartilaginous extensions of the sternum were likely present both anteriorly and posteriorly. Although the shapes of these extensions are difficult to infer, the anterior one likely formed a plate articulating with the coracoids as reconstructed for *Iguanodon* (Normal 1980), though without the mineralised intersternal element. The thin, lightly grooved outer margins of the ossified sternal elements themselves seem unsuitable for direct contact with the much thicker coracoids. In this reconstruction, the width of the anterior notch would approximate the distance between the coracoids, considering the convexity of the coracoids themselves. The posterior cartilaginous extension of the sternum may have been long, resembling the mesosternum and / or xiphisternum in modern crocodilians (e.g. Cong et al. 1998; Sanders and Farmer 2012; Baier et al. 2018) and providing seemingly necessary space for attachment of the posterior pairs of sternal ribs.

On hadrosaurid carpals

It is known that at least some iguanodontids possess block-like or wedge shaped, ossified carpals (Norman and Weishampel 1990; Rasmussen 1998; Carpenter and Wilson 2008). Hadrosaurids undoubtedly possessed carpals, but they are rarely found in the literature or in collections. Brett-Surman and Wagner (2007) argued that this is because of their unique shape that is not easily identified by excavators and preparators. While this may be the case for at least some taxa, I would argue that carpals are simply not preserved in the vast majority of hadrosaurid dinosaur remains. TMP2015.044.0036 is exceptionally well preserved, with all manual elements preserved and mostly in articulation. However, there are no carpals preserved. There is, however, a clear gap of several centimetres between the radius and ulna proximally, and the metacarpals distally, in the left forelimb of TMP2015.044.0036, the least distorted of the two. This spacing would be consistent in location and size for carpals. Therefore, it is most likely that in TMP2015.044.0036 the carpals were cartilaginous and degraded after burial of the animal, as suggested by Norman (2002) in the case of *Probactrosaurus*. This likely also occurred in other articulated hadrosaurid specimens, such as CMN 57016, an articulated right manus and distal portion of radius and ulna of *Lambeosaurus* which has been reconstructed with a wedge-shaped carpal resting over the proximal articular surface of metacarpal II. While it is possible that this element represents the radiale of CMN 57016, it bears a striking resemblance to phalanx II of digit III or even IV, which happen to be missing in CMN 57016, raising the possibility that this element is simply a displaced phalanx. Indeed, no other carpals are present in CMN 57016 so the placement of the element is questionable at best. The fact remains that there have been no hadrosaurid specimens described in the literature thus far that possess structures morphologically similar enough to be confidently classified as genuine carpals. Thus, one cannot confidently

describe which individual ossified or cartilaginous elements were present within the wrist itself or draw any meaningful conclusions on their structure or articular relationships within the manus.

Functional morphology of the manus in TMP2015.044.0036

The manus of TMP2015.044.0036 is functionally tridactyl. Metacarpals II, III, and IV form a pillar-like structure, with metacarpal III sitting anterior to the others, as in *Maiasaura peeblesorum* and *Lambeosaurus magnacristatus* (Dilkes 2000; Brett-Surman and Wagner 2007; Evans and Reisz 2007). This pillar-like structure would be particularly advantageous for weight bearing since the mechanical load of the body's mass is transmitted to compressional force that is spread over a greater combined cross-sectional area than any one metacarpal on its own. This would be particularly effective in the configuration seen in TMP2015.044.0036 considering the close proximity of these elements suggest there was a negligible amount of movement that could occur between adjacent metacarpals, given their close proximity to each other, resulting in a mechanical bracing effect in the manus. Indeed, most hadrosaurid metacarpals seem to be shaped in such a way that would allow for a very close proximity to one another (Brown 1916; Brett-Surman and Wagner 2007; Prieto-Márquez 2008; Campione 2014). Metacarpal V is significantly reduced and sits posterior to the manus, so that digit V is directed posteriorly, and would likely not have contacted the ground. Maryańska and Osmólska (1984) attribute this lateral splaying of digit 5 to a laterally compressed distal articular surface of metacarpal V, causing phalanx I of digit V and the distal half of metacarpal V to experience lateral torsion (Maryańska and Osmólska 1984; Brett-Surman and Wagner 2007). The terminal phalanx of digit V is much smaller than those of digits II, III, and IV, and though it largely resembles the shape of the

terminal unguals of the manus in being anteriorly convex, posteriorly flat, and rounded on the ventral edge, it is laterally compressed, and its small size suggests negligible involvement in bearing weight. Digit I is consistently absent among hadrosaurids (Brown 1916; Brett-Surman and Wagner 2007; Prieto-Márquez 2008; Campione 2014). Digits II, III, and IV, in contrast, all possess well-developed hoof-like unguals as their distal phalanx. The presence of unguals alone suggests that these animals used their forelimbs at least in part during locomotion and/ or in bearing weight to some degree.

Summary of forelimb features that vary taxonomically among hadrosaurids

Scapula

As described by Brett-Surman and Wagner (2007), there are two morphotypes present within hadrosaurid scapulae: the saurolophine type whose blade is anteroposteriorly long and dorsoventrally short, and the lambeosaurine type whose blade is anteroposteriorly short and dorsoventrally wide. The findings of the present study also suggest that lambeosaurines that possess a generally narrow and long scapular neck, and the dorsoventrally wide blade is accompanied by a curved ventral hump along the bottom margin of the blade (Sternberg 1935; Evans and Reisz 2007; Ostrom 1963; Prieto-Márquez 2008; Prieto-Márquez 2014; Lull and Wright 1942; Brett-Surman and Wagner 2007). In contrast, Saurolophines possess a scapula whose neck is, in general, dorsoventrally similar in width to the blade, an anterior head that is anteroposteriorly short, and whose blade maintains a straight edge dorsally and ventrally, with a less dramatic flare in dorsoventral width posteriorly (Hu et al. 1973; Brett-Surman and Wagner 2007; Campione 2014; Dilkes 2000; Prieto-Márquez 2008; Prieto-Márquez 2014; Cuthbertson

and Holmes 2010; Maryańska and Osmólska 1984; Lull and Wright 1942). However, there is much variation in these proportions taxonomically at both the genus and species level, so they should be used to evaluate specific taxonomic classification.

Coracoid

The most obvious taxonomic variation in the coracoid is between early hadrosauroids and the Hadrosauridae proper. *Iguanodon, Probactrosaurus, Camptosaurus,* and *Gilmoresaurus* have all been described to possess coracoids that are round and plate-like (flat and mediolaterally thin) in lateral view (Carpenter and Wilson 2008; Norman 2002; Prieto-Márquez and Norell 2010; Prieto-Márquez 2008; Brett-Surman and Wagner 2007). The hadrosaurids universally possess coracoids that are thick mediolaterally (at least a few centimeters) with prominent bicipital tubercles dorsal to the ventral ridge for attachment of the biceps tendon (Hu et al. 1973; Brett-Surman and Wagner 2007; Campione 2014; Dilkes 2000; Prieto-Márquez 2008; Prieto-Márquez 2014; Cuthbertson and Holmes 2010; Maryańska and Osmólska 1984; Lull and Wright 1942 Sternberg 1935; Evans and Reisz 2007; Ostrom 1963).

Sternal Plates

As with the scapulae, there are two distinct morphs that separate saurolophines and lambeosaurines. Brett-Surman and Wagner (2007) proposed that in general, the lambeosaurine main plate of the sternal is anteroposteriorly long, whereas the posterolateral process is the longer portion of the element in saurolophines, the exception being *Lambeosaurus*. Further comparisons by Prieto-Márquez (2008) seems to agree with this idea, however it is difficult to

draw any relevant conclusions due to the tendency of sternal plates to be heavily damaged, underprepared, and frequently unidentified or incorrectly attributed. *Camptosaurus*, however, displays the primitive condition in having a sternal plate that is roughly semi-circular with no posterolateral processes (Carpenter and Wilson 2008; Brett-Surman and Wagner 2007; Prieto-Márquez 2008).

Humerus

There is a common morphology to the humeri of juvenile hadrosaurids (Egi and Weishampel 2001). Through ontogeny, this very similar shape among taxa can change quite drastically (Brett-Surman and Wagner 2007; Egi and Weishampel 2002). For this reason, humeri are not typically used as a taxonomic determinant, but nonetheless possess some features that vary with taxonomic groups in the adult individuals.

The largest divide in hadrosauroid morphology, unsurprisingly, exists between early hadrosauroids (namely *Iguanodon* and *Ouranosaurus* for which morphometric analyses have been conducted (Egi and Weishampel 2002)), and Hadrosauridae proper. These early forms have been described as having "gracile"' humeri that are comparatively long and slender. The deltopectoral crest, which is the major site of attachment for M. pectoralis and some other forelimb retractors and adductors, does not reach part the midpoint of the humeral shaft in *Iguanodon, Ouranosaurus, Probactrosaurus, Bactrosaurus, Camptosaurus, Gilmoreosaurus, Lophorhothon,* and *Tanius* (Egi and Weishampel 2002; Norman 2002; Carpenter and Wilson 2008, Prieto-Márquez 2008; Prieto-Márquez and Norell 2010). Due to its commonality, this character seems to be a primitive feature of early hadrosauroids.

More differences are observable between the humeral morphologies of Lambeosaurinae and Saurolophinae. Lambeosaurines possess humeri that are, in general, thicker and more robust than those of hadrosaurines (Brett-Surman and Wagner 2007; Egi and Weishampel 2002). Saurolophines fall in between those of early forms and lambeosaurines, in being more slender and longer than lambeosaurines, but still more robust than in non-hadrosaurid hadrosauroids (Brett-Surman and Wagner 2007; Egi and Weishampel 2002). Similarly, saurolophines tend to have thinner radii an ulnae than those of lambeosaurines. In saurolophines, the lateromedial width of the deltopectoral crest is less than a third as long as it is dorsoventrally wide. In lambeosaurines, the dorsoventral length of the deltopectoral crest is twice as long as it is lateromedially long (Brett-Surman and Wagner 2007). The distal end of the deltopectoral crest in saurolophines also terminates at or above (proximal to) the midpoint of the humeral shaft, whereas in lambeosaurines it terminates at or below (distal to) the midpoint of the humeral shaft (Brett-Surman and Wagner 2007; Egi and Weishampel 2002). In lambeosaurines, the humeral shaft and deltopectoral crest are comparatively wider than those of saurolophines, and the deltopectoral crest also protrudes more obviously anterolaterally in lambeosaurines.

Comparisons of antebrachium (measured from radial length) and brachium length (measured from humeral length) in hadrosaurids can also be taxonomically useful. The length ratio of the brachium to the antebrachium is greatest in non-hadrosaurid hadrosauroids, intermediate in saurolophines, and smallest in lambeosaurines (Brett-Surman and Wagner 2007; Egi and Weishampel 2002; Lull and Wright 1942). In other words, the humeral length relative to the radial length is shorter in lambeosaurines than in hadrosaurines (Egi and Weishampel 2002) due to a relatively longer antebrachium in hadrosaurines. Humerus length is also frequently compared to femoral length in hadrosaurids and seems also to be taxonomically relevant (Egi

and Weishampel 2002). These analyses indicate that iguanodontians possess a humerus to femur length ratio that is longer than those of hadrosaurids proper, and of those. Lambeosaurines yield a smaller humerus to femoral length ratio than hadrosaurines, and this difference become more pronounced in larger individuals (Egi and Weishampel 2002). This fact, coupled with the significant variation in growth rates throughout the ontogeny of groups of hadrosaurids (Egi and Weishampel 2002; Dilkes 2001), makes these comparisons reliable only in adult individuals.

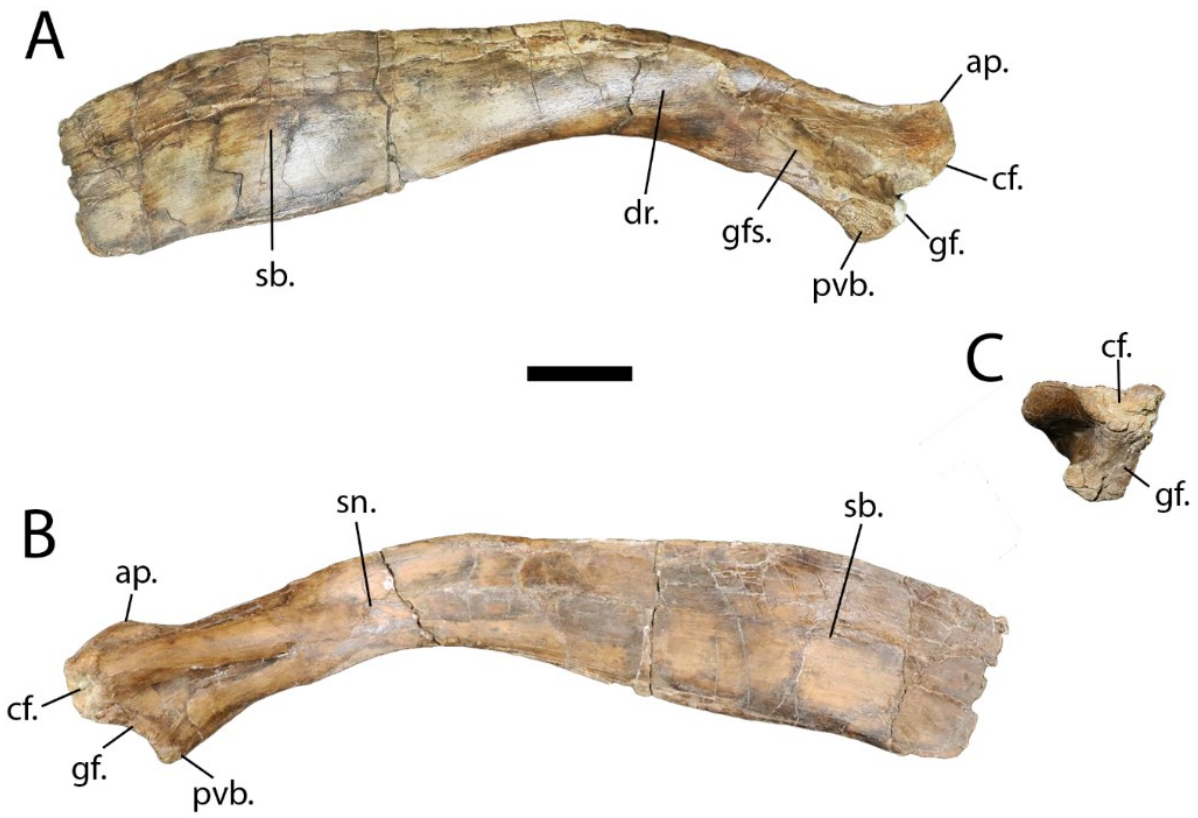

Figure 1. Right Scapula (TMP2015.044.0036) in (**A**) lateral; (**B**) medial; and (**C**) anterior views. Scale bar = 10cm. **Abbreviations: ap**, acromion process; **cf**, coracoid facet; **dr**, deltoid ridge; **gf**, glenoid facet; **gfs**, glenoid fossa; **pvb**, proximoventral buttress; **sb**, scapular blade; **sn**, scapular neck.

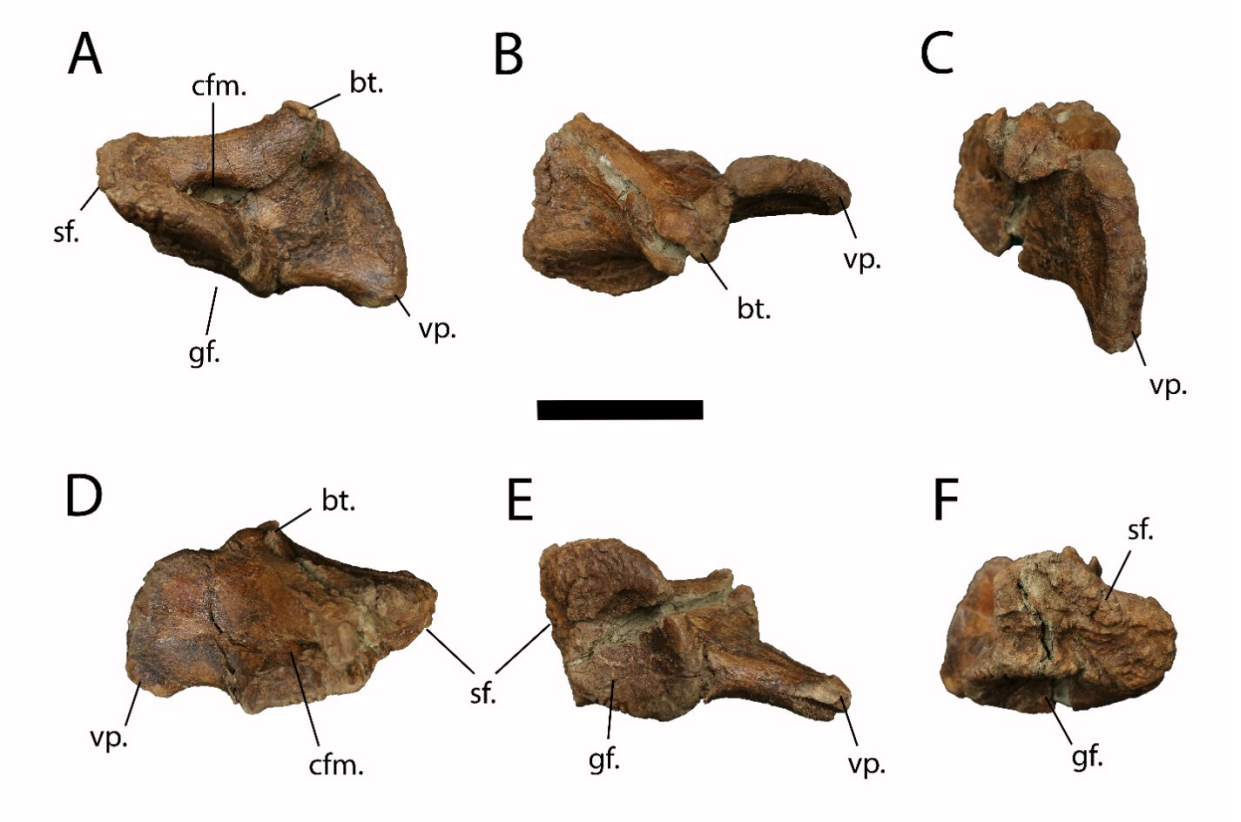

Figure 2. Right Coracoid (TMP2015.044.0036) in (**A**) lateral; (**B**) dorsal; (**C**) anterior; (**D**) medial; (**E**) ventral; and (**F**) caudal views. Scale bar = 10cm. **Abbreviations: bt**, bicipital tubercle; **cfm**, coracoid foramen; **gf**, glenoid facet; **sf**, scapular facet; **vp**, ventral process.

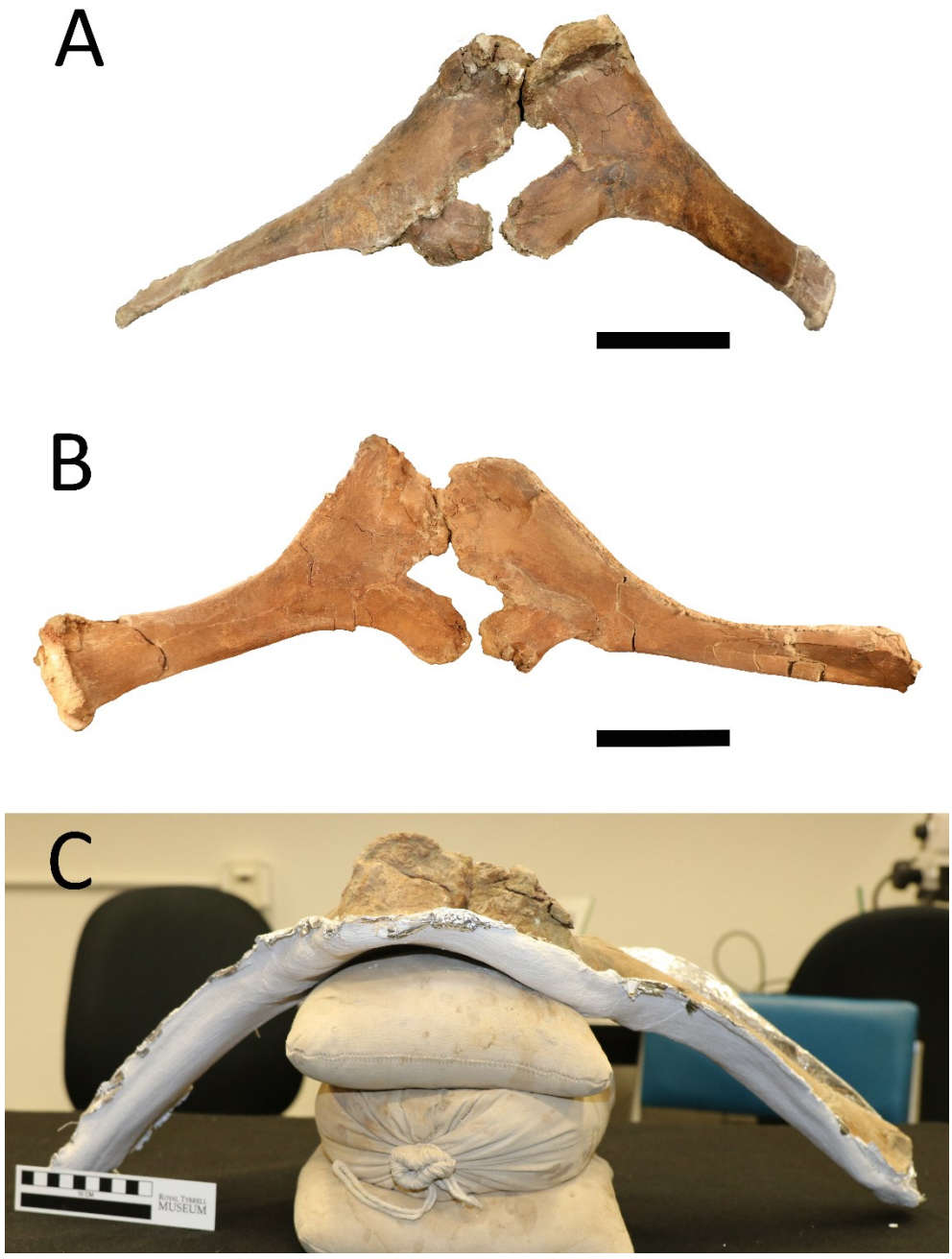

Figure 3. Sternal Plates (TMP2015.044.0036) in (**A**) ventral; (**B**) dorsal; and (**C**) anterior views. Scale bars = 10cm.

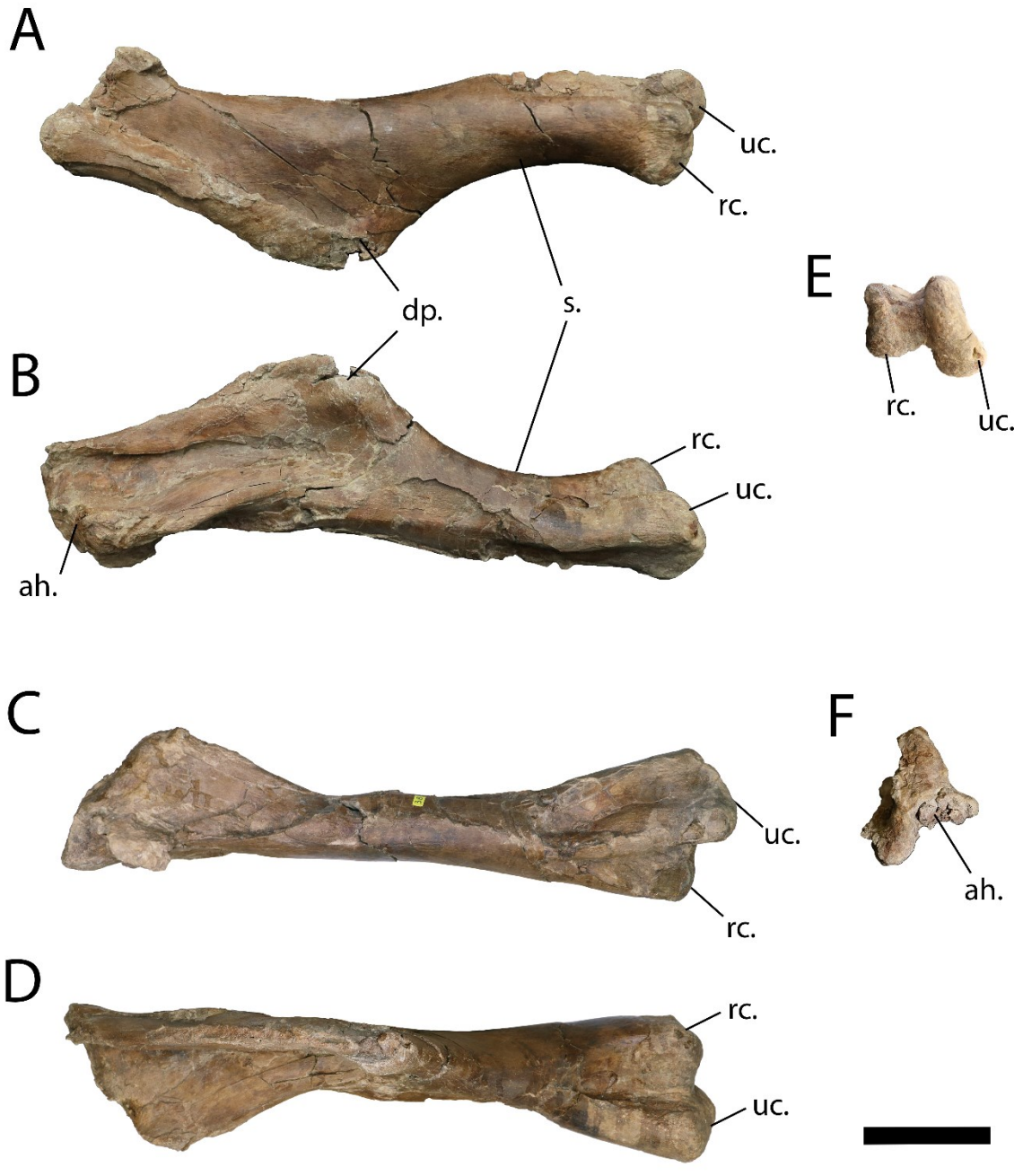

Figure 4. Left humerus (TMP2016.044.0036) in (A) lateral; (B) medial; (C) posterior; (D) anterior views; (E) distal; and (F) proximal views. Scale bar = 10cm. Abbreviations: ah, articular head; dp, deltopectoral crest; rc, radial condyle; s, humeral shaft; uc, ulnar condyle.

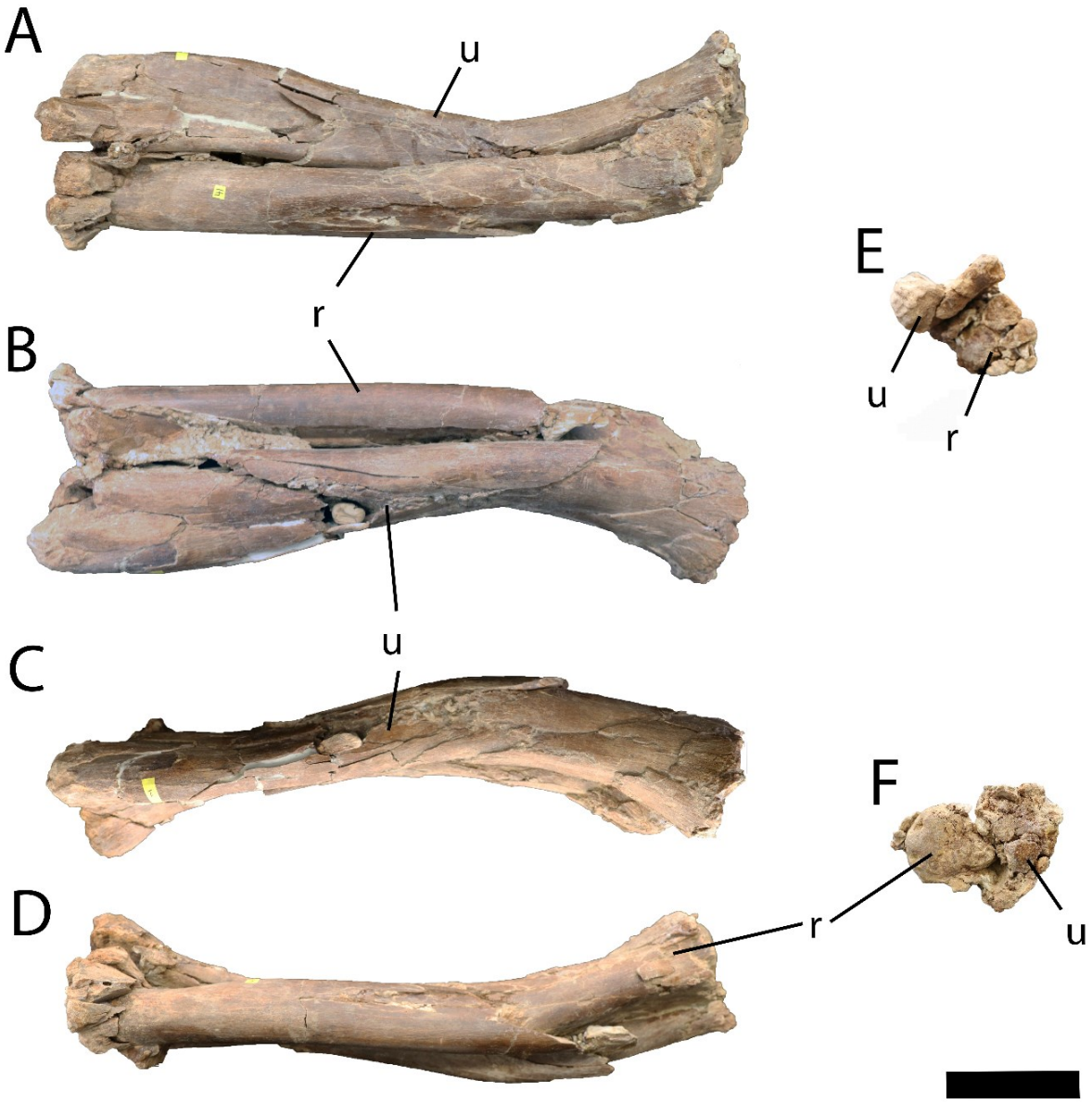

Figure 5. Left radius and ulna (TMP2016.044.0036) in (**A**) anterior; (**B**) posterior; (**C**) lateral, (**D**) medial); (**E**) proximal; and (**F**) distal views. Scale bar = 10cm. **Abbreviations: r**, radius; **u**, ulna.

Figure 6. Right radius (TMP2016.044.0036) in (**A**) anterior; (**B**) posterior; (**C**) medial; (**D**) lateral; (**E**) proximal; and (**F**) distal views. Scale bar = 10cm.

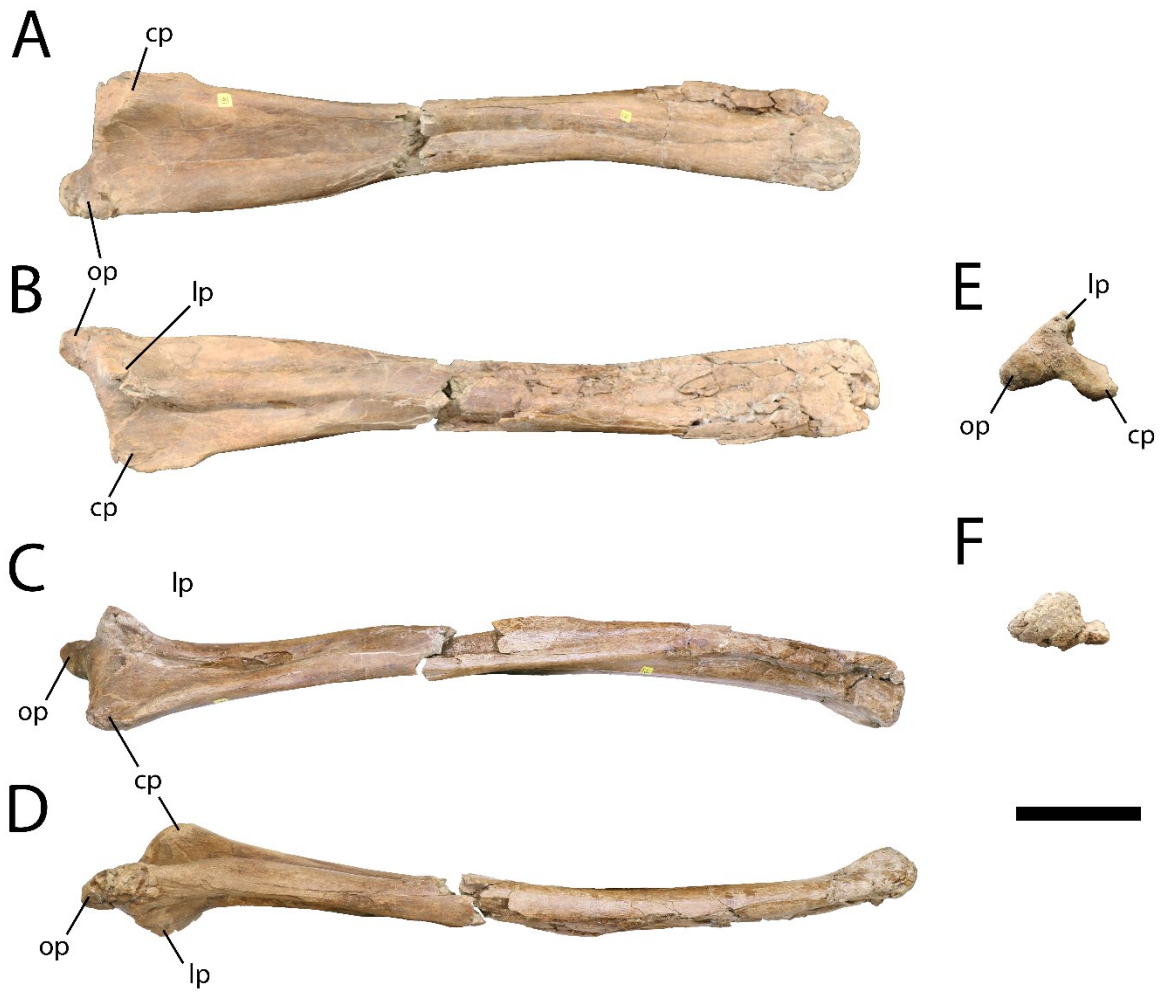

Figure 7. Right ulna (TMP2016.044.0036) in (**A**) lateral; (**B**) medial; (**C**) anterior; (**D**) posterior; (**E**) proximal; and (**F**) distal views. Scale bar = 10cm. **Abbreviations: cp**, cranial process; **lp**, lateral process; **op**, olecranon process.

Figure 8. metacarpal II (TMP2016.044.0036). Left (A-F) and Right (G-L) metacarpal II in (**A, G**) anterior; (**B, H**) medial; (**C, I**) posterior; (**D, J**) lateral; (**E, K**) proximal; and (**F, L**) distal views. Scale bar = 5 cm.

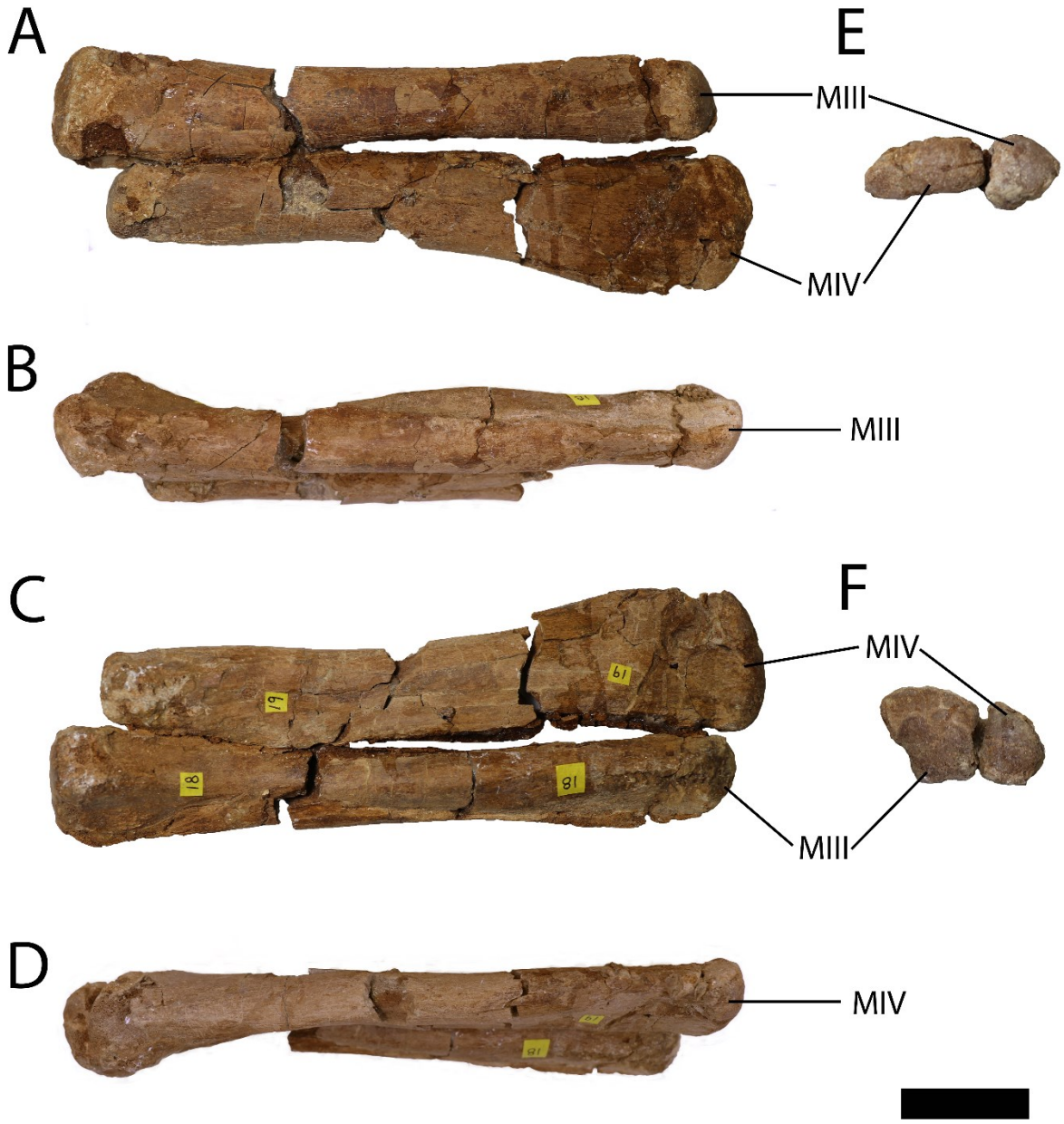

Figure 9. Left metacarpals III and IV (TMP2016.044.0036) in (A) anterior; (B) medial; (C) posterior; (D) lateral; (E) proximal; and (F) distal views. Scale bar = 5 cm. Abbreviations: MIII, metacarpal III; MIV, metacarpal IV.

Figure 10. Right metacarpal III (TMP2016.044.0036) in (**A**) anterior; (**B**) medial; (**C**) posterior; (**D**) lateral; (**E**) proximal; and (**F**) distal views. Scale bar = 5 cm.

Figure 11. Right metacarpal IV (TMP2016.044.0036) in (**A**) anterior; (**B**) medial; (**C**) posterior; (**D**) lateral; (**E**) proximal; and (**F**) distal views. Scale bar = 5 cm.

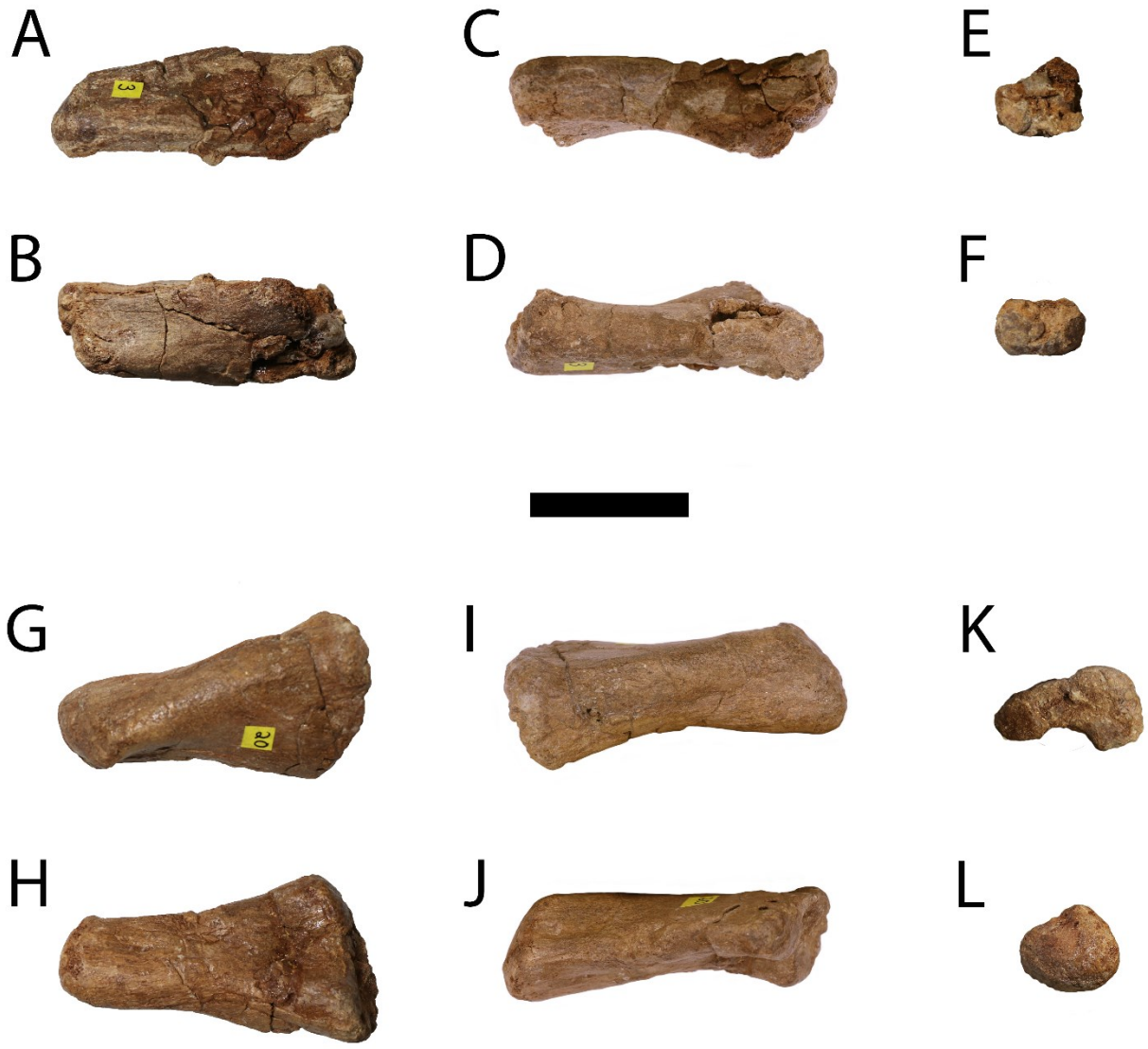

Figure 12. Metacarpal V (TMP2016.044.0036). Right (**A-F**) and Left (**G-L**) in (**A**, **G**) anterior; (**B**, **H**) posterior; (**C**, **I**) medial; (**D**, **J**) lateral; (**E, K**) proximal; and (**F, L**) distal views. Scale bar = 5 cm.

Figure 13. Phalanx I of digit II (TMP2016.044.0036). Right (**A-D**) and Left (**E-H**) in (**A**, **E**) medial; (**B**, **F**) lateral; (**C**, **G**) proximal; and (**D**, **H**) distal views. Scale bar = 5 cm.

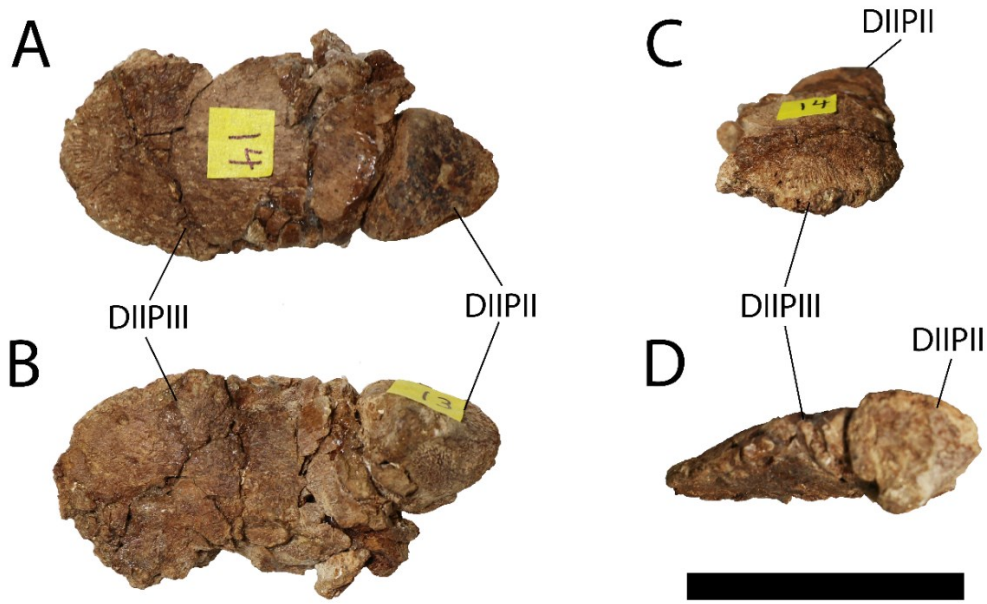

Figure 14. Right digit II phalanx II and III (TMP2016.044.0036) in (**A**) anterior; (B) posterior; (**C**) distal; and (**D**) proximo-lateral views. Scale bar = 5 cm. **Abbreviations: DIIPIII**, digit II phalanx II; **DIIPIII**, digit II phalanx III.

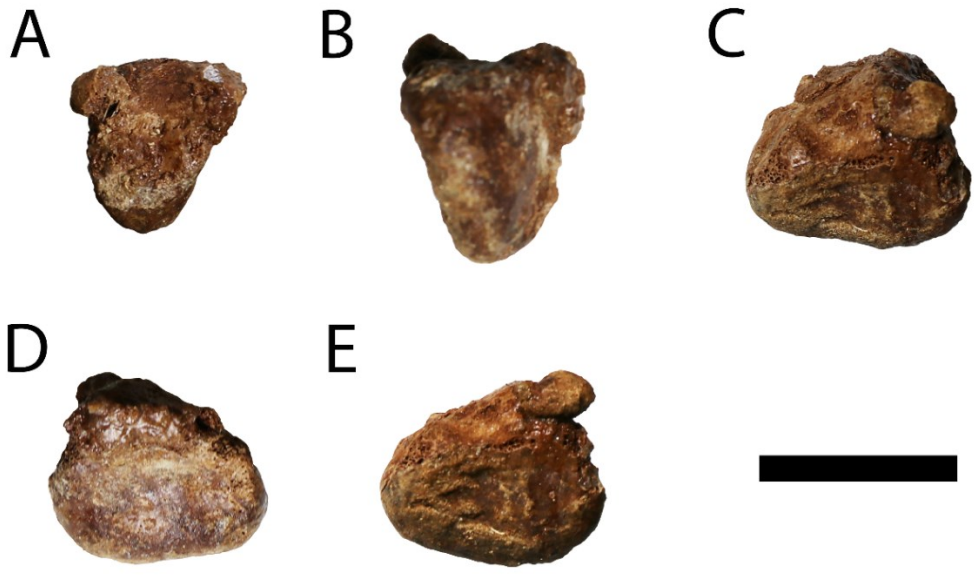

Figure 15. Left digit II phalanx II (TMP2016.044.0036) in (**A**) anterior; (**B**) posterior; (**C**) antero-distal; (**D**) proximal; and (**E**) distal views. Scale bar = 2.5 cm.

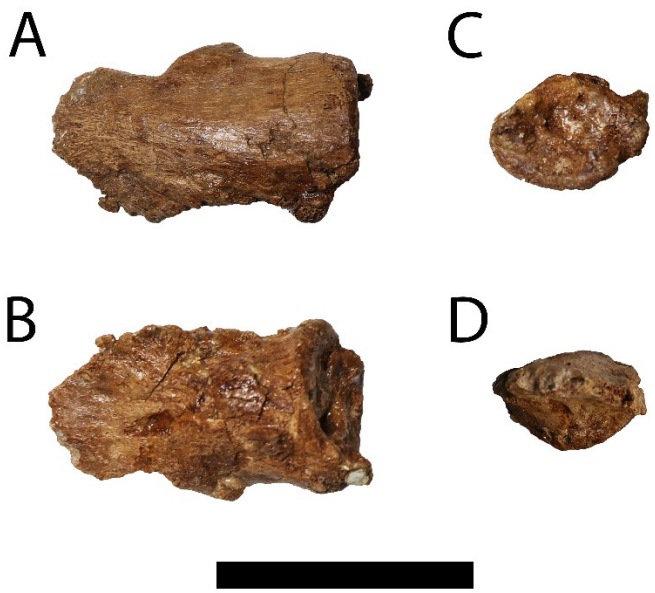

Figure 16. Left digit II phalanx III (TMP2016.044.0036) in (**A**) anterior; (**B**) posterior; (**C**) proximal; and (**D**) distal views. Scale bar = 5 cm.

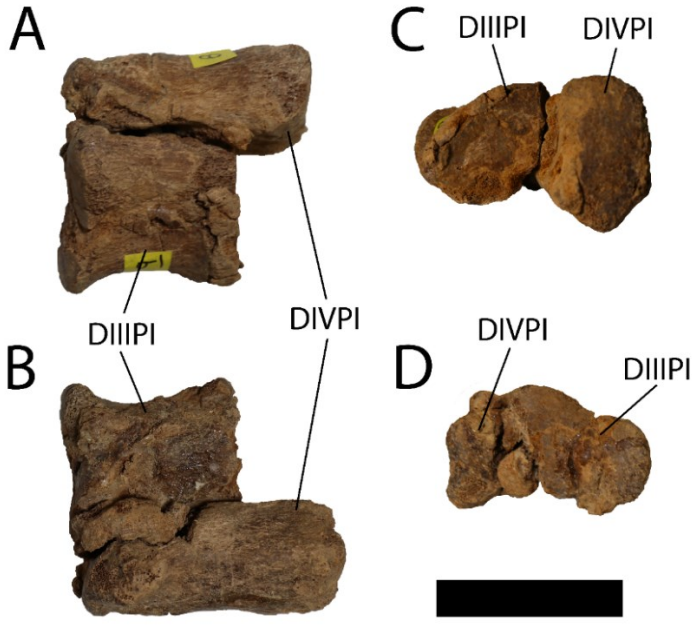

Figure 17. Right digit III phalanx I and digit IV phalanx I (TMP2016.044.0036) in (**A**) anterior; (**B**) posterior; (**C**) proximal; and (**D**) distal views. Scale bar = 5 cm. **Abbreviations: DIIIPI**, digit III phalanx I; **DIVPI**, digit IV phalanx I.

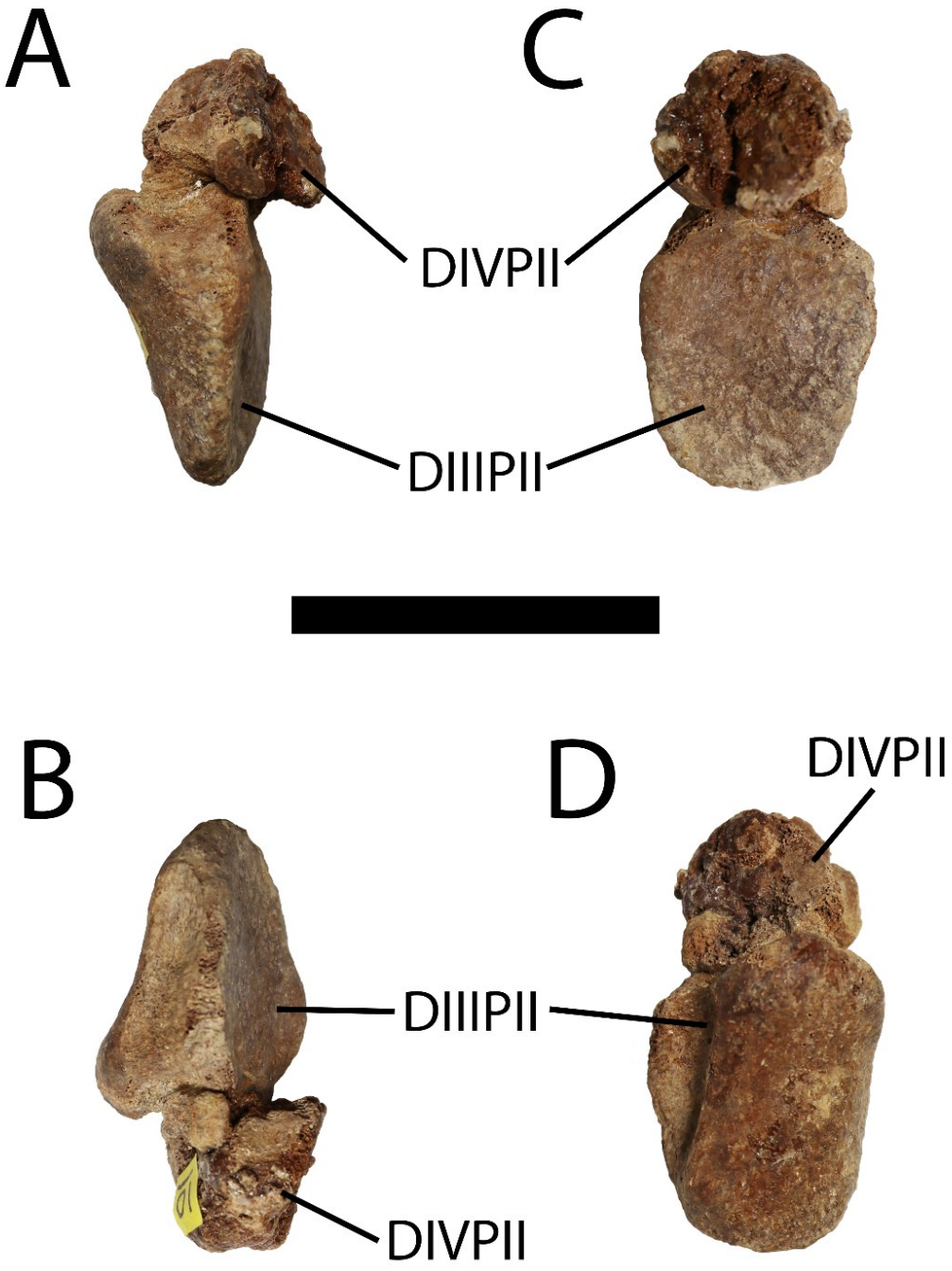

Figure 18. Right digit III phalanx II and digit IV phalanx II (TMP2016.044.0036) in (**A**) anterior; (**B**) posterior; (**C**) proximal; and (**D**) distal views. Scale bar = 5 cm. **Abbreviations: DIIIPII**, digit III phalanx II; **DIVPII**, digit IV phalanx II.

Figure 19. Left digit III phalanx I (TMP2016.044.0036) in (**A**) anterior; (**B**) posterior; (**C**) proximal; and (**D**) distal views. SCale bar = 5 cm.

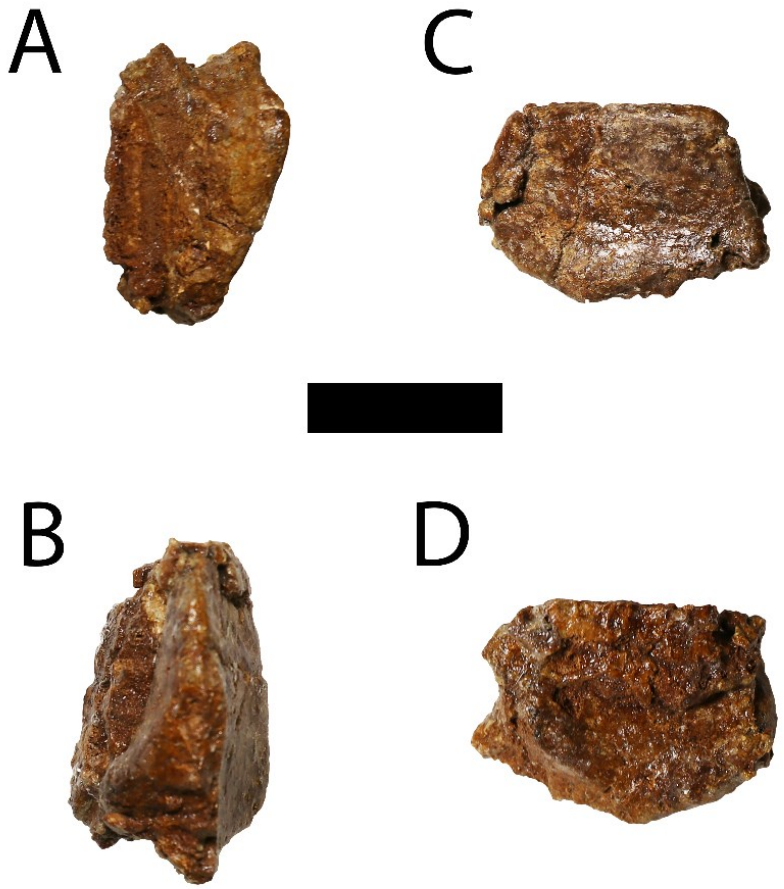

Figure 20. Left digit III phalanx II (TMP2016.044.0036) in (**A**) anterior; (**B**) posterior; (**C**) proximal; and (**D**) distal views. Scale bar = 2.5 cm.

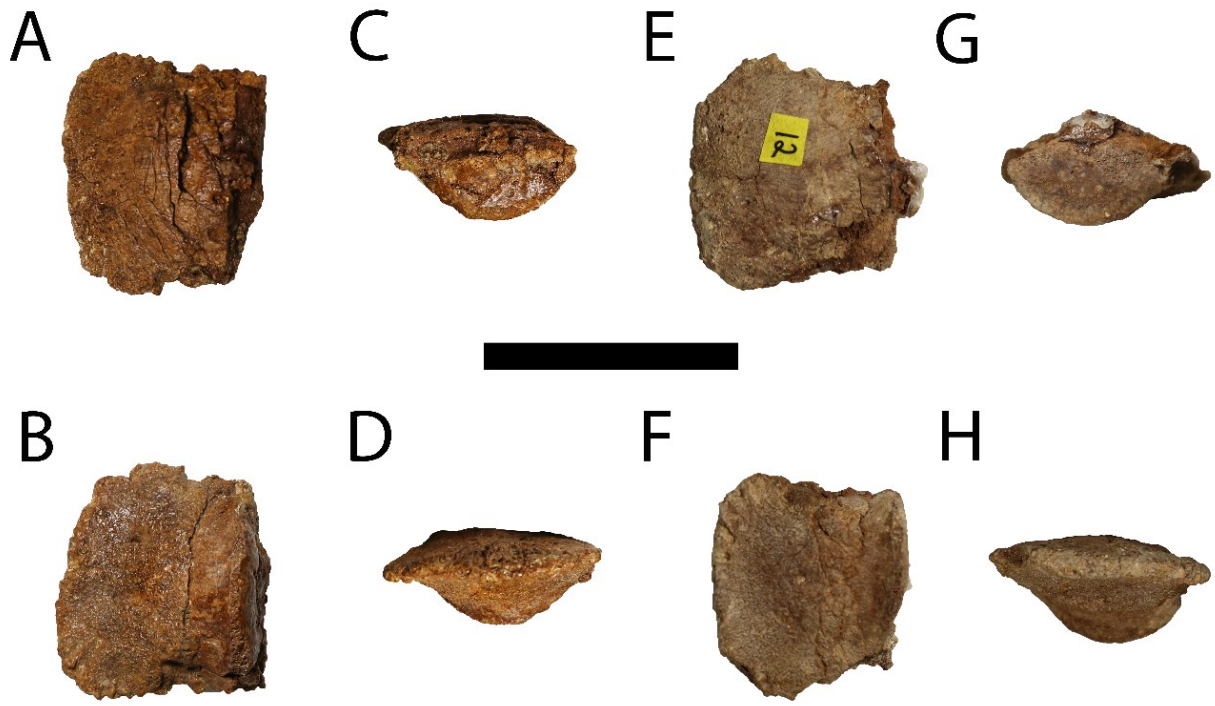

Figure 21. Digit III phalanx III (TMP2016.044.0036). Left (**A-D**) and right (**E-H**) in (**A, E**) anterior; (**B, F**) poterior; (**C, G**) proximal; and (**D, H**) distal views. Scale bar = 5 cm.

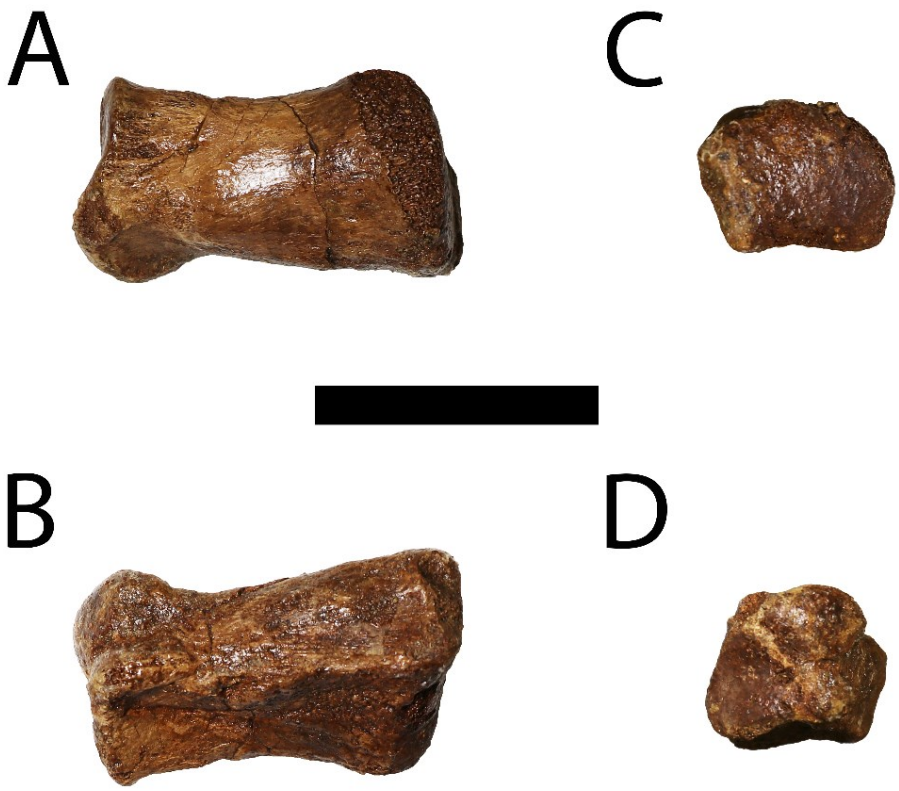

Figure 22. Left digit IV phalanx I (TMP2016.044.0036) in (**A**) anterior; (**B**) postero-lateral; (**C**) proximal; and (**D**) distal views. Scale bar = 5 cm.

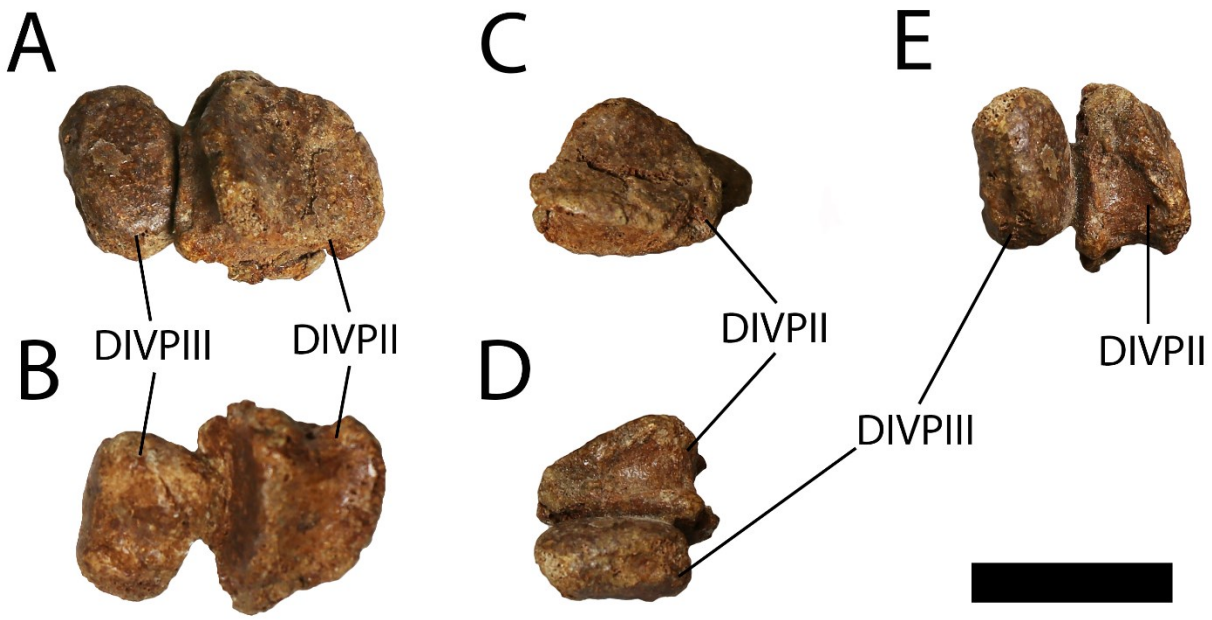

Figure 23. Left digit IV phalanx II and III (TMP2016.044.0036) in (**A**) anterior; (**B**) posterior; (**C**) proximal; (**D**) distal; and (**E**) anterolateral views. Scale bar = 2.5 cm. **Abbreviations: DIVPII**, digit IV phalanx II; **DIVPIII**, digit IV phalanx III.

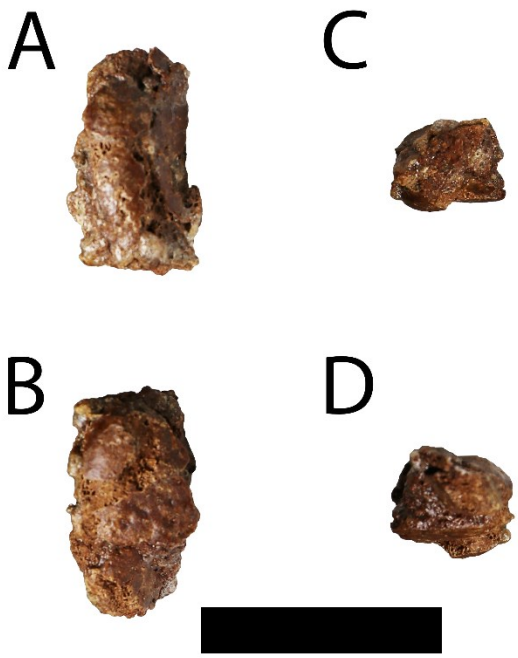

Figure 24. Right digit IV phalanx III (TMP2016.044.0036) in (**A**) anterior; (**B**) posterior; (**C**) medial; and (**D**) lateral views. Scale bar = 2.5 cm.

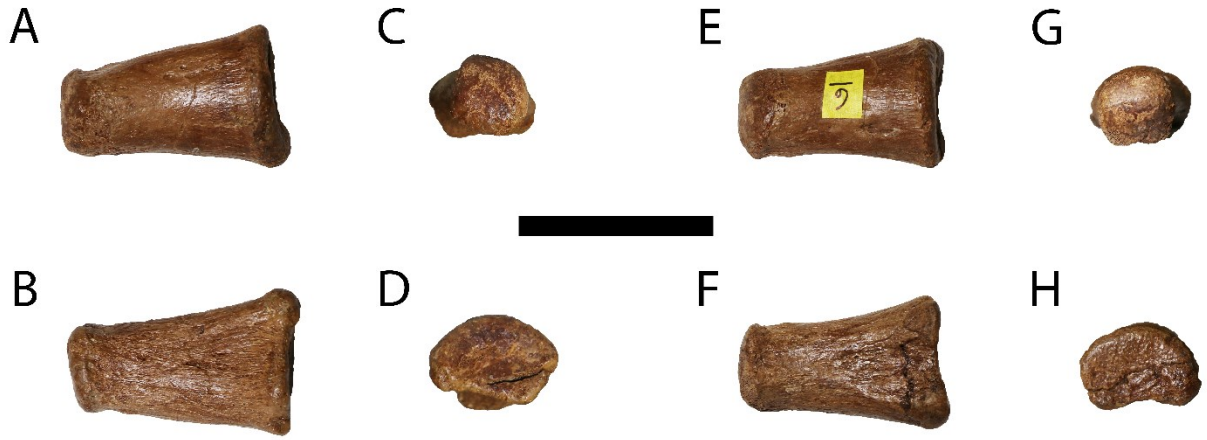

Figure 25. Digit V phalanx I (TMP2016.044.0036). Left (**A-D**) and Right (**E-H**) in (**A, E**) anterior; (**B, F**) posterior; (**C, G**) distal; and (**D, H**) proximal views. Scale bar = 5 cm

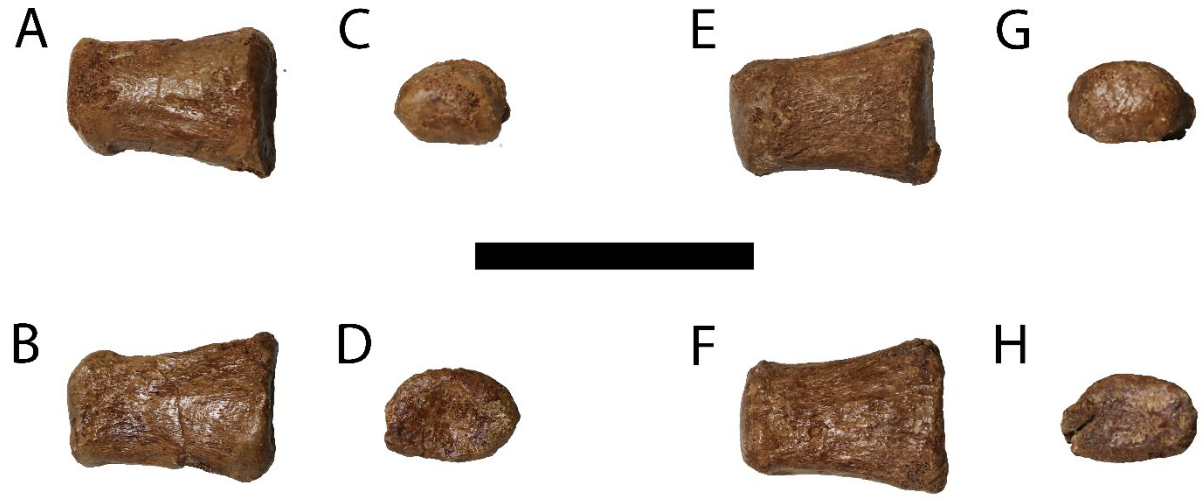

Figure 26. Digit V phalanx II (TMP2016.044.0036). Left (**A-D**) and right (**E-H**) in (**A, E**) anterior; (**B, F**) posterior; (**C, G**) distal; and (**D, H**) proximal views. Scale bar = 5 cm.

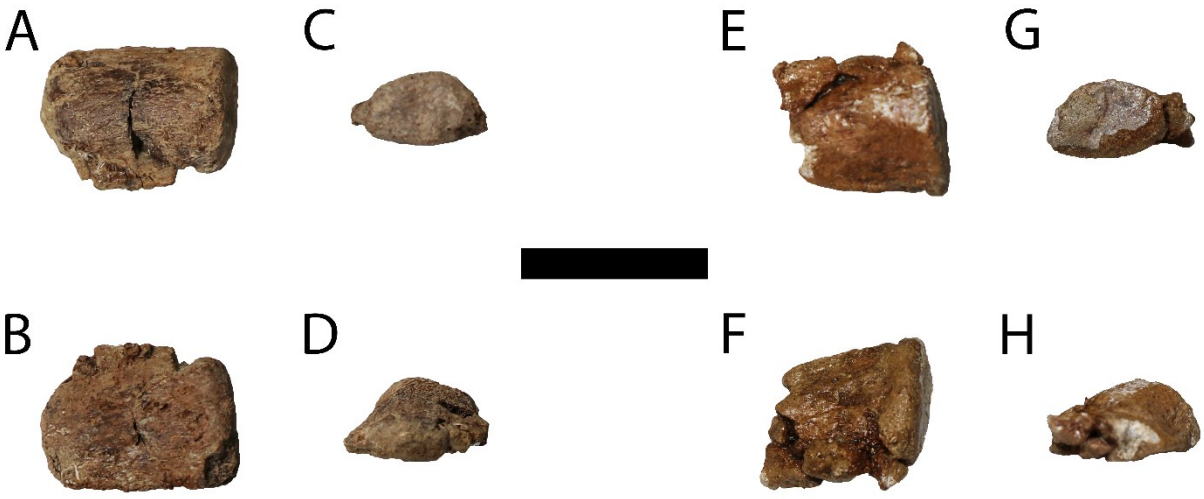

Figure 27. Digit V phalanx III (TMP2016.044.0036). Left (**A-D**) and right (**E-H**) in (**A, E**) anterior; (**B, F**) posterior; (**C, G**) proximal; and (**D, H**) distal views. Scale bar = 2.5 cm.

Figure 28. Manus (TMP2016.044.0036). Right (**A**) and left (**B**) in anterior views. Scale bar = 10 cm. **Abbreviations: DII**, digit II; **DIII**, digit III; **DIV**, digit IV; **DV**, digit V.

Figure 29. Manus (TMP2016.044.0036). Right (**A**) and left (**B**) in posterior views. Scale bar = 10 cm. **Abbreviations: DII**, digit II; **DIII**, digit III; **DIV**, digit IV; **DV**, digit V.

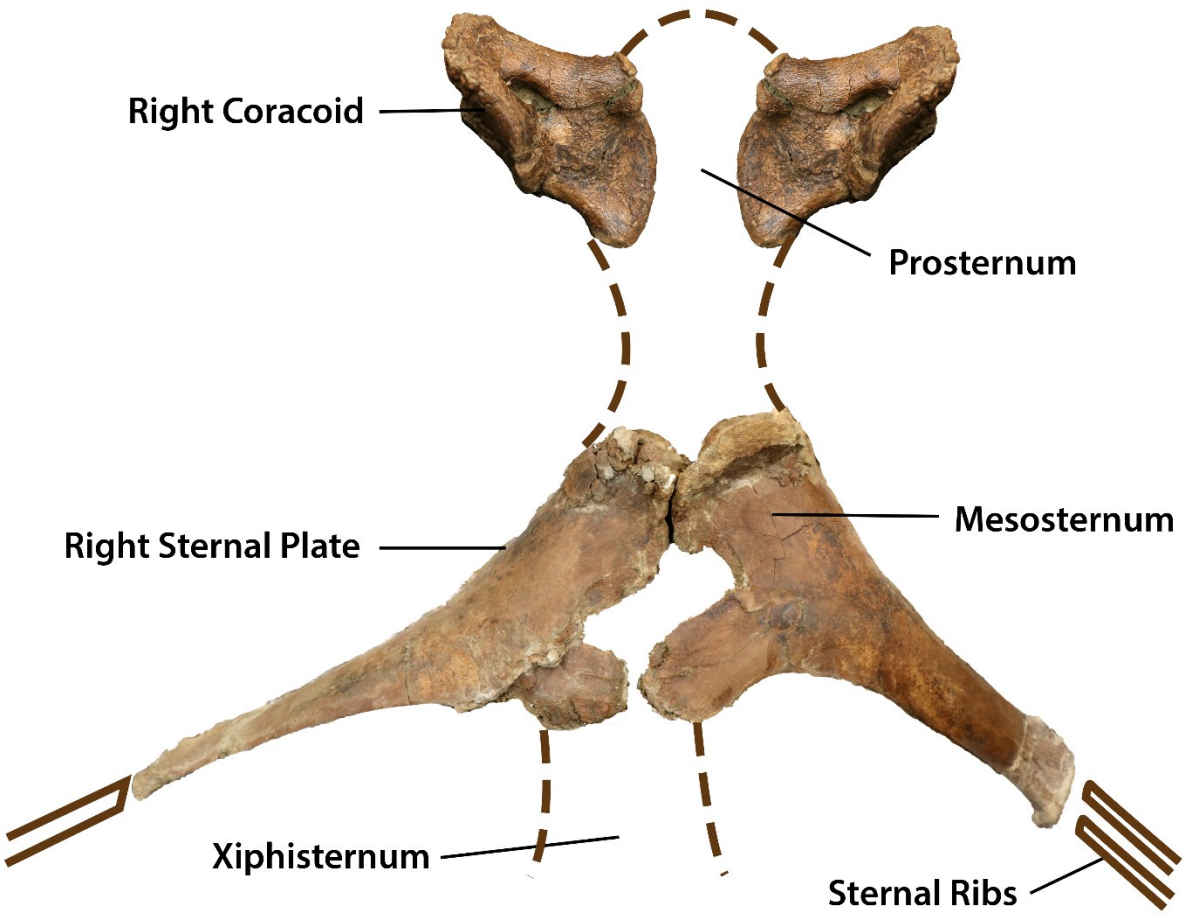

Figure 30. Proposed sternum reconstruction for TMP2016.044.0036. Based especially on crocodilian sternal morphology.

2.5 Measurements of the Postcranial Skeleton of TMP2015.044.0036

Table 1A. Pectoral Girdle Skeleton Measurements in Millimeters

Measurement	Right	Left
Scapula		
Length	845.20	
Width at constriction	97.43	
Width at distal end	157.00	
Width at coracoid	15.11	
Glenoid length	96.34	
Coracoid		
Glenoid width	96.77	
Length	177.70	
Width of ventral process	20.31	
height of ventral process	92.48	

Table 1B. Sternal Plate Measurements in Millimeters

Measurement	Right	Left
Sternal plate		
Main plate length	152.58	181.27
Main plate width (anterior)	84.86	79.58
Main plate width (posterior)	46.46	48.83
Anterior plate thickness	56.22	60.32
Posterolateral process length	229.44	211.76
Posterolateral maximum width	72.57	63.85
Posterolateral process minimum width	42.90	43.63
Distal head width	49.67*	71.31

Table 1C. Forelimb Skeleton Measurements in Millimeters

Measurement	Right	Left
Humerus		
Length		524.12
Minimum shaft circumference		216.44
Deltopectoral crest length		265.00
Deltopectoral crest width		25.48
Proximal head width		145.29
Mediolateral width of condyle		32.70
Distal head width		108.94
Minimum shaft width (craniocaudal)		70.46
Ulna		
Length	474.80*	633.16
Prearticular length	63.33*	113.45
Minimum circumference	171.50*	152.17
Minimum shaft width (mediolateral)	35.49	53.17
Minimum shaft width (craniocaudal)	43.72*	30.99*
Mid-shaft width (mediolateral)	55.44	55.50
Mid-shaft width (craniocaudal)	51.60	40.39
Radius		
Length	448.56*	546.88*
Mid-shaft width (mediolateral)	27.85*	49.25
Mid-shaft width (craniocaudal)	51.20	31.49
Proximal head width (mediolateral)	83.26*	68.12
Proximal head width (craniocaudal)	75.00*	67.98
Distal head width (mediolateral)	62.19	67.56
Distal head width (craniocaudal)	65.03	35.37*
Minimum circumference	138.00*	130.66

Table 1D. Manus Skeleton Measurements in Millimeters

Measurement	Right	Left
Metacarpal II		
Length	229.13*	212.03
Minimum width (mediolateral)	20.81*	24.79
Minumim width (craniocaudal)	25.86*	22.45
Proximal head width	36.56	42.49
Distal Head width	19.66*	30.38
Metacarpal III		
Length	258.66	259.15
Minimum width (mediolateral)	33.84	28.14
Minumim width (craniocaudal)	23.85*	25.25
Proximal head width	41.71	29.22
Distal Head width	52.37	43.48
Metacarpal IV		
Length	244.80	251.23
Minimum width (mediolateral)	35.13	32.95
Minumim width (craniocaudal)	22.23	16.93*
Proximal head width	54.28	53.95
Distal Head width	45.07	32.24
Metacarpal V		
Length	97.40	96.64
Minimum width (mediolateral)	28.18	28.28
Minumim width (craniocaudal)	19.30	22.30
Proximal head width	32.47*	52.50
Distal Head width	33.49	26.69
First phalanx of digit II		
Length	80.91	80.65
Minimum width (mediolateral)	27.42	26.82
Minumim width (craniocaudal)	16.19	18.77
Proximal head width	34.37	32.67
Distal Head width	37.72	37.29
Second phalanx of digit II		
Length	20.58	27.14
width (mediolateral)	24.37	26.86
width (craniocaudal)	22.50	23.72
Proximal head width	25.27	26.76
Distal Head width	24.72	26.38
Third (distal) phalanx of digit II		
Length	59.43	60.60

Minimum width (mediolateral)	32.24*	28.50
Maximum width (craniocaudal)	19.26*	24.96
Proximal head width	35.27	33.44
Distal Head width	38.33*	33.99*
First phalanx of digit III		
Length	44.06	44.01
Minimum width (mediolateral)	39.43*	49.75
Minumim width (craniocaudal)	23.80	25.03
Proximal head width	43.36	49.40
Distal Head width	48.53	50.99
Second phalanx of digit III		
Length	22.28	23.73
width (mediolateral)	40.19	37.70
Maximum width (craniocaudal)	30.79	28.94
Proximal head width	41.87	37.96*
Distal Head width	42.13	42.59
Third (distal) phalanx of digit III		
Length	40.56	38.22
Minimum width (mediolateral)	42.29	40.06
Maximum width (craniocaudal)	22.56	21.79
Proximal head width	36.56	40.73
Distal Head width	47.90	44.71
First phalanx of digit IV		
Length	67.31	65.21
Minimum width (mediolateral)	22.00*	23.77
Minumim width (craniocaudal)	31.98	25.25
Proximal head width	28.96	33.54
Distal Head width	28.36	29.02
Second phalanx of digit IV		
Length	17.50	14.51
Minimum width (mediolateral)	19.85*	17.87
Minumim width (craniocaudal)	19.08	22.11
Proximal head width	20.60	21.35
Distal Head width	21.85	19.51
Third (distal) phalanx of digit IV		
Length	12.85*	15.84
Minimum width (mediolateral)	24.36*	21.06
Minumim width (craniocaudal)	9.95*	10.25
Proximal head width	23.31*	21.80
Distal Head width	24.18*	21.10
First phalanx of digit V		

Length	51.81	54.36
Minimum width (mediolateral)	22.11	22.70
Minumim width (craniocaudal)	17.76	17.78
Proximal head width	35.21	34.81
Distal Head width	21.13	21.76
Second phalanx of digit V		
Length	36.72	36.55
Minimum width (mediolateral)	19.42	19.63
Minumim width (craniocaudal)	15.00	12.26
Proximal head width	27.57	26.48
Distal Head width	20.29	20.33
Third (distal) phalanx of digit V		
Length	21.29*	26.77
Minimum width (mediolateral)	17.75*	17.32
Minumim width (craniocaudal)	7.08*	7.42
Proximal head width	21.82*	17.28
Distal Head width	16.96*	19.63

Chapter 3. Muscular reconstruction of the forelimb and shoulder girdle of a lambeosaurine hadrosaurid

3.1 Introduction

Reconstructing the musculature of fossil vertebrates is difficult. The soft tissues of large animals are typically lost during the process of fossilization, so other steps must be taken to reconstruct the most likely placement of muscles in extinct vertebrates. Muscle scarring, roughened surfaces on the bone for muscle anchoring, can indicate areas of muscle and tendon attachment, however only some muscles leave scars and though muscle scarring provides an indication of the presence of a muscle, it cannot provide information on which muscle it represents, its orientation, and what function it may provide. For this information I rely on the extant phylogenetic bracket, observing the most closely related animals possible, and assuming the muscles of the closest living relatives are mostly homologous to those of their ancient relatives. Theropod dinosaurs have direct living descendants in birds, and studies of theropod musculature are common (e.g., Nicholls and Russell 1985; Carrano and Hutchinson 2002; Jasinoski et al. 2006; Snively and Russell 2007; Hutchinson and Allen 2009; Hutchinson et al. 2011; Burch 2014; Burch 2017; Meso et al. 2021; Rhodes et al. 2020; Smith 2021). Ornithischian dinosaurs did not survive past the end-Cretaceous extinction, and therefore have no living representatives. Birds remain the most closely related living group and are heavily relied upon for muscular inferences in both ornithischian and saurischian dinosaurs, as are crocodilians who are less closely related (e.g., Nicholls and Russell 1985; Jenkins 1993; Paul and Christiansen 2000; Jasinoski et al. 2006; Carpenter and Wilson 2008). However, their mode of locomotion is fundamentally different from most ornithischians which, for the most part, were

large, quadrupedal animals and not gracile or bipedal like most birds. Those ornithischians that were bipedal were not especially bird or crocodilian-like in their posture and limb kinematics, birds holding the femur in a near-horizontal position and employing a knee-driven gait (Baumel et al. 1998), while crocodilians typically possess a sprawling gait but occasionally can also move with a semi-erect hindlimb gait (Meers 2003; Cong et al. 1998). For this reason, coupled with the fact that ornithischian dinosaurs tend to receive less research attention than theropods, muscular reconstructions for representatives of Ornithischia are comparatively few in the scientific literature (e.g., Dilkes 2000; Carpenter and Wilson 2008; Maidment and Barrett 2011; Bates et al. 2012; Maidment and Barrett 2012; Maidment et al. 2014a; Maidment et al. 2014b).

Hadrosaurids were abundant in the Campanian-Maastrichtian ecosystems of the northern continents, and indeed their remains are the most common terrestrial vertebrate fossils in the Cretaceous record (Cullen and Evans 2016), yet the forelimb muscular anatomy and kinematics of these animals remain especially poorly understood. Given that carefully assessed forelimb musculature can inform on the behavioural ecology of extinct groups such as migration (Calmaestra and Moreno 2005), prehension (Böhmer et al. 2019), and physical prowess (Grand 1997), reconstructing the forelimb musculature of hadrosaurid dinosaurs is an important step in understanding ecological interactions in Late Cretaceous faunal communities. In any case, reconstructing muscular anatomy is a prerequisite for drawing further inferences about muscle function, and potential muscle performance during various activities. Previous muscular reconstructions of the ornithopod forelimb has been done on the iguanodontids *Camptosaurus* (Carpenter and Wilson 2008) and *Iguanodon atherfieldensis* (Norman 1986), and the hadrosaurids *Edmontosaurus annectens* (Lull and Wright 1942) and *Maiasaura peeblesorum* (Dilkes 2000). Currently, the general consensus is that all hadrosaurids were mostly facultatively

bipedal (Carrano 2001; Horner et al. 2004; Evans 2007; Sellers et al. 2009; Maidment et al. 2014a). This chapter aims to reconstruct the musculature associated with the forelimb, shoulder girdle, and sternum of a newly recovered, unidentified lambeosaurine hadrosaurid (TMP2015.044.00360) with remarkably preserved forelimbs, providing a good representative specimen for Lambeosaurinae. I will also discuss the biomechanical implications of the inferred musculature and compare it with reconstructions for other known representatives of Hadrosauridae.

3.2 Methods

To reconstruct the musculature of TMP2015.044.0036, observations of muscle scarring on the fossil bones were used as a primary indication of muscle attachment sites. Representative living archosaurs, namely a common raven (*Corvus corax*, adult), a savannah monitor lizard (*Varanus exanthematicus*, adult) and a caiman (*Caiman crocodilus*, 9 kg adult) were dissected to provide comparative information on muscle origin and insertion sites as well as their functional relationships with the skeleton. As lizards are an outgroup to birds and crocodilians, a savannah monitor lizard (*Varanus exanthematicus*) was also dissected. Literature on crocodilian (Meers 2003; Cong et al. 1998; Klinkhamer et al. 2017) and bird (Howell 1937; Hudson et al. 1972; Baumel et al. 1998) forelimbs was also heavily consulted, and the work of Dilkes (2000), Jasinoski et al. (2006), and Burch (2014) was utilized to interpret muscle origin and insertion sites based on their phylogenetic-bracketing-based reconstruction of the forelimb musculature of *Maiasaura peeblesorum.* Musculature nomenclature used in this chapter follows Romer (1922, 1944). Descriptions of musculature are written assuming a quadrupedal animal in the resting phase of its step cycle. Therefore, the vertebral column is dorsal to the body and the humerus is

oriented perpendicular to the trunk of the body, sitting downward in the glenoid facet. This assumption is simply for the sake of standardization since it is unknown where TMP2015.044.0036 sits on the spectrum of bipedalism to quadrupedalism. Since it is not possibly to reasonably estimate the cross sectional area, mass, or potential force generated by these muscles, muscle descriptions here only reconstruct the anatomical location and extent of muscle origin and insertion sites, as well as estimating the function of each muscle.

3.3 Myological Description

3.3.1 Axial Muscles

M. trapezius

In crocodilians and lepidosaurs, M. trapezius (Fig. 31) is a large superficial muscle that originates on the thoracodorsal facia and can appear continuous with the origin of M. latissimus dorsi caudally (Meers 2003; Jasinoski et al. 2006; Klinkhamer et al. 2017). In these taxa, M. trapezius inserts on the anterior margin of the acromion process of the scapula where it functions in protraction of the scapula (Meers 2003; Jasinoski et al. 2006). Birds lack both M. trapezius and M. levator scapulae (Howell 1937; Hudson et al. 1972; Baumel et al. 1998), making the presence of these muscles equivocal in hadrosaurids on strict phylogenetic bracketing grounds. The avian scapula is comparatively thin, and is largely immobile due to attachment to the coracoid which articulates with an ossified sternum in addition to bracing by the furcula (Howell 1937; Hudson et al. 1972; Baumel et al. 1998). This provides a sturdy pectoral girdle for which the presence of M. rhomboideus and M. dorsalis scapulae can effectively stabilize the scapula, making M. trapezius and M. levator scapulae functionally unnecessary in birds (Howell 1937;

Jasinoski et al. 2006). The morphology of the scapula is broadly similar in at least eumaniraptoran theropods, and there is no scarring on the scapula to indicate the presence of M. levator scapulae or M. trapezius (Jasinoski et al. 2006), likely indicating an absence of these muscles. However, many eumaniraptorans lack an ossified sternum, making the absence of M. trapezius and M. levator scapulae less plausible in this group. Nonetheless, at least some theropod dinosaurs do show anterodorsally oriented muscle scarring on the proximal scapular blade along the anterior margin consistent with the location of these muscles in crocodilians and lepidosaurs (Currie and Zhao 1993), and TMP2015.044.0036 possesses similar scarring on the anterior dorsal margin of the scapula, so it can be assumed that M. trapezius and M. levator scapulae were present in this individual. This scarring is, of course, consistently absent in birds (Howell 1937; Hudson et al. 1972; Baumel et al. 1998).

In lambeosaurines, M trapezius likely inserted on the dorsal margin of the scapular blade (Fig. 31), as evidenced by muscle scarring on the anterior dorsal margin of the scapula of TMP2015.044.0036. This is corroborated by the position of the scapula in crocodilians, in which the anterior portion of the scapula would be held roughly in the same position relative to the trunk musculature and sternum as the equivalent portion of the scapula in hadrosaurids. Since the origin of M. trapezius would presumably have lain on the medial dorsal fascia as in crocodilians, or on the dorsal vertebrae as in *Varanus exanthematicus*, then M. trapezius would function in pulling the scapula dorsally and medially in TMP2015.044.0036.

M. levator scapulae

In crocodilians and most tetrapods, M. levator scapulae (Fig. 31) is a deep muscle that lies under M. trapezius. Birds seem not to possess M. levator scapulae, and claims to the contrary

may be explained by the fact that M. serratus is easily mistaken for M. levator scapulae due to their similar locations of insertion along the cervical vertebrae (Howell 1937; Hudson et al. 1972; Baumel et al. 1998). In crocodilians, M. levator scapulae is bifurcated into two heads: M. levator scapulae superficialis and M. levator scapulae profundus (Meers 2003; Cong et al. 1998; Jasinoski et al. 2006). M. levator scapulae superficialis originates from the cervical ribs, increases in thickness ventrally, and inserts along the anteromedial margin of the scapular blade (Meers 2003; Cong et al. 1998; Jasinoski et al. 2006). M. levator scapulae profundus originates below M. levator scapulae superficilais, is comparatively smaller, and inserts on the dorsal coracoid and ventral scapula anteromedially. In *Varanus*, M. levator scapulae has a similar arrangement, but the ventral portion inserts on the dorsal surface of the clavicle and on the anterior margin of the scapula. In these groups, M. levator scapulae functions to protract the scapula and coracoid (Meers 2003; Cong et al. 1998; Jasinoski et al. 2006; Klinkhamer et al. 2017).

It has been argued that since there is no osteological correlate that specifically indicates the presence of M. levator scapulae among eumaniraptoran theropods, this muscle might have been absent in these animals (Jasinoski et al. 2006). Similar to the case of M. trapezius, the scapula in eumaniraptorans lies almost directly lateral to the vertebral column. In this position, M. rhomboideus could function in protraction of the scapula, making the presence of M. levator scapulae unnecessary (Jasinoski et al. 2006; Howell 1937). However, at least some theropods (some ceratosaurs, tetanurans, and tyrannosaurids) do show a shallow trough with muscle scarring on the medial surface of the proximal two-thirds of the scapula that would be consistent with the presence of M. levator scapulae (Currie and Zhao 1993; Jasinoski et al. 2006; Burch 2014). This suggests that M. levator scapulae was present in at least some dinosaur lineages but

may have been lost convergently or homologously with birds. TMP2015.044.0036 does possess similar scarring on the proximal scapula medially, so although the scapula is oriented somewhat parallel to the vertebral column in the models presented here, it is likely that M. levator scapulae was present in at least some lambeosaurine dinosaurs, even though its functional role would be similar to that of M. rhomboideus. However, the absence of this muscle in birds makes it equivocal in hadrosuarids.

Though TMP2015.044.0036 does possess muscle scarring on the anterior dorsal scapula, ventral scapula, and dorsal coracoid, these areas of the ventral scapula and dorsal coracoid have been assigned to musculature of the brachium, namely M. scapulohumeralis posterior and M. supracoracoideus, respectively (see below). As both parts of M. levator scapulae are present in crocodilians and in *Caiman* and *Varanus*, it is likely that both parts of this muscle were present in hadrosaurids (Fig. 31). However, since their trajectories in TMP2015.044.0036 would have been functionally the same, we will discuss pars superficialis and pars profundus together as one muscle. The muscular arrangement seen in hadrosaurids would almost certainly be consistent with modern tetrapods indicating that M. levator scapulae would originate on the anterior cervical vertebrae and insert on the anterior dorsal margin of the scapula, corroborated by light muscle scarring on TMP2015.044.0036 that would be consistent with this arrangement. Hadrosaurids do not possess clavicles, and since a clavicular insertion seems not to be widespread among reptilia, it is possible that the insertion of M. levator scapulae may have extended onto the sternum, but there is no direct evidence to support this. This muscle would function in protracting the scapula and offer slight rotation anteriorly and dorsally as well as lend support to the shoulder by resisting excessive depression.

M. serratus

Crocodilians possess two serratus muscles: M. serratus superficialis and M. serratus profundus (Fig 31). M. serratus superficialis attaches directly to the anterior dorsal ribs and some thoracic muscles at its origin and inserts on the posteromedial surface of the scapular blade and suprascapular cartilage (Jasinoski et al. 2006; Cong et al. 1998; Dilkes 2000; Meers 2003; Nicholls and Russell 1985). M. serratus profundus lies below M. serratus superficialis in crocodilians, originating from the anterior ribs dorsally. Its insertion is just below that of M. rhomboideus and M. serratus superficialis, covering a broad area of the dorsomedial surface of the scapula. M. serratus superficialis acts in retracting the scapula posteroventrally, while M. serratus profundus adducts the scapula (Jasinoski et al. 2006; Cong et al. 1998; Dilkes 2000; Meers 2003; Nicholls and Russell 1985). Similarly, in *Varanus,* M. serratus originates on several cervical and thoracic ribs and inserts on the posterior edge of the scapula and suprascapular cartilage.

In birds, M. serratus is also divided into M. serratus superficialis and M. serratus profundus. M. serratus superficialis is further divided into pars cranialis and pars caudalis. Pars cranialis originates on the lateral surface of the first cervical or last thoracic ribs, while pars caudalis originates posteriorly to that of M. serratus superficialis pars cranialis on the anterior thoracic ribs. The insertion from pars cranialis is located dorsally to the glenoid on the medial edge of the scapular blade between the insertion for the two heads of M. subscapularis. Similarly, pars caudalis inserts on the dorsal portion of the scapular blade in birds on the posteromedial edge. Both pars cranialis and pars caudalis of M. serratus superficialis function in retraction of the scapula in neognaths and have a role in expiration (Jasinoski et al. 2006; Baumel et al. 1993). M. serratus profundus in birds can present as one muscle or it can be made up of several divisions. In either case, this muscle originates on the posteriormost cervical vertebrae and ribs

as well as the first few thoracic vertebrae and ribs laterally. Similar to the insertion of M. serratus superficialis, M. serratus profundus of neognaths inserts over a large area (more than half) of the medial scapula, posterior to that of M. rhomboideus. M. rhomboideus profundus has a role in inspiration as well as adduction as protraction of the scapula (Jasinoski et al. 2006; Baumel et al. 1993).

Given the similar morphology in crocodilians, lizards, and birds, M. serratus was almost certainly present in two parts in hadrosaurids: M. serratus superficialis and M. serratus profundus (Fig. 31). Both these muscles would have originated on the posterior cervical and anterior thoracic vertebrae and ribs, as in these groups. Previous reconstructions of ornithopod musculature place the insertion of M. serratus superficialis on the posteroventral margin of the scapula, and M. serratus profundus on the dorsomedial surface of the scapula, covering a quite large area in both cases (Dilkes 2000), which is supported by phylogenetic bracketing especially when the lepidosaur condition is taken into account. However, in TMP2015.044.0036, there is a distinct space on the ventral medial surface of the scapula posteriorly, located between the origin of M. subscapularis and the insertion of M. rhomboideus that would be more consistent with the insertion for M. serratus profundus in crocodilians (Meers 2003; Cong et al. 1998; Jasinoski et al. 2006; Klinkhamer et al. 2017). These muscles would then function mostly in stabilization of the scapula, resisting excessive lateral, anterior, or posterior movement of the scapula, as well as assisting in retraction and adduction of the scapular blade.

M. rhomboideus

M. rhomboideus (Fig. 31) is a single muscle in Crocodilians (Cong et al. 1998; Jasinoski et al 2006; Nicholls and Russell 1985), which is different from other living taxa. Birds possess two parts to M. rhomboideus: M. rhomboideus superficialis and M. rhomboideus profundus (Cong et al 1998; Jasinoski et al. 2006). In both birds and crocodilians M. rhomboideus originates on the neural spines of the last several cervical and first few thoracic vertebrae, fleshily in birds (Baumel et al. 1993; Jasinoski et al. 2006) and from the fascia overlying these vertebrae in crocodilians (Meers 2003; Cong et al. 1998; Jasinoski et al. 2006). This origin can extend quite far dorsally, reaching the pelvis in some birds. In crocodilians, M. rhomboideus inserts on the dorsomedial surface of the suprascapula (Dilkes 2000), and in birds both pars superficialis and pars profundus insert on the anteromedial edge of the scapula directly. Pars superficialis can sometimes extend onto the clavicular shaft, and pars profundus can cover a considerable portion of the dorsal scapular blade and suprascapula in a few bird groups (Baumel et al. 1993; Jasinoski et al. 2006). In crocodilians M. rhomboideus functions in adduction of the scapula. In birds, both M. rhomboideus superficialis and M. rhomboideus profundus function in protraction of the scapula.

Pars profundus of M. rhomboideus is only found in birds but it was reconstructed as present in dromaeosaurids by Jasinoski et al. (2006) due to the horizontal position of the scapula in this group. However, Burch (2014) argues that the scapular blade in theropods was ancestrally at a steeper incline indicating no functional need for a second head to M. rhomboideus. This combined with the lack of osteological correlates makes it unlikely that theropods possessed pars profundus to M. rhomboideus. Therefore, pars profundus is equivocal in hadrosaurids. The origin of M. rhomboideus in hadrosaurids was certainly on the neural spines of the last few cervical vertebrae and the first few thoracic vertebrae either directly as in birds or via the overlying fascia

as in crocodilians (fig. 31). As there is no evidence for an ossified or cartilaginous suprascapula in hadrosaurids, the insertion for M. rhomboideus would most likely have been on the dorsal surface of the anterior scapula and possibly extending medially. In this position, the muscle would function in both elevating and protracting the scapula.

M. costocoracoideus

In crocodilians the costocoracoideus complex (Fig. 31) is composed of M. costocoracoideus pars superficialis and the smaller M. costocoracoideus pars profundus (Meers 2003; Cong et al. 1998; Jasinoski et al. 2006; Klinkhamer et al. 2017). Both these muscles originate on the anterior surfaces of the first two sternal and gastral ribs. The insertion for M. costocoracoideus superficialis covers a large area ventral to the glenoid on the dorsal surface of the coracoid, and on the craniolateral edge of the sternal plate. M. costocoracoideus profundus inserts medially onto the scapulosternal ligament, extending over the medial coracoid, occasionally reaching onto the sternal plate and functioning in retraction of the coracoid (Meers 2003; Nicholls and Russell 1985; Jasinoski et al. 2006). Crocodylia is the only group in which M. costocoracoideus is overlain by M. pectoralis (Cong et al. 1998).

The muscular arrangement seen in birds suggests that M. sternocoracoideus of birds and lepidosaurs is homologous to M. costocoracoideus of crocodilians (Howell 1936; Jasinoski et al. 2006). In birds, M. sternocoracoideus originated directly onto the anterolateral process of the coracoid and occasionally onto the sternal ribs. This muscle inserts on the ventromedial coracoid as in crocodilians making this muscle relatively short. Similar to crocodilians, this muscles functions in retraction of the coracoid (Jasinoski et al. 2006).

Since modern birds utilize their forelimbs quite differently than crocodilians and presumably lambeosaurine dinosaurs, it is most likely that hadrosaurids would have a morphology that closely resembles that of crocodilians. It has been argued that in the case of dromaeosaurs, M. costocoracoideus likely did not attach directly to the sternum due to the animal's lack of well-developed anterolateral processes (Jasinoski et al. 2006), resembling the condition seen in birds which is corroborated by their bird-like pectoral girdle and sternal anatomy. However, the sternum of TMP2015.044.0036 possesses very well developed and large posterolateral processes, which seem a very likely attachment site for the origin of M. costocoracoideus (Fig. 31). This muscle may have also originated along the sternal ribs as in birds, though with an osteology more similar to that of crocodilians it is unlikely. In extant taxa, pars profundus and pars superficialis have close but different insertion points. It is unclear how many divisions it may have had in hadrosaurids, but slight anteroposteriorly centred scarring on the ventral-most medial surface of the coracoid in TMP.2015.044.0036 suggests a fleshy insertion on this area. This muscle then would function in retraction of the coracoid and stabilization of the shoulder by inhibiting lateral movement of the coracoid.

3.3.2 Appendicular muscles

3.3.2.1 Brachium (dorsal)

M. latissimus dorsi

In most tetrapods, M. latissimus dorsi (Fig. 32) is a superficial muscle that overlies much of the dorsal pectoral musculature such as M. trapezius and M. levator scapulae. It is a broad muscle with a fan shape and a long origin attaching to the neural spines of the thoracic vertebrae in *Varanus*, and along the thoracodorsal fascia in crocodilians (Cong et al. 1998; Meers 2003; Jasinoski et al. 2006; Klinkhamer et al. 2017). This origin begins at the anterior-most thoracic vertebrae and extends over most of the ribs. In crocodilians, the insertion for M. latissimus dorsi is via a strong tendon that attaches via a distinct muscle scar on the proximal posterior surface of the humerus, just behind the deltopectoral crest.

M. latissimus dorsi in birds is divided into pars cranialis and pars caudalis, as well as a couple of extra slips that run along feather tracts in some avian taxa. Like crocodilians, M. latissimus dorsi pars cranialis originates on the neural spines of the posterior cervical and anterior thoracic vertebrae (Baumel et al. 1993; Jasinoski et al. 2006). M. latissimus dorsi pars caudalis originates just posterior to the origin of pars cranialis, on the neural spines of the thoracic vertebrae and on the ribs. Pars cranialis and pars caudalis insert separately on the dorsal humerus, but in close proximity and both muscle slips become thinner toward their attachment sites. The humerus is textured for muscle attachment, typically posterior to the deltopectoral crest and the insertion of M. deltoideus on the anterior margin (Jasinoski et al. 2006). In both birds and crocodilians, M. latissimus dorsi retracts and abducts the humerus.

As in modern taxa, one could expect that the origin of M. latissimus dorsi would occur on the cervical and thoracic neural spines and be comprised of both pars cranialis and pars caudalis. Crocodylians, birds and lepidosaurs as well as dromaeosaurids, troodontids, and many other non-avian theropods, display a muscle scar for insertion of M. latissimus dorsi on the posterior deltopectoral crest (Jasinoski et al. 2006; Burch 2014). In TMP2015.044.0036, the proximal posterior portion of the humerus is damaged, but a long, prominent muscle scar on the dorsal surface of the humerus distal to the humeral head and opposite the deltopectoral crest is remarked in both *Maiasaura*, and *Edmontosaurus* (Dilkes 2000; Campione et al. 2014). It seems likely that this would be a reasonable insertion for M. latissimus dorsi for TMP2015.044.0036 (Fig. 32). M. latissimus dorsi would function in flexion and retraction of the humerus.

M. teres major

M. teres major (Fig. 31, 32) is only present in crocodilians, leading many authors to believe that this muscle is autapomorphic to crocodilians (Howell 1936; Jasinoski et al. 2006). There is also a muscled named M. teres major in mammals, however the mammalian M. teres major is a derivative of M. latissimus dorsi and is clearly not homologous to the crocodilian one (Dilkes 2000; Koizumi 2021). In crocodilians, M. teres major is thought to have formed from a splitting of M. latissimus dorsi (Howell 1936; Jasinoski et al. 2006). M. teres major originates on the lateral surface of the scapular blade posterodorsally and inserts via a common tendon with M. latissimus dorsi on the dorsal humerus, opposite the deltopectoral crest (Howell 1936; Cong et al. 1998; Meers 2003; Jasinoski et al. 2006;), where it retracts the humerus and contributes to humeral abduction.

Since this muscle is present only in crocodilians, Jasinoski et al. (2006) argued that this muscle was likely absent in dromaeosaurids, and indeed presence of this muscle is equivocal in hadrosaurids. However, there is good indication of the presence of M. teres major in TMP2015.044.0036 via a pronounced muscle scar on the lateral scapular blade, presumably following the morphology of crocodilians. If this is indeed the case, it would imply that M. teres major is primitive for archosaurs and lost along the lineage leading to birds. This muscle would then originate ventral to the origin of M. deltoideus scapularis on the lateral scapular blade and insert together with M. latissimus dorsi on a small area on the lateral surface of the humerus, below the insertion of M. coracobrachialis as in crocodilians (Fig. 31, 32). This muscle would aid in retraction of the humerus and flexion of the shoulder joint.

M. deltoideus scapularis

In *Varanus* M. deltoideus scapularis (Fig. 31, 32) originates on the lateral surface of the anterior scapula, suprascapular cartilage, and clavicle. The insertion is via a tendon to the proximal head of the humerus caudolaterally. M. deltoideus scapularis in crocodilians and lepidosaurs takes its origin from the anterodorsal scapular blade, where there is a corresponding shallow depression in the bone to accommodate its attachment (Jasinoski et al. 2006; Cong et al. 1998). There is a midline ridge separating the attachment of M. deltoideus scapularis from that of M. teres major (Jasinoski et al. 2006). The insertion for this muscle is distal to the anterior tuberosity of the humerus, contributing to humeral abduction.

In birds, M. deltoideus can be present as a single head or in two parts: caput craniale and caput caudale (Jasinoski et al. 2006; baumel et al. 1993). Where both heads are present, caput

caudale is significantly larger and overlies the smaller division. M. deltoideus major caput craniale typically takes its origin from a sesamoid bone that overlies the shoulder joint and inserts onto the dorsal side of the deltopectoral crest of the humerus. M. deltoideus major caput caudale typically originates on the lateral end of the furcula or on the acromion process of the scapula and inserts along with caput craniale onto the deltopectoral crest of the humerus. Caput craniale and caput caudale both function in retraction and abduction of the humerus in birds (Jasinoski et al. 2006).

Dilkes (2000) discusses a probable attachment site for M. deltoideus scapularis in *Maiasuara* to be a depression on the anterolateral surface of the scapula above the acromial process since the acromial process is most likely the attachment site for M. deltoideus clavicularis. TMP2015.044.0036 also possesses this dorsal depression posterior to the acromion process of the scapula. Anteriorly, this depression is slightly roughened which could indicate muscle or tendon attachment. As M. deltoideus clavicularis originates only on the acromion itself, this depression would be free for attachment of M. deltoideus scapularis on TMP2015.044.0036. However, as crocodilians and lepidosaurs possess a large area of origin for M. deltoideus scapularis on the anterodorsal scapular blade, it has been postulated that in at least dromaeosaurid dinosaurs, this would be a more likely origin for M. deltoideus scapularis than the location of origin in birds (Jasinoski et al. 2006). The scarring above the acromion on TMP2015.044.0035 indicates the presence of a muscular or tendinous attachment, but attachment more posteriorly onto the dorsal scapula would provide a greater protractive moment arm in hadrosaurids for the brachium, which seems to be the intended function of this muscle. Therefore, in our models, M. deltoideus scapularis is reconstructed as originating above the acromion, with the origin extending dorsally onto the anterodorsal scapular blade. The insertion

for M. deltoideus scapularis is much simpler to place in TMP2015.044.0036 since in extant taxa, regardless of the number of muscular heads present, have a common insertion on the dorsal deltopectoral crest of the humerus (Fig. 31, 32). This would make M. deltoideus scapularis a large muscle that likely stabilizes the shoulder by counteracting excessive depression of the humerus or may aid in protraction and abduction of the humerus.

M. deltoideus clavicularis

Crocodilians lack a clavicle, but do possess a large, prevalent deltoideus clavicularis muscle (Fig. 31, 32) that overlies M. supracoracoideus. In crocodilians, M. deltoideus clavicularis originates directly on the anterior acromion process of the scapula and inserts over a large surface on the dorsal side of the deltopectoral crest of the humerus (Meers 2003; Jasinoski et al. 2006). As remarked by Jasinoski et al. (2006), this insertion interdigitates distally with the origin of M. humeroradialis. M. deltoideus clavicularis functions in protraction of the humerus in crocodilians. M. deltoideus clavicularis originates on the clavicle and interclavicle in lizards and, as in crocodilians, inserts below the humeral head on the dorsal surface of the humerus to protract the humerus (Howell 1936). In birds, the equivalent muscle to M. deltoideus clavicularis is M. deltoideus pars propatagialis, which is a small, superficial muscle, originates on the epicleideum of the furcula, and occasionally the acromion process of the scapula (Dilkes 2000; Jasinoski et al. 2006; Baumel et al. 1993). M. deltoideus pars propatagialis inserts on the antebrachium musculature in birds and is a muscle specialized for flight (Jasinoski et al. 2006) and is consequently absent in ratites. Interestingly, this muscle is present in tinamous (Hudson et al. 1972) as a broad muscle that, as in neognath birds, originates on the epicleideum and inserts as two parts over the wrist.

The ancestral state for M. deltoideus clavicularis is to originate on the clavicle (Howell 1936) and in groups in which the clavicle has been lost, the origin has migrated onto the anterior scapula near the acromion process as in crocodilians (Meers 2003; Jasinoski et al. 2006; Klinkhamer et al. 2017). As hadrosaurids lack a clavicle, the origin of M. deltoideus clavicularis is likely the acromion process, which is heavily scarred in TMP2015.044.0036. Similarly, Burch (2014) places the origin of this muscle in early theropods on the anterior acromion process and the acromial expansion since this was the place of origin in all taxa they studied, with no additional attachments on the scapula as Jasinoski et al. (2006) reconstructed for dromaeosaurids. The insertion in TMP2015.044.0036 may then be located on the dorsal aspect of the deltopectoral crest (Fig. 31, 32) as in crocodilians and likely some theropods (Jasinoski et al. 2006; Burch 2014), and likely did not have multiple heads at its insertion as in birds since this is a derived condition for Aves. This muscle would be a powerful protractor of the humerus and forelimb.

M. subcoracoideus

In *Iguana* and in most lepidosaurs, M. subcoracoideus originates over the whole medial surface of the coracoid and anteromedial epicoracoid and inserts on the medial tuberosity of the humerus within the tendon of M. subscapularis (Howell 1936; Jasinoski et al. 2006; Otero 2018), acting as a retractor of the brachium. In contrast, the crocodilian M. subcoracoideus (sometimes called M. subcoracoscapularis) is unique in having one head and originating only on the medial scapular blade and like lepidosaurs, inserts onto the medial tuberosity of the humerus (Romer 1944; Jasinoski et al. 2006; Otero 2018). In birds, M. subcoracoideus has both a ventral and a dorsal head, whose presence and attachments differ among avian taxa. Generally, the dorsal head

originates on the medial surface of the coracoid and the ventral head, when present, originates on the anterior edge of the coracoid and the ventral coracoid shaft. When both ventral and dorsal heads are present, they typically insert along with the tendon of M. subscapularis on the posterior tubercle of the humerus (Jasinoski et al. 2006; Otero 2018). In birds, M. subcoracoideus adducts and rotates the humerus.

Howell (1936) argues that in derived reptiles, M. subcoracoideus developed from M. subscapularis, extending its fibres to cover the medial scapula at its origin, a claim that is supported by the nervous input to this muscle. This theory would explain why M. subcoracoideus is not present in mammals, never being mechanically necessary in the mammalian shoulder arrangement as a retractor and only being developed in those reptiles whose scapula is oriented parallel with the ground. Jasinoski et al. (2006) reconstruct the dromaeosaurid M. subcoracoideus as originating on the medial coracoid, over the coracoid foramen like the majority of neognaths, and inserting on the posterior tuberosity of the humerus along with M. subscapularis. It is difficult to say for certain if M. subcoracoideus was present in hadrosaurids, but at least in TMP2015.044.0036, the scapula is presumably somewhat parallel to the ground, making M. subcoracoideus useful mechanically as a retractor and adductor of the humerus if it were present. In this case, the medial coracoid seems an appropriate site of origin as most of the medial surface of TMP2015.044.0036 is scarred from muscle attachment. M. subcoracoideus undoubtedly would have inserted along a common tendon with M. subscapularis as in most birds and reptiles (Howell 1936; Howell 1937; Jasinoski et al. 2006).

M. subscapularis

As discussed above, reptiles and birds typically have a division of M. subscapularis which has differentiated into M. subcoracoideus that aids in adduction and rotation of the humerus (Fig. 31, 32). In crocodilians, M. subscapularis proper is comprised of only one head which is located directly below M. scapulohumeralis posterior. It has a large origin on the medial surface of the scapular blade, ventral to the insertion of M. serratus ventralis cervicis and converges to form a narrow insertion on the posterior tuberosity of the humerus (Meers 2003; Jasinoski et al. 2006; Otero 2018). Here, it plays a role in retraction and adduction of the humerus and stabilizes the shoulder joint.

Birds possess two heads to M. subscapularis at their origin: caput laterale and caput mediale. This interruption is typically caused by the intruding path of M. serratus superficialis cranialis (Jasinoski et al. 2006; Otero 2018). Caput laterale is a small muscle that originates on the posterolateral edge of the scapular blade ventrally, and caput mediale originates on the medial surface of the scapular blade somewhat centrally (Jasinoski et al. 2006; Howell 1937; Baumel et al. 1993). Both caput laterale and caput mediale insert via a large common tendon with M. subcoracoideus onto the posterior tubercle of the proximal humerus where it retracts and adducts the humerus.

Dromaeosaurids and many other theropods possess a ridge on the medial scapula that extends at least half the length of the scapula (Jasinoski et al. 2006; Burch 2014). There is a horizontal depression beginning at the scapular neck of TMP2015.044.0036 and ending halfway along the length of the scapular blade that would be consistent with an attachment site for M. subscapularis. The insertion of M. subscapularis should be consistent with extant tetrapods and would therefore be on the dorsomedial surface of the proximal end of the humerus (Fig. 31, 32).

This surface of this area in TMP2015.044.0036 is damaged, but Dilkes (2000) reports scarring on the medial humeral shoulder of *Maiasaura* that would be consistent with this placement. The function of M. subscapularis would be in retraction and elevation of the humerus, as well as some stabilization of the shoulder joint.

M. scapulohumeralis anterior

There is some debate on the occurrence of M. scapulohumeralis anterior (Fig. 31, 32) in reptiles. Cong et al. (1998) identify M. scapulohumeralis in *Alligator sinensis* as a deep muscle of the shoulder that occurs as a single head. Romer (1922) postulated that M. teres minor is derived from M. scapulohumeralis anterior where present, as is M. supracoracoideus. M scapulohumeralis anterior is absent in crocodilians (Romer 1922; Meers 2004) and in some birds, including ratites, but is present in tinamous, who seem to be an odd case among flightless birds (Baumel et al. 1993; Jasinoski et al. 2006; Hudson et al. 1972; Romer 1922). When present in birds, M. scapulohumeralis anterior originates on the lateral surface of the scapula, behind the glenoid process, and inserts on the posterodorsal part of the proximal humerus. In *Varaus* and many lepidosaurs, M. scapulohumeralis anterior has two heads, one originating on the posterior edge of the scapular blade and the other on the coracoid. Both heads converge and insert on the head of the humerus.

Dilkes (2000) suggests that the plesiomorphic condition for M. scapulohumeralis anterior in dinosaurs is to originate above the origin of M. suprcoracoideus on the lateral surface of the scapula, and to insert adjacent to M. deltoideus clavicularis on the dorsal surface of the humerus proximally. However, this suggestion is dependent on the deep fibres of the deltoideus

clavicularis being homologous to M. scapulohumeralis anterior in crocodilians, but as stated above, M. scapulohumeralis has been lost in crocodilians. In TMP2015.044.0036, this area is too damaged to retain muscle scarring, so this placement is equivocal. Jasinoski et al. (2006) place M. scapulohumeralis anterior as originating on the posterior edge of the scapular blade similarly to the condition seen in lepidosaurs, corroborated by an ovoid scar on the dromaeosaurid scapula. This scar is not observed in TMP2015.044.0036, but the placement seems appropriate, given its similar arrangement in lepidosaurs. The insertion site for M. scapulohumeralis anterior is similar in most lizards and birds where it is present in being on the posterodorsal edge of the proximal humerus, below the humeral head (Fig. 31, 32). This location in TMP2015.044.0036 is marked by well pronounced scarring that extends partially onto the dorsal deltopectoral crest distally, making M. scapulohumeralis anterior in this lambeosaurine an effective retractor and adductor of the humerus.

M. scapulohumeralis posterior

In both birds and crocodilians, M. scapulohumeralis posterior (Fig. 31, 32) is a powerful retractor of the humerus (Jasinoski et al. 2006). M. scapulohumeralis posterior in crocodilians is a large muscle overlying M. subscapularis that originates on the posterior portion of the dorsal surface of the scapula and inserts on the posterior humerus, just distal to the humeral head (Meers 2003; Jasinoski et al. 2006; Klinkhamer et al. 2017). In *Varanus* this muscle is also large, originating on the posterior margin of the scapula and suprascapula, and inserting on the tubercle of the humerus. M. scapulohumeralis posterior in birds is also a significant retractor of the humerus and covers most of the dorsal surface of the scapular blade where it originates (Baumel

et al. 1993; Jasinoski et al. 2006;). It inserts via a tendon onto the crus ventral fossae, on the proximal humerus.

As in crocodilians and birds, the origin of M. scapulohumeralis posterior in hadrosaurids was likely near or on the posterolateral surface of the scapula. There are striations along the ventral margin of the posterior half of the scapular blade in TMP2015.044.0036 that seems a likely origin for M. scapulohumeralis posterior. These striations begin just distal to the scapular angle and end approximately halfway along the scapular blade distally on the ventral margin. Much of the lateral surface of the scapula in TMP2015.044.0036 possesses long striations, so it is difficult to determine the extent of this origin, but a difference in the angle of striations suggests that the origin extends several centimeters dorsally from the ventral margin of the scapula both medially and laterally (Fig. 31, 32). The insertion would be the dorsomedial surface of the humerus just below the humeral head, the same region as the insertion for M. subscapularis that was identified in *Maiasaura* (Dilkes 2000), contributing to retraction of the humerus.

M. triceps

The triceps complex (Fig. 31, 32) varies greatly within tetrapoda, but universally acts to extend the forearm (Jasinoski et al .2006). M. triceps brachii of *Alligator sinensis* is the only dorsal extensor of the humerus and has four heads originating on the humerus, scapula, and coracoid (Cong et al. 1998). Crocodilians possess five heads (Meers 2003; Klinkhamer et al. 2017) to the triceps complex, *Varanus* has three heads, while some birds possess only two. In general, the triceps complex can be broken down into four parts: M. triceps brachii caput

scapulare, M. triceps brachii caput mediale, M. triceps brachii caput coracoideum, and M. triceps brachii caput laterale.

M. triceps brachii caput scapulare is the largest of the triceps muscles in crocodilians (Meers 2003; Jasinoski et al. 2006). It originates on the dorsal edge of the scapula, above the glenoid. M. triceps brachii caput mediale originates from the entire dorsal side of the humeral shaft. M. triceps brachii caput coracoideum partially overlies caput mediale and originates via two seprate tendons, one on the medial surface of the scapula along the dorsal edge, the other on the lateral scapula on the dorsal edge, above the glenoid and distal to the insertion of caput scapulare (Jasinoski et al. 2006). Finally, M. triceps brachii caput laterale sits below M. triceps brachii caput scapulare and the origin is on the dorsal humerus, distal to the insertion of M. deltoideus scapularis. M. triceps brachii caput scapulare, M. triceps brachii caput mediale, M. triceps brachii caput coracoideum, and M. triceps brachii caput laterale all converge on a single, large tendon which inserts onto the olecranon process of the ulna (Cong et al. 1998; Meers 2003; Otero 2018).

The divisions and attachments of the M. triceps brachii complex can vary greatly among bird taxa. In general, birds possess only M. triceps brachii caput scapulare, M. triceps brachii caput mediale, and M. triceps brachii caput coracoideum (Baumel et al. 1993; Jasinoski et al. 2006). M. triceps brachii caput scapulare takes its origin on the dorsal scapula, posterior to the glenoid, and can have additional attachments on the dorsal humeral shaft which typically leave an ovoid scar when present (Jasinoski et al. 2006; Otero 2018). M. triceps brachii caput mediale (M. humerotriceps in neognaths) has a two or occasionally three headed origin on the dorsal humerus, along the posterior edge and surrounds the insertion of M. scapulohumeralis cranialis. M. triceps brachii caput coracoideum (M. coracotriceps in neognaths) is a small vestigial muscle

in birds (Baumel et al. 1993; Jasinoski et al. 2006). It originates on the sternoscapular ligament and the posterior humerus and inserts close on the proximal ulna close to that of the rest of the triceps complex which inserts on the olecranon process of the ulna via a common tendon. It is thought that this muscle is no longer used for locomotion when present, possibly being used as a mechanoreceptor to detect the amount of contraction being performed by the rest of the triceps complex (Rosser and George 1985; Jasinoski et al. 2006).

Outgroup analysis by Dilkes (2000) indicates that dinosaurs possessed two heads of M. triceps brachii: a scapular head (caput scapulare) and a humeral head (caput mediale). As in crocodilians, which possess two scapular heads for M. triceps, the scapular head would likely originate on the dorsal surface of the scapula in hadrosaurids, posterior to the glenoid fossa. Dilkes (2000) noted a scarring on the proximoventral buttress in *Maiasaura* and argues that this is the origin of M. triceps brachii. TMP2015.044.0036 also possesses this scarred region on the proximoventral buttress of the scapula that could accomodate the scapular head of M. triceps, according to Dilkes' (2000) assessment. The origin of M. triceps brachii caput mediale is somewhat easier to place as crocodilians and birds have a common area of origin for this division of M. triceps on the posterior humeral shaft, extending proximally just below the humeral head. This area is damaged in TMP2015.044.0036 so scarring is not visible. Although M. triceps brachii caput coracoideum is vestigial in birds, Jasinoski et al. (2006) suggest that a vestigial coracoid head may have been present in dromaeosaurids, based on its functionality in limiting movement of the humerus and thereby increasing the ability to protract he forelimb, since striking and grasping prey would have been important in these predatory animals. Since there is no evidence to suggest that hadrosaurids would possess a similar evolutionary pressure, it is unlikely that a coracoid head would have posed any kind of advantage to the hadrosaurid

forelimb and so will not be considered further in this study. As in other tetrapods, M. triceps would certainly converge on a common tendon and insert on the olecranon process of the ulna (Fig. 31, 32), which is very well develped in TMP2015.044.0036, making M. triceps a primary extensor of the antebranchium.

3.3.2.2 Brachium (ventral)

M. pectoralis

M. pectoralis (Fig. 31, 32) in most extant tetrapods is a very powerful retractor and adductor of the humerus. In crocodilians, this muscle has an extensive origin on much of the sternum and distal portion of the sternal ribs and inserts onto the deltopectoral crest of the humerus on the ventral edge (Meers 2003; Jasinoski et al. 2006). In *Varanus,* the origin for M. pectoralis is the sternum, interclavicle, sternal ribs, and midline abdominal fascia. In most birds, M. pectoralis is significantly expanded to provide a powerful downstroke for flight, making this muscle the main adductor in birds. This large muscle takes its fleshy origin on the entire surface of the sternal keel and lateral surfaces of the anterior sternum, the lateral furcula, and sometimes also the sternoclavicular membrane (Jasinoski et al. 2006; Baumel et al. 1993). In all taxa, M. pectoralis inserts onto the deltopectoral crest of the humerus.

TMP2015.044.0036 possesses very well-preserved, articulated sternal plates with a dorsoventrally expanded anterior portion of the plate and quite long dorsolaterally extending processes. The anterior portion of the ventral side of the ossified sternal plates in TMP2015.044.0036 is strongly curved ventrally, creating a dorsoventrally broad anterior faces that would likely have been in contact with a block of cartilage situated between the sternal

plates and the coracoids (see discussion in chapter 2). It is possible that these cartilage-covered surfaces might have accommodated the pectoralis muscle origins, but since M. pectoralis has a fleshy origin directly onto the sternal bones in birds and crocodilians, it is more likely that M. pectoralis originated on the posterolateral extensions of the sternum and would be a similar arrangement to the attachment of M. pectoralis along the sternal ribs of crocodilians (Meers 2003; Klinkhamer et al. 2017). The insertion of M. pectoralis would almost definitely be centered proximodistally onto the apex of the deltopectoral crest of the humerus as in birds and crocodilians Fig. 31, 32), making M. pectoralis the primary retractor and adductor of the forelimb in TMP.2015.044.0036.

M. supracoracoideus

There is variation in the number of divisions of the supracocacoideus complex (Fig. 31, 32) in crocodilians. In crocodilians, this muscle group historically comprises three separate muscles, M. supracoracoideus longus, M. supracoracoideus intermedius, and M. supracoracoideus brevis (Meers 2003; Jasinoski et al. 2006; Klinkhamer et al. 2017). *Alligator sinensis,* however, possesses only two divisions of M. supracoracoideus (M. supracoracoideus and M. epicoracohumeralis) (Cong et al. 1998). In crocodilians that possess all three divisions, M. supracoracoideus longus typically has two heads which originate on the anterodorsal coracoid and medial coracoid. Jasinoski et al. (2006) note that the second head of M. supracoracoideus longus which originates on the medial coracoid is only distinguishable at its origin and coalesces into a single belly before the insertion of M. supracoracoideus longus onto the deltopectoral crest along with M. pectoralis, which can share a tendon. This second head then is likely the M. supracoracoideus intermedius identified by Meers (2003), meaning that there is only two true

divisions of M. supracoracoideus in crocodilians: M. supracoracoideus longus and M. supracoracoideus brevis. M. supracoracoideus longus therefore is a large, bifurcated muscle that sits partly above the much thinner M. supracoracoideus brevis. M. supracoracoideus brevis is a deep muscle that originates on the ventral acromion process of the scapula and on the dorsal coracoid (Jasinoski et al. 2006; Meers 2003) and inserts on the deltopectoral crest proximal to the insertion of M. supracoracoideus longus. This muscle group is important in protraction of the humerus in crocodilians.

In *Varanus*, M. supracoracoideus originates on the anterolateral surfaces of the coracoid and coracoid cartilage and inserts on the proximal head of the deltopectoral crest. In neognaths, the arrangement of M. supracoracoideus is altered to assist the pectoralis in adduction of the forelimb, so M. supracoracoideus is large and underlies M. pectoralis. It originates on the sternal keel, ventral sternum, and the medial surface of the coracoid or sternoclavicular membrane (Baumel et al. 1993; Jasinoski et al. 2006; Otero 2018). Since this muscle is utilized for flight in flying birds, this muscle condenses onto a thick tendon that passes through the triosseal canal of the shoulder and inserts distal to the humeral head on the anterior tubercle of the humerus, just proximal to the deltopectoral crest. This canal effectively changes the trajectory of the tendon, causing M. supracoracoideus to elevate the wing in birds.

Phylogenetic based reconstructions of musculature of *Maiasaura* (Dilkes 2000) indicate a similar arrangement to crocodilians, with the origin of M. supracoracoideus on the lateral surface of the coracoid from the base of the biceps tubercle extending onto the proximal portion of the scapula. Jasinoski et al. (2006), however, argue that since the scapular origin in crocodilians is possibly autapomorphic (Romer 1922), and the only osteological origin common to crocodilians, birds, and lepidosaurs is the coracoid, it is likely that the ancestral condition would be for M.

supracoracoideus to originate on the anteroventral coracoid. A sternal origin is also not likely since the sternum in both dromaeosaurids and hadrosaurids did not possess a keel, the site of attachment when a sternal origin is present. When combined with evidence from muscle scarring, Jasinoski et al. (2006) place the origin of M. supracoracoideus in dromaeosaurids on the anterolateral coracoid ventral to the coracoid foramen, extending from the biceps tubercle to the ventral-most point of the coracoid anteriorly. Scarring on the lateral surface of the coracoid of TMP2015.044.0036 corroborates this placement in hadrosaurids. The insertion of M. supracoracoideus in dinosaurs is a mechanically interesting question, since M. supracoracoideus in birds inserts onto the proximal humerus via a tendon that passes through the triosseal canal, which does not exist in hadrosaurids. Burch (2014) argues that an insertion on the greater tubercle in theropods would cause M. supracoracoideus to be ineffective, and that an insertion on the apex of the deltopectoral crest would allow M. supracoracoideus to be an effective protractor of the humerus like the condition in crocodylians. Given the arrangement of the existing musculature and the osteology in TMP2015.044.0036, it would make functional sense to place the insertion of M. supracoracoideus in the same place (Fig. 31, 32). Therefore, the insertion of M. supracoracoideus on TMP2015.044.0036 would likely have been on the apex of the deltopectoral crest proximally as in crocodilians where it would act as an important protractor of the humerus.

M. coracobrachialis

M. coracobrachialis (Fig. 31, 32) in general can be divided into two muscles: M. coracobrachialis brevis and M. coracobrachialis longus. In crocodilians, M. coracobrachialis brevis originates fleshily from the lateral surface of the coracoid posteriorly and inserts onto the

ventral deltopectoral crest of the humerus posterior to the insertion of M. pectoralis (Jasinoski et al. 2006; Klinkhamer et al. 2018), where it effectively protracts the humerus. Although M. coracobrachialis longus may be present in some adult crocodilian specimens, Jasinoski et al. (2006) found this muscle to be absent in all crocodilian specimens dissected.

Birds possess both M. coracobrachialis brevis (cranialis) and M. coracobrachialis longus (caudalis). The majority of neognaths have an origin for M. coracobrachialis cranialis on the acrocoracoid process dorsally but can occasionally also originate on the tendon of M. biceps brachii (Baumel et al. 1993; Jasinoski et al. 2006; Otero 2018). The insertion of this muscle is the same as in crocodilians, on the proximal portion of the ventral side of the humerus, posterior to the insertion of M. pectoralis, making it a protractor of the humerus. M. coracobrachialis caudalis in birds is a large muscle originating from the lateral coracoid along the ventral margin and the posterior process of the coracoid and can extend onto the sternum in a few cases (Jasinoski et al. 2006; Baumel et al. 1993). This muscle inserts onto the posterior tubercle of the humerus where it rotates and adducts the humerus.

There is little doubt that hadrosaurids possessed at least one division if M. coracobrachialis. The origin of M. coracobrachialis brevis differs from crocodilians and ratites from that of neognaths but universally originates posterior to the origin of M. biceps brachii (Jasinoski et al. 2006; Otero 2018). Therefore, in TMP2015.044.0036, M. coracobrachialis likely attached to the posterior of the lateral surface of the coracoid, posterior to the biceps tubercle where M. biceps brachii would have attached. The insertion then would almost certainly be on the deltopectoral crest of the humerus, posterior to the insertion of M. pectoralis as this homology is conserved in birds and crocodilians. There is heavy scarring on the lateral posterior side of the deltopectoral crest in TMP2015.044.0036 which may, at least in part, contribute to the

insertion of M. coracobrachialis (Fig. 31, 32). M. coracobrachialis longus is mostly absent in crocodilians, but when reported in lepidosaurs, birds, and crocodilians it always originates on the posterior coracoid along the ventral margin (Jasinoski et al. 2006) and inserts onto the dorsal humerus, distally in crocodilians and lepidosaurs, and proximally in birds (Meers 2003; Klinkhamer et al. 2017; Otero 2018). At either insertion this muscle would assist in humeral adduction. However, M. coracobrachialis longus is absent in crocodyliforms, and the homology of this muscle in neognaths and lepidosaurs is uncertain, being related to different muscle groups and functions in those taxa (Burch 2014). Furthermore, there is no scarring on TMP2015.044.0036 to definitively place M. coracobrachialis longus or confirm its existence in this group. In any case, M. coracobrachialis longus would not contribute significantly to adduction of the forelimb in TMP2015.044.0036 so this division of M. coracobrachialis will be excluded from biomechanical analysis. The M. coracobrachialis muscle would function in flexion of the humerus.

M. biceps brachii

In crocodilians, M. biceps brachii (Fig. 31, 32) originates via a large tendon onto the shaft of the coracoid anteriorly, runs along the length of the ventral humerus, and inserts onto the proximal radius below the proximal radial head via a common tendon with M. brachialis inferior (Meers 2003; Jasinoski et al. 2006; Cong et al. 1998). In most lizards and birds, there are two heads to the biceps brachii at its origin on the lateral surface of the coracoid and sometimes humerus which converge on a single tendon at its insertion via a tendon on the proximal end of the radius and ulna. In birds specifically, the humeral head is the larger of the two and the muscle

can have one or two bellies, and one or two tendons of insertion (Baumel et al. 1993; Otero 2018). M. biceps brachii retracts the forearm, and in crocodilians also protracts the humerus.

TMP2015.044.0036 possesses strong scarring on the entire lateral surface of the coracoid, and a prominent biceps tubercle anteriorly and dorsally on the lateral side. In all archosaurs, this tubercle is present and marks the tendinous attachment of M. biceps brachii (Jasinoski et al. 2006). This tubercle would make up at least part of the origin in TMP2015.044.0036. There are light striations near the radial and ulnar heads on the posterior side which likely pertain to the insertion of M. biceps brachii (Fig. 31, 32). Neognaths and tinamous possess a second origin of M. biceps brachii from the humerus (Jasinoski et al. 2006; Otero 2018). Crocodilians, ratites, and lepidosaurs do not possess a second head in this position, and there are no obvious osteological features that would indicate a second head to M. biceps brachii in TMP2015.044.0036. With this configuration, the single head of M. biceps brachii in TMP2015.044.0036 would be an effective flexor of the forearm.

M. brachialis

The origin of M. brachialis (Fig. 32) is fairly consistent across Tetrapoda, being along the anterior surface of the humerus (Jasinoski et al. 2006). In crocodilians this origin extends from the distal apex of the deltopectoral crest and reaches across the anterior deltopectoral crest (Jasinoski et al. 2006; Meers 2003). This muscle inserts with a common tendon with M. biceps brachii onto the posterior surface of the proximal end of the radius. *Alligator sinensis* differs in having two heads at its origin, both attaching to the humerus (Cong et al. 1998). In birds, M. brachialis is a short muscle originating distally on the humerus and inserting only on the

proximal lateral side of the ulna (Baumel et al. 1993; Jasinoski et al. 2006; Otero 2018). In both crocodilians and birds, M. brachialis flexes the forelimb. The presence of M. brachialis in both crocodilians and birds makes this muscle unequivocal for Dinosauria based on phylogenetic bracketing and indeed, the proximal radius and ulna of TMP2015.044.0036 possess scarring along much of their anterior surfaces just distal to the proximal head of these elements and extending distally about a third of their length (Fig. 32). The origin for M. brachialis in hadrosaurids would likely be on the medial surface of the humerus posteriorly to the deltopectoral crest and proximal to the humeral shaft and converging with a common tendon to M. biceps brachii as is the case in crocodilians (Otero 2018). M. brachialis would serve to flex the forearm and possibly lend support to the elbow joint in avoiding overextension of the antebranchium.

3.3.2.3 Antebrachium (dorsal)

M. extensor carpi ulnaris

In crocodilians, M. extensor carpi ulnaris (Fig. 32, 33) originates on the anterior epicondyle of the humerus and inserts at the base of metacarpal II (Meers 2003), on the extensor side of the ulna and proximal ulnare (Dilkes 2000). M. extensor carpi ulnaris in *Alligator sinensis* differs by inserting onto the dorsal ulna rather than reaching the manus (Cong et al. 1998). In *Varanus*, M. extensor carpi ulnaris originates on the distal end of the humeral condyle and inserts on metacarpal V, the pisiform bone and the ulnare. In birds, this muscle originates both on the distal humerus and proximal end of the ulna and inserts onto the carpometacarpus at the base of metacarpal II (Dilkes 2000; Baumel et al. 1993; Burch 2014), which Burch (2014)

argues may be a derived feature for archosaurs. As discussed by Dilkes (2000), M. extensor carpi ulnaris may have originated on the anterior of the ulna and carpals, however in TMP2015.044.0036 and indeed in most hadrosaurid forelimbs, there is space to accommodate carpals in situ, but no genuine ossified carpal material has been recovered for hadrosaurids (see discussion in chapter 2). Conversely, Otero (2018) places the origin of M. extensor carpi ulnaris unequivocally on the humeral ectepicondyle for sauropodomorphs based on the common origin of crocodilians, lepidosaurs, and birds. For these reasons, an unequivocal origin of M. extensor carpi ulnaris for TMP2015.044.0036 is placed on the anterior epicondyle of the humerus as well as the anterior ulna, centered proximodistally onto the shaft of the ulna. Dilkes (2000) also discusses a depression on metacarpal IV of *Maiasaura* on the anterolateral side. There is a similar depression on metacarpal IV of TMP2015.044.0036 although the surface is smoother than described for *Maiasaura*. Though placement of the insertion of this muscle in hadrosaurids is quite uncertain due to the apparent lack of carpals for observation, this depression seems a logical insertion point for M. extensor carpi ulnaris for the elements that we do possess (Fig. 32, 33). There, this muscle would function in extending the manus as in all living archosaurs (Meers 2003; Jasinoski et al. 2006; Otero 2018).

M. extensor carpi radialis

M. extensor carpi radialis (Fig. 32, 33) (sometimes called M. abductor pollicis longus) is present in all living reptiles (Otero 2018), making this muscle unequivocal for Dinosauria. In crocodilians, this muscle is divided into radial and ulnar parts. These originate on the distal portions of the medial sides of the radius and ulna respectively and combine to insert onto the radiale proximally (Meers 2003; Klinkhammer et al. 2018). The extensor radialis complex in

Varanus is divided into three muscles that originate on the medial to distal humerus and insert onto the distal radius and radiale. In lepidosaurs, this muscle originates on the distal-most ulna and inserts medially on the proximal end of metacarpal I (Otero2018). In birds, M. extensor carpi radialis also originates on the distal humerus, typically from two separate heads dorsally and ventrally and inserts onto the carpometacarpus (Baumel et al. 1993; Otero 2018) and is modified for flexion and extension of the wrist and elbow in the avian wing (Burch 2014). It is possible that this muscle originated on the distal radius medially in hadrosaurids, as in lizards and crocodilians (Fig. 32, 33). Since there are no preserved carpals in TMP2015.044.0036, the insertion for M, extensor carpi radialis may have been on the radiale as in crocodilians and lizards, however, it is also possible that it inserted onto the metacarpals like the condition in birds, as suggested by Dilkes (2000) for *Maiasaura.* Burch (2014) argues that at least in *Tawa*, the osteology is more like that of crocodylians and lepidosaurs rather than birds and place the insertion on the radiale. There is no clear definitive answer for the placement of the insertion in TMP2015.044.0036 but in either case the primary function of M. extensor carpi radialis would be to extend the forearm.

M. extensor digitorum longus

M. extensor digitorum longus and its homologous muscles vary across Tetrapoda. In all tetrapods, M. extensor digitorum longus originates above the radial condyle of the humerus on the distal end of the lateral side (Meers 2003; Jasinoski et al. 2006; Otero 2018). This particular location in TMP2015.044.0036 bears strong striations. In most tetrapods, M. extensor digitorum longus inserts onto metacarpals or to digits. In crocodilians, this insertion is reduced to metacarpals II and III (Meers 2003; Otero 2018). In birds, M. extensor digitorum communis

originates on the distal end of the ulna, passes over the dorsal wrist, and inserts anteriorly onto the phalanges (Baumel et al. 1993). We cannot be certain of the insertion of M. extensor digitorum longus in TMP2015.044.0036 since there is very little to no scarring on the phalanges and metacarpals, however, assuming that the digits themselves did not extend much, it seems reasonable to place the insertion for M. extensor digitotrum longus on metacarpals II to IV, as appears to be plesiomorphic for reptiles (Otero 2018) or on the proximal ends of the first phalanges. Burch (2014) suggests that in Theropods this insertion would not extend to metacarpal IV since this bone is highly diminished in theropods. Hadrosaurids possess a very well-developed metacarpal IV and insertion of M. extensor digitorum longus across the metacarpals would provide an extensive and strong attachment site for this muscle, making it a highly functional extensor of the digits.

3.3.2.4 Antebrachium (ventral)

M. palmaris communis

M. palmaris communis (Fig. 32, 33) is an important flexor of the manus in most tetrapods so was unequivocally present among Dinosauria and likely performed the same function as living tetrapods (Jasinoski et al. 2006). In Varanus, however, M. palmaris communis originates with the other flexors on the epicondyle of the humerus distally and inserts across all of the carpals in the wrist though this arrangement is quite different from other reptiles. In crocodilians, this muscle originates on the flexor epicondyle of the ulna and inserts via multiple tendons onto the unguals of digits II to V, as in most other taxa (Dilkes 2000; Meers 2003). Dilkes (2000) reports a proximal ridge on the ventral side of the third ungual in *Maiasaura* which they attribute

to the insertion of this muscle. TMP2015.044.0036 has a similar ridge on the ventral side of unguals II to IV. These three unguals are the only digits that would have contacted the ground in TMP2015.044.0036, and the overlying metacarpals are arranged in such a way that it would be unlikely for these unguals to move independently of one another. Therefore, it is likely that one, two, or all of these digits were insertion sites for M. palmaris communis (Fig. 32, 33) where, regardless of which digits this muscle spanned, contraction would lead to palmarflexion of the manus.

M. flexor carpi ulnaris

In all reptiles, M. flexor carpi ulnaris (Fig. 32, 33) originates on the distal epicondyle of the humerus (Meers 2003; Jasinoski et al. 2006; Otero 2018). In both crocodilians and lepidosaurs, this muscle inserts onto the carpals. In birds, M. flexor carpi ulnaris originates on the flexor surface of the humerus (the entepicondyle), ocasionally in a common tendon with M. extensor carpi ulnairs and crosses the elbow joint through a tract on the proximal ulna to insert onto the ulnare (Baumel et al. 1993; Burch 2014; Otero 2018). This muscle functions in flexion of the wrist in birds but also is utilized in positioning of flight feathers. As this muscle is apparently plesiomorphic for archosaurs in both anatomy and function (Jasinoski et al. 2006; Otero 2018), the presence of this muscle in TMP2015.044.0036 is unequivocal. M. flexor carpi ulnaris would almost certainly originate on the distal epicondyle of the humerus in hadrosaurids as it does in all other reptiles (Fig. 32, 33). Due to the presumed cartilaginous nature of the carpals in TMP2015.044.0036, it is likely that the insertion for M. flexor carpi ulnaris has shifted from the carpals to the flexor surface of the metacarpals, as suggested by Dilkes (2000) for *Maiasaura.* There, it would act as a palmarflexor of the manus.

M. flexor carpi radialis

M. flexor carpi radialis (Fig. 32, 33) in *Varanus* originates on the epicondyle of the humerus and inserts on the ventral surface of the radiale. In crocodilians, this muscle also originates on the epicondyle of the humerus on the flexor (posterior) side and inserts on the anterolateral surface of the ulna (Cong et al. 1998; Meers 2003), which differs from lizards whose insertion rest upon the carpals. The origin in hadrosaurids was likely the epicondyle of the humerus as in M. flexor carpi ulnaris (Fig. 32, 33), and like this muscle it probably inserted onto the carpals or the metacarpals of TMP2015.044.0036 where it could aid in flexion of the manus.

3.4 Discussion

Carpenter and Wilson (2008) reconstructed the major forelimb muscles of *Camptosaurus* by deforming digital models of a crocodilian and an avian scapula, coracoid, and humerus to resemble those of *Camptosaurus*, and observing the resulting position of the crocodilian and avian muscle origins and insertions on these elements. Although written muscle descriptions are not presented in their paper, attachment sites are illustrated and can provide a good basis for comparing results (Fig. 31, 32, 33). Muscles reconstructed as having the same areas of attachment and insertion as in this study include M. biceps, M. deltoideus scapularis, M. latissimus dorsi, M. teres major, and M. triceps. The origins of M. coracobrachialis and M. supracoracoideus in TMP2015.0044.0036 are similar to those reconstructed for *Camptosaurus* but in TMP2015.044.0036 these muscles are both reconstructed as occurring more posteriorly and dorsally on the lateral coracoid rather than along the anteroventral edge as in *Camptosaurus*

(Carpenter and Wilson 2008). These muscles are also reconstructed with second heads, called M. coracobrachialis posterior and M. supracoracoideus intermedius, that originate on the anterior scapular head and just ventral to the anterior scapular head, respectively. Carpenter and Wilson (2008) also place the origin for M. deltoideus clavicularis on the lateral dorsal scapular neck whereas in TMP2015.044.0036 its origin is placed on the acromion process. There is only one origin for M. scapulohumeralis shown for *Camptosaurus* that is located at the site of origin for M. scapulohumeralis posterior in TMP2015.044.0036. M. teres major is shown to originate ventrally on the lateral scapula in *Camptosaurus* whereas in TMP2015.044.0036 it is shown to originate dorsally, above the origin of M. deltoideus scapularis. Additionally, the insertion for M. coracobrachialis in *Camptosaurus* is on the deltopectoral crest while in TMP2015.044.0036 it inserts in a large area closer to the humeral head. *Camptosaurus* is an ornithopod but is not closely related to lambeosaurines. Its forelimb morphology is broadly similar to that of TMP2015.044.0036 though with some remarkable differences. The coracoid of *Camptosaurus* is somewhat semi circular with a simpler morphology than in the hadrosaurids and the humerus is elongated, whereas in TMP2015.044.0036, the humerus is more robust with a very pronounced deltopectoral crest.

The pectoral girdle and forelimb musculature of another iguanodontid, *Iguanodon atherfieldensis*, was described by Norman (1986) based on muscle scars and the musculature of extant crocodilians. His findings are quite similar to the reconstruction presented here, and lend themselves to more extensive comparisons than do Carpenter and Wilson (2008) since Norman's (1986) descriptions are quite complete and the author reconstructs all muscles of the upper forelimb and shoulder. Muscles whose attachments are consistent between the present study and that of Norman (1986) are M. levator scapulae, M. serratus profundus, M. costocoracoideus, M.

latissimus dorsi, M. scapulohumeralis posterior, M. deltoideus scapularis, M. pectoralis, M. coracobrachialis, M. biceps, and M. brachialis. M. trapezius's position is similar in both *Iguanodon* and TMP2015.044.0036, but in *Iguanodon* its insertion is located along the scapular buttress, anterior to the insertion of M. levator scapulae. In *Iguanodon*, M. serratus superficialis is also reconstructed to insert on the medial surface of the scapula only, whereas in TMP2015.044.0036, it inserts on the ventral and lateral scapula. M. teres major is reconstructed similarly to *Camptosaurus* (Carpenter and Wilson 2008) in that it originates on the lower lateral scapula, ventral to the origin of M. deltoideus scapularis. This muscle then inserts in a common tendon with M. latissimus dorsi on the dorsal proximal humerus. In TMP2015.044.0036, M. teres major inserts vis its own tendon on the lateral humerus. Norman (1986) describes the origin of M. subscapularis as being much smaller than that reconstructed here, and on the ventral scapular neck. M. scapulohumeralis anterior is also described by Norman (1986) as inserting on the lateral shaft of the humerus whereas here, it is postulated to have a common insertion with M. deltoideus scapularis on the proximal part of the deltopectoral crest. M. supracoracoideus is shown in *Iguanodon* to insert on the proximal deltopectoral crest whereas in TMP2015.044.0036 it is reconstructed to insert on the distal deltopectoral crest. The largest difference is that in Norman's (1986) reconstruction, all five heads of the crocodilian M. triceps are conserved with an additional head on the posterolateral coracoid, and three heads originating on the humerus, two of which are similarly placed as in TMP2015.044.0036, but there is an additional site of attachment on the medial humerus between the insertions of M. deltoideus scapularis and M. subscapularis. Outgroup analysis by Dilkes (2000) states that two heads for M. triceps is decisively ancestral for the node Dinosauria, and so here TMP2015.044.0036 is reconstructed to possess only the two scapular and humeral heads. The most substantial difference in Norman's

(1986) paper from the present study is in placement of M. supracoracoideus which is reconstructed as attaching proximal to the deltopectoral crest whereas in TMP2015.044.0036 it is reconstructed on the ventral surface of the deltopectoral crest. However, this placement by Norman (1986) was attributed to a visible muscle scar on the proximal humerus above the deltopectoral crest, and states that this placement was uncertain. It is probable that this muscle scarring noted by Norman (1986) was due to a more extensive insertion for M. deltoideus scapularis rather than a separate site of attachment for M. supracoracoideus. In any case, the deltopectoral crest of *Iguanodon* is substantially less well developed than that of TMP2015.044.0036 so it is not surprising that there are anatomical differences in the attribution of this musculature. Furthermore, we have reconstructed M. deltoideus clavicularis and M. scapulohumeralis posterior as inserting on the proximal deltopectoral crest, while Norman reconstructs M. scpulohumeralis posterior in the same location as is inferred here on the posterior humerus proximally, Norman does not include M. scapulohumeralis anterior in their analysis claiming that it is absent from crocodilians and thus equivocal in *Iguanodon*. However, Norman does state that if it were present in *Iguanodon* it would undoubtedly occupy a similar position to that of M. deltoideus clavicularis, which is where we have placed it for TMP2015.044.0036.

This study mostly agrees with the findings of Lull and Wright (1942) for *Anatosaurus* (now *Edmontosaurus*), namely with regard to the anatomy of M. latissimus dorsi, M. pectoralis, M. deltoideus, M. brachialis, M. biceps, M. flexor carpi ulnaris, M. extensor carpi radialis, and M. extensor carpi ulnaris. However, Lull and Wright (1942) state that the origin of M. coracobrachialis is at the posteriormost dorsolateral edge of the coracoid, while here it is reconstructed as originating on the lateral surface of the coracoid, further anteriorly than

posteriorly but occupying most of the lower portion of the lateral surface of the coracoid. Lull and Wright (1942) also place the insertion of M. flexor carpi radialis on the radius as well as the carpus whereas, here it is reconstructed as only inserting on the metacarpus, as this study considers the carpals of hadrosaurids to be largely cartilaginous (see discussion in chapter 2). This was done following Dilkes (2000) who suggests that although insertion on the radius is ancestral for M. flexor carpi radialis in dinosaurs, the lack of muscle scarring on the radius, coupled with scarring on the metacarpals of *Maiasaura* and TMP2015.044.0036 suggest a possible shift of the insertion. Functionally, this may also have provided M. flexor carpi radialis with a longer moment arm about the wrist joint by extending the line of action (muscle trajectory) by several inches. Additionally, Lull and Wright (1942) describe an additional origin for M. triceps on the coracoid. Here, I conservatively place origins on the scapula and humerus of TMP2015.044.0036 to create a two-headed M. triceps as is suggested on the basis of phylogenetic bracketing by Dilkes (2000). Indeed, my findings strongly corroborate the reconstructed forelimb musculature of Dilkes (2000) for *Maiasaura* except for placement of the insertion of M. supracoracoideus and M. coracobrachialis which we reconstruct as more centered antero-posteriorly on the lateral coracoid rather than on the dorsal-most posterior and anterior edges, respectively. Dilkes attributed this placement to clear striations on the lateral coracoid for *Maiasaura* and as we have also used clear muscle scarring to assign these sites of muscle attachment it may simply be a taxonomical difference which would be corroborated by the overall shape difference between *Maiasaura* and TMP2015.044.0036. Specifically, the coracoid of *Maiasaura* is comparatively antero-posteriorly stretched with a markedly ventrally-hooked anterior coracoid process whereas TMP2015.044.0036's coracoid is antero-posteriorly compressed and more rounded overall. This yields less space on the lateral face of the coracoid

of TMP2015.044.0036 so it would make sense for these muscles to take origin closer together in TMP2015.044.0036 and for those of *Maiasaura* to be spaced further apart. In any case, as our methodologies for phylogenetic bracketing are extremely similar to that of Dilkes (2000) (ie a strong focus on the crocodilian and avian condition), the similarity in our muscular reconstructions is unsurprising and lends support to Dilkes' assessment.

The proposed arrangement of musculature for the forelimb of TMP2015.044.0036 supports the hypothesis that TMP2015.044.0036 was capable of walking quadrupedally and likely spent its life that way. Large attachment sites for stabilizing muscles such as M. subscapularis and M. rhomboideus as well as a close proximity of the scapula, coracoids, sternum, and presumably the ribs, suggest that the scapula mostly remained in place with little movement of the scapula-coracoid complex independent of the body. The highly ossified sternal plates in combination with the anterior ventral curve to the sternals in TMP2015.044.0036 would provide a robust attachment site for M. pectoralis which would insert on the highly developed deltopectoral crest. This arrangement would have enabled M. pectoralis to act as a powerful forelimb retractor, and to aid in propelling the body forward during locomotion. Unsurprisingly, attachment sites for the flexors and extensors of the wrist are small and few. The pillar-like structure of the metacarpals in TMP2015.044.0036 and most other hadrosaurids, lends support to the hypothesis that the metacarpus acted mainly to provide structural support rather than being capable of fine movements. Attachment of various flexor and extensor muscles to the proximal part of the metacarpus suggests some anterior-posterior movement of the manus. M. palmaris communis has small areas of insertion on unguals II to IV, suggesting that some flexion of these unguals may have been possible, but would be extremely limited given the proximity of the

adjacent phalanges. The forelimb of TMP2015.044.0036 appears to possess the biomechanical framework to support a massive quadrupedal herbivore.

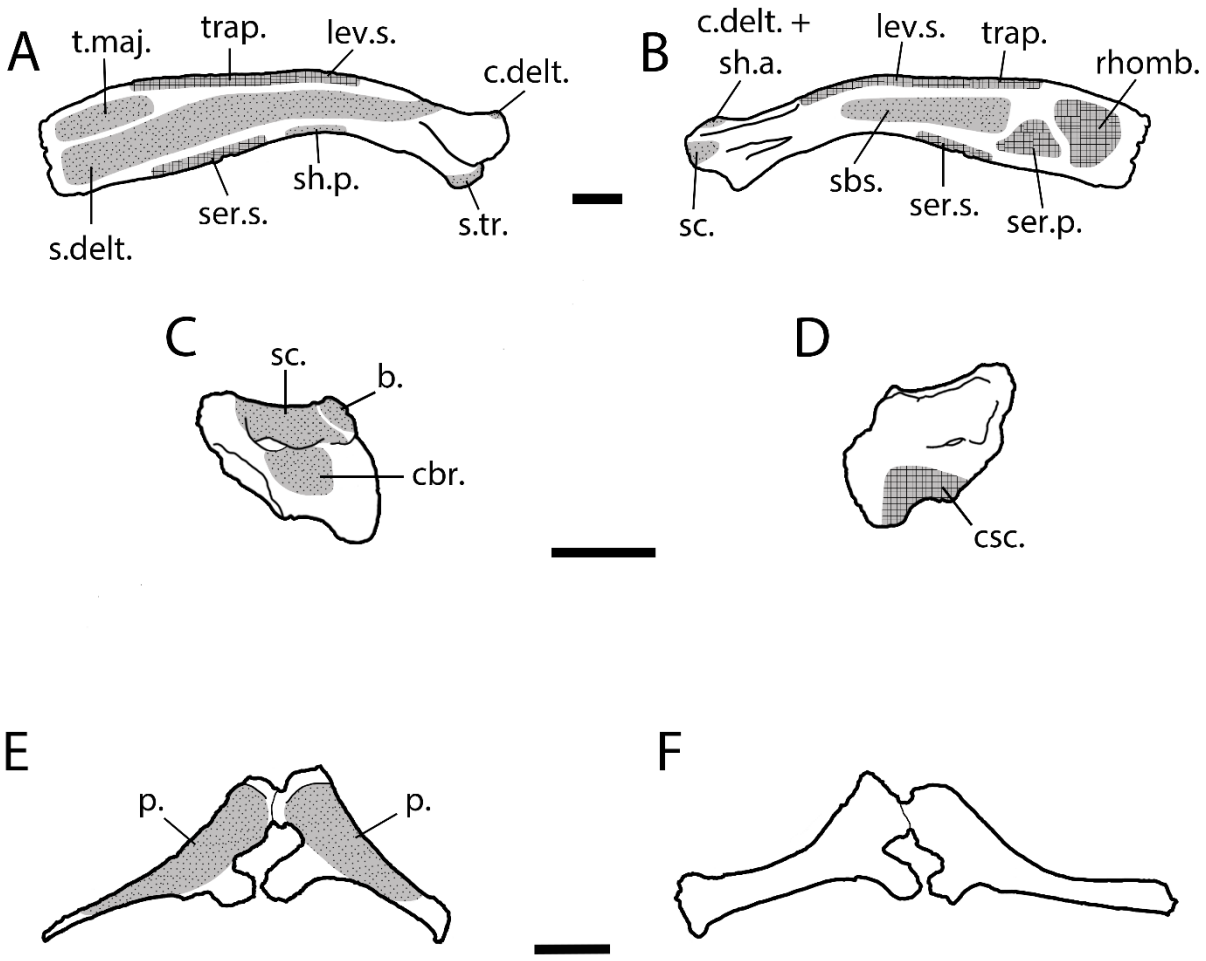

Figure 31. Restored muscle attachments of the shoulder girdle and thoracic region of TMP2015.044.0036. Right scapula in lateral (A) and medial (B) views; right coracoid in lateral (C) and medial (D) views; sternal plates in ventral (E) and dorsal (F) views. Scale bars = 10cm. Stippled areas denote muscle origins and cross-hatching denotes muscle insertions. **Abbreviations: b**, M. biceps brachii; **cbr.**, M. coracobrachialis; **c.delt.**, M. deltoideus clavicularis; **csc.**, M costocoracoideus; **lev.s.**, M. levator scapulae; **p.**, M. pectoralis; **rhomb.**, M. rhomboideus; **s.delt.**, M. deltoideus scapularis; **s.tr.**,M. triceps (scapular head); **sbs.**, M. subscapularis; **sc.**, M. supracoracoideus; **ser.p.**, M. serratus profundus; **ser.s.**, M. serratus superficialis; **sh.a.**, M. scapulohumeralis anterior; **sh.p.**, M. scapulohumeralis posterior; **t.maj.**, M. teres major; **trap.**, M. trapezius.

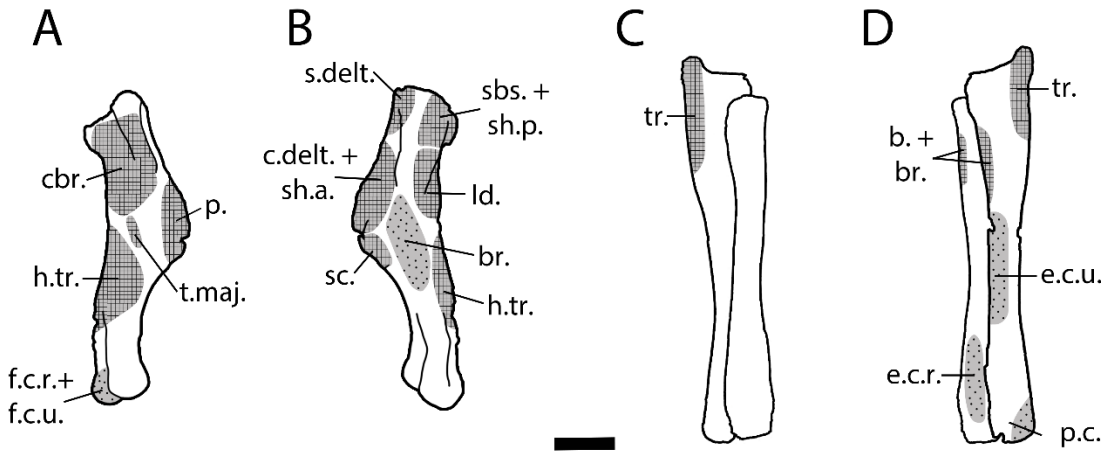

Figure 32. Restored muscle attachments of the right humerus, radiua, and ulna of TMP2015.044.0036. Right humerus in lateral (**A**) and medial (**B**) views; right radius and ulna in medial (**C**) and lateral (**D**) views. Scale bar = 10cm. Stippled areas denote muscle origins and cross-hatching denotes muscle insertions. **Abbreviations: b.**, M. biceps brachii; **br.**, M. brachialis; **c.delt.**, M. deltoideus clavicularis; **cbr.**, M. coracobrachialis; **e.c.r.**, M. extensor carpi radialis; **e.c.u.**, M. extensor carpi ulnaris; **f.c.r.**, M. flexor carpi radialis; **f.c.u.**, M. flexor carpi ulnaris; **h.tr.**, M. triceps (humeral head); **ld.**, M. latissimus dorsi; **p.**, M. pectoralis; **p.c.**, M. palmaris communis; **s.delt.**, M. deltoideus scapularis; **sbs.**, M. subscapularis; **sc.**, M. supracoracoideus; **sh.a.**, M. scapulohumeralis anterior; **sh.p.**, M. scapulohumeralis posterior; **t.maj.**, M. teres major; **tr.**, M. triceps.

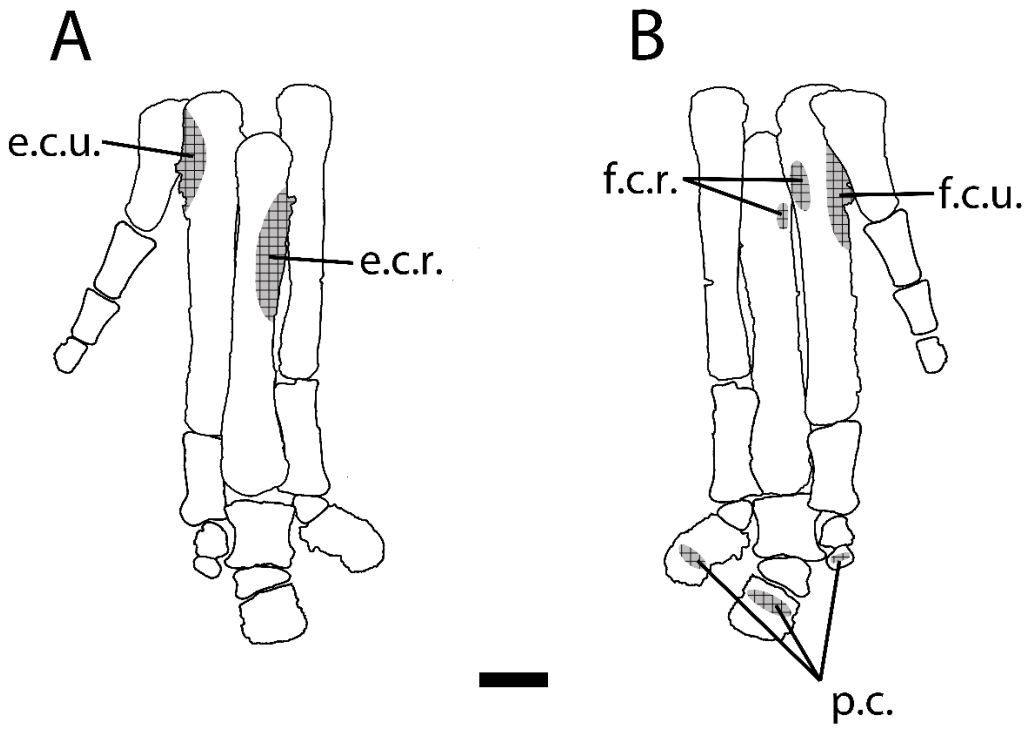

Figure 33. Restored muscle attachments of the manus of TMP2015.044.0036. Right manus in anterior (**A**) and posterior (**B**) views. Scale bar = 5 cm. Stippled areas denote muscle origins and cross-hatching denotes muscle insertions. **Abbreviations: e.c.r.**, M. extensor carpi radialis; **e.c.u.**, M. extensor carpi ulnaris; **f.c.r.**, M. flexor carpi radialis; **f.c.u.**, M. flexor carpi ulnaris; **p.c.**, M. palmaris communis.

Chapter 4. Range of motion analysis and muscle moment arm estimates for the forelimb and shoulder girdle of a lambeosaurine hadrosaurid

4.1 Introduction

Studying non-avian dinosaur gait and locomotion presents a unique challenge since their closest living relatives (birds, crocodilians, and lepidosaurs) differ drastically in osteology and myology from members of this extinct grade. Muscular anatomy can be inferred based on the extant phylogenetic bracket but determining how those muscles acted on the skeletal frame poses a more challenging problem. Using the principles of moment arm analysis, one can use muscular reconstructions of extinct animals to generate numerical data which can inform us of how effectively the linear force produced by a muscle can be converted to torque about a joint. By assessing the distance between an anatomical joint and the line of action of a muscle acting to produce rotation at that joint, we can generate an approximation of the torque that could be applied by that muscle. A large moment arm indicates a muscle attachment further away from the joint it is acting on, meaning greater leverage applied to that joint and a consequently greater force applied. This technique is particularly well suited to assessing the mechanics of extinct animals because it does not rely on precise knowledge of the morphology, especially cross-sectional area, and fibre orientation of those muscles, only of their attachments and trajectories, which can often be inferred with reasonable confidence and precision based on muscle scarring and comparisons to dissections of extant taxa. When combined with realistic constraints on range of motion about those joints, we can approximate how these animals moved, what muscles provided the most torque about joint axes for different movements and define limits on the extent of those movements.

Moment arm extrapolation and three-dimensional computational modelling techniques are relatively new approaches to assessing locomotor mechanics in extinct animals but are steadily increasing in popularity amongst functional paleo-anatomists (e.g., Sellers et al. 2009; Hutchinson and Allen 2009; Hutchinson 2011; Hutchinson et al. 2011; Bates et al. 2012; Maidment et al. 2014; Bishop et al. 2021). This technique has been applied to address many evolutionary queries such as: evaluating convergence in muscle moment arms between birds and basal ornithischians (Bates et al. 2021), gauging gait and anatomical position of appendicular elements in various dinosaur groups (Maidment et al. 2013; Sellers 2009), and assessing muscular and gait changes throughout the evolution of ornithischians (Maidment et al. 2014a; Maidment et al. 2014b). The evolution of quadrupedalism in ornithischian dinosaurs is especially interesting given that at least some early ornithischians like *Iguanodon* possessed forelimbs modified for grasping, as evidenced by a supinated manus preserved in trackways (Wright 1999; Maidment et al. 2014a) and even a spike-like pollex in *I. bernissartensis* specifically (Norman 1980; Maidment et al. 2014a). Quadrupedalism arose independently in the clade at least three times (Maidment and Barrett 2012). Muscle moment arm studies have historically mostly been performed on the pelvis of both saurischian and ornithischian dinosaurs (e.g., Hutchinson and Allen 2009; Bates and Schachner 2011; Maidment and Barrett 2011; Bates et al 2012; Maidment et al. 2013; Maidment et al. 2014), but moment arm analyses of the forelimb and pectoral girdle have only been presented for theropod dinosaurs (e.g., Senter and Sullivan 2019. This area of study is still relatively new, and more data are required to draw meaningful conclusions about locomotion and the evolution thereof in many dinosaur groups. However, this requires particularly well-preserved fossil material, since the process of fossilization inherently destroys much of the original shape, texture, and association of most fossils. TMP2015.044.0036, a newly

recovered set of complete forelimbs from a juvenile lambeosaurine hadrosaurid from southern Alberta, lends itself particularly well to three-dimensional computational modelling due to its exceptional preservation and completeness. In this chapter, I will assess the range of motion of the shoulder girdle, forelimb, and manus of TMP2015.044.0036, and use the reconstructed musculature of the forelimbs to estimate moment arms. This will add a new taxonomic group to the existing dataset of moment arm analyses that exists in the literature for ornithischian dinosaurs.

4.2 Methods

4.2.1 Three-dimensional model generation

An HDI Advance structured light scanner and Flexscan 3D (Polyga) software were used to generate a three-dimensional, digital mesh of each of the selected skeletal elements of TMP2015.044.0036 (Table 2). When both the right and left examples of a given element were present, the more intact of the two was selected for scanning. The posterolateral processes of the sternal plates of TMP2015.044.0036 extend dorsally at slightly different angles, even though neither process is obviously deformed or damaged. This, in conjunction with the practical difficulties that would accompany scanning either sternal plate separately, led to the decision to scan the sternal plates together to preserve the three-dimensional geometry of the sternum in its presumed natural midline contact and to protect the delicate fossils. Hole filling, digital retro-deformation of major damage to some bones, and reduction of file sizes of the models was done using the digital sculpting program ZBrush (Pixologic Inc) and the open-source three-dimensional creation suite Blender 2.83.1 LTS (the Blender Foundation). Digital reparation of

fossil elements and retro-deformation was guided by comparisons with other hadrosauroid forelimb elements in the literature (e.g. Sternberg 1935; Lull and Wright 1942; Cuthbertson and Holmes 1953; Ostrom 1963; Maryańska and Osmólska 1984; Brett-Surman 1989; Dilkes 2000; Egi and Weishampel 2002; Evans and Reisz 2001; Brett-Surman and Wagner 2007; Carpenter and Wilson 2008; Prieto-Márquez 2008; Prieto-Márquez 2010; Campione et al. 2014; Prieto-Márquez 2014) and from the collections and galleries of the University of Alberta Laboratory for Vertebrate Palaeontology (Edmonton, Alberta), Royal Tyrrell Museum of Palaeontology (Drumheller, Alberta), Royal Ontario Museum (Toronto, Ontario), and the Canadian Museum of Nature (Ottawa, Ontario).

4.2.2 Biomechanical setup

3D models of the pectoral girdle, arm, and hand of TMP2015.044.0036 were imported into Maya 2018 (© Copyright 2020 Autodesk Inc). When required, bones from the opposing side of the body were mirrored to create a complete and fully articulated right pectoral girdle and forelimb. Both right and left sternal plates were scanned together and placed in the model as one block. Articulation of the skeleton and creation of a moveable model of the pectoral girdle and forelimbs (Fig. 34) was done following Sullivan 2007. Each element was aligned along Maya's three-dimensional axis, of which one unit (grid square length) is equal to 51.56 mm, calculated after the final models were re-sized to fit into Maya's 3D space. On this coordinate plane, the anatomically anterior direction corresponds to the positive z axis and posterior the negative z axis. Dorsal is along the positive y axis, ventral the negative y axis. Medial to the body is along the positive x axis and lateral, the negative x axis. All final 3D meshes of each element were imported into Maya individually and their centroids were placed at the origin of the coordinate

system, with their distal ends directed towards the negative z axis. For each element, the command “center pivot” was applied to set the origin of the coordinate system as the centre of rotation and translation so that a controller could be created to record the position, translation, and rotation of each bone, quantifying its position in world space with respect to the grid origin after the skeleton was digitally re-articulated.

In the context of biomechanics, vertebrate skeletons can be divided into functional segments that move as units. Such segments can move with respect to one another at anatomical joints, but parts of any given segment remain fixed in place relative to one another. For example, the coracoid was digitally frozen at its articulation with the scapula, creating a functionally rigid segment due to the negligible movement between the scapula and coracoid. An anatomical joint is defined in this study as a centre of rotation that exists between articular surfaces of two adjoining body segments, or the centre of rotation of a segment itself. As described by Sullivan (2007), an anatomical joint in Maya is defined as the combination of three centres of rotation, each belonging to one Cardan axis. These are yaw (movement about the y axis), pitch (movement about the z axis), and roll (movement about the x) axis.

Modelling the movements of entire limbs requires the creation of joint chains in which the joints are arranged in a hierarchical relationship. For example, yaw, pitch, and roll of the pectoral girdle as a whole will, by default, move the entire limb together with the pectoral girdle itself. However, distal joints can also move independently of the more proximal ones that stand above them in the hierarchy: for example, movement of the wrist joint does not affect the elbow or shoulder. This hierarchy is created in Maya using a function called “parenting”, in which each joint becomes the “child” of the successively more proximal one and the “parent” of the successively more distal one (for further explanation see Sullivan 2007). The bones belonging to

each segment also become the children of the joints just proximal to them, so that, for example, the radius, ulna, and wrist joint are all treated as children of the elbow joint and are moved by translations and rotations of the elbow.

Articulation of the skeleton in Maya was done assuming the position of the bones in situ was an accurate approximation of their position in the living animal. To approximate this, quarry photos were examined, and each jacketed block of the skeleton was carefully photographed and measured. Blocks containing forearm and manus elements were 3D modelled via photogrammetry before being removed from the matrix. The sternum was collected separately from the forelimb so its positioning relative to the rest of the model was accomplished through comparisons with hadrosauroid sterna in the literature (e.g. Osborn 1912; Norman 1980; Dodson and Madsen Jr. 1981; Norman 1986; Forster 1990; Bultynck 1992; Carpenter and Wilson 2008; Wang et al. 2011; Campione 2014; Wang et al. 2017; Prieto-Márquez 2014; Verdú et al. 2017) and evaluation of extant archosaur sternal morphology from collections (UALVP, RTMP, CMN, ROM) and from the literature (e.g. Kälin 1929; Baumel et al. 1993; Cong et al. 1998; Sanders and Farmer 2012; Baier et al. 2018). Known and inferred respiratory physiology of extant and extinct archosaurs was also considered (e.g. Codd 2004; Schachner et al. 2009; Farmer 2015; Codd 2010). Further discussion on the evaluation of the sternum can be found in chapter 2. Step by step instructions showing the workflow for the creation of this model in Maya can be found in appendix A.

4.2.3 Range of motion analysis

During excavation, the scapula and coracoid were recovered separately from the humerus and thus an approximation of their natural articulation was necessary. The proximal-most margin of the humerus was set at an initial vertical distance of 77.34 mm (1.5 grid units) from the centre of the contact between the scapula and coracoid (also the origin in Maya) (Fig. 35). This placement was chosen to represent a minimum distance of the humeral head to the glenoid fossa as it was the shortest vertical distance from the glenoid where the proximal humerus could maintain a realistic amount of mobility. Since the addition of cartilage significantly increases the maximum humeral length in extant archosaurs (Holliday et al. 2010), a second set of measurements were done at an additional 41.88 mm (0.81 grid units) of vertical distance (a total of 119.22 mm) from the glenoid to the proximal margin of the humerus (Fig. 35). This increase was calculated based on an average 7.99% increase ($n = 15$; $p<0.01$) across multiple ontogenetic stages (sizes ranging from 0.5 m to 2.5 m total length) in maximum humeral length found for *Alligator mississippiensis* when cartilage was considered (Holliday et al. 2010).

Using the biomechanical model set up in Maya (Autodesk), where the animal displays a hypothetical resting phase of its step cycle (Fig. 34), with the forearm extending vertically downward from the glenoid, two separate range of motion analyses were performed for both estimated vertical distances (77.34 mm and 119.22 mm) of the proximal humerus from the glenoid. Maximum degrees of protraction, retraction, adduction, abduction, and long axis rotation were measured for the shoulder, elbow, and wrist joints (Fig. 36 – 43). The first analysis evaluated the maximum range of rotational movement permitted for body segments before colliding with another element (bone) (Table 3). The complete manus, radius, ulna, humerus, scapula, coracoid, and both sternal plates were present in the model during analysis. When this

analysis consistently yielded unrealistically high degrees of rotation (several above 360˚), a second analysis was performed that observed the maximum degrees of rotation permitted while articular surfaces remained in contact (Table 4). Once an articular surface "slipped" out of contact with that of an opposing bone, it was considered above the maximum threshold of movement. For each type of movement (protraction / retraction, adduction / abduction, long axis rotation), the smallest degrees of rotation from either "crashing" or "slipping" analyses were chosen for later moment arm extrapolation, as these represent the most likely range of motion in the living animal.

4.2.4 Muscle moment arm extrapolation

Muscle moment arm analyses were performed in SIMM 7.0 (Software for Interactive Musculoskeletal Modeling) motion analysis powered by Cortex™. The model used the same 3D meshes that were used in Maya for range of motion analyses, but these meshes were decimated and scaled down by a factor of 4.96 to achieve the small file sizes required by SIMM as the 3D space available in SIMM's animation window is limited to the dimensions afforded a fully functioning human musculoskeletal model. Articulation of the humerus with the scapula and coracoid required some assumptions. It is likely that the true vertical distance of the proximal humerus in the living animal would have fallen somewhere between the initial proposed distance of 77.34 mm based on the position of articular surfaces and the calculated maximum distance of 119.22 mm based on an average increase in crocodilian humeral length with the addition of cartilaginous caps (Holliday et al. 2010). However, as one cannot know the anatomy of the living animal and since the minimum distance of 77.34 mm yielded the most conservative range of motion estimates, this minimum value was selected for moment arm analysis. In any case,

moment arm lengths are calculated from the placement of muscle attachment points and any deviation from the proposed vertical distance of the humerus from the glenoid would change all moment arm lengths by the same vertical amount. As this would not change the direction of muscle action, assuming a vertical humeral distance of 77.34 mm from the glenoid is reasonable. Moment arm analysis was limited to the right shoulder (scapula, coracoid, humerus, sternal plates) of TMP2015.044.0036, and specifically to muscles that acted on the humerus: M. teres major, M. deltoideus scapularis, M. deltoideus clavicularis, M. subscapularis, M. scapulohumeralis posterior, M. triceps (scapular head), M. pectoralis, M. supracoracoideus, and M. coracobrachialis. A full description of how the shoulder musculature of TMP2015.044.0036 was reconstructed can be found in chapter 3. These muscles were placed on bone meshes in SIMM via attachment points and where necessary, additional attachment points and wrap objects were added to the model (Fig. 44). Wrap objects are digital meshes that can be manually placed within the model, for example over a bone surface, to act as barriers to muscle trajectories. This ensured that muscle trajectories would rest upon bone surfaces when at rest, and glide along the bone surface when in movement. Prior to the creation of wrap objects and additional attachment points, muscle trajectories would cut directly through bone meshes, decreasing moment arm lengths and generating data suggesting improbable directions of muscle action upon bones for their anatomical arrangement. Since this study estimated moment arm lengths only, muscles constructed in SIMM were limited to muscle paths and were not assigned any force parameters (Fig. 45). Bates et al. (2015) describe a correction required for similarly constructed pelvic models in GaitSym based on how the orientations of the axes of rotation used in the model may change relative to the pelvis. The flexion-extension axis maintains a consistent (lateromedial) orientation relative to the pelvis, but as the hip is flexed or extended, the axes of adduction-

abduction and long axis rotation pivot together with the limb. By contrast, SIMM inherently takes this information into account, pivoting the humerus at its proximal articular surface while automatically calculating moment arm trajectories across the shoulder joint, automatically accounting for changes in joint axis orientation. This was tested in SIMM by observing joint axis orientations as movements were performed. Motion files were created using the ranges of shoulder protraction/retraction, adduction/abduction, and long axis rotation estimated in this study. The range of motion results obtained in this chapter for the shoulder of TMP2015.044.0036 were used to create script-based motion files that could then be observed as animations in the SIMM model viewer. These motion files were then used to generate plots of moment arm length versus shoulder position for all recreated muscles. A detailed explanation of how the model was created in SIMM, together with the script used to construct the model, can be found in Appendix B.

4.3 Results

4.3.1 Range of motion results

A complete list of range of motion results can be found in Tables 3 and 4 (Fig. 35 – 43). The first range of motion analysis assessed the maximum degrees of rotation permitted before a bone crashed into another bone, marking a definite maximum of rotation (crashing model criteria). At a vertical humeral distance of 77.34 mm from the surface of the glenoid, the humerus could undergo a maximum of 26˚ of protraction, 13˚ of retraction, 76˚ of adduction, and 40˚ of abduction. Rotation about the long axis terminated at 70˚ of supination and 44˚ of pronation. At an increased vertical distance of 119.22 mm from the surface of the glenoid fossa, intended to account for the likely presence of a substantial cartilaginous cap on the humeral head,

the humerus could undergo a maximum of 224˚ of protraction, 34˚ of retraction, 66˚ of adduction, and 279˚ of abduction. Rotation along the long axis could reach a maximum of 242˚ of supination and 91˚ of pronation. Articulation of the radius, ulna, and manus was based on their associations observed during excavation and preparation as well as comparisons with the literature (see above). Using the crashing model criteria, the forearm (radius and ulna) was observed to rotate at the elbow joint to a maximum of 32˚ protraction, 92˚ of retraction, 41˚ of adduction, 13˚ of abduction, 148˚ of supination, and 122˚ of pronation. The manus yielded a range of motion of 42˚ of dorsiflexion, 79˚ of palmarflexion, 12˚ of adduction, 28˚ of abduction, 145˚ of supination, and 55˚ of pronation.

Several of the maximum angles of rotation obtained using the crashing model criteria are unrealistic for a living animal. Specifically, these were 224˚ of humeral protraction, 279˚ of humeral abduction, 242˚ of humeral long axis rotation medially, 148˚ of supination of the forearm (radius and ulna), 122˚ of pronation of the forearm, and 145˚ of supination of the hand. These movements would be physically impossible for the animal to perform without failure of the joint resulting in dislocation of the moving element from the joint that houses it. Consequently, the results obtained using the crashing model criteria were considered unreliable for use in any realistic moment arm analyses and alternate criteria were established for a separate range of motion analysis. This second analysis entailed careful observation of the joints as they performed each movement and taking note of the angle at which the proximal articular surface of the moving element lost contact with the articular surface of the opposing element, representing a dislocation of the moving element from the joint and thus failure of the joint. Using this slipping model criteria, the maximum degrees of humeral rotation permitted at a vertical distance of 77.34 mm from the glenoid, the maximum angle of humeral abduction decreased from 40˚

under the crashing model criteria to 26˚ under the slipping model criteria. All other values at this distance from the glenoid remained consistent across both analyses (26˚ of protraction, 13˚ of retraction, 31˚ of adduction, 34˚ of long axis rotation medially, and 63˚ of long axis rotation laterally). More substantial differences were observed in the maximum degrees of rotation permitted under the slipping model criteria at a humeral distance of 119.22 mm from the glenoid as compared to the crashing model. A single maximum rotation value of 91˚ of lateral long axis rotation remained consistent across both analyses, however all other results decreased considerably under the slipping model criteria. These alternate maximum angles of rotation were 44˚ of protraction, 10˚ of retraction, 44˚ of adduction, 41˚ of abduction, 64˚ of long axis, and rotation medially.

Under the slipping model criteria, maximum rotation of the forearm (radius and ulna) and manus was also reduced from the crashing model criteria for several movements. For the forearm, maximum angles obtained that were consistent with the crashing model criteria were protraction (32˚), adduction (41˚), and abduction (13˚). Degrees of retraction and long axis rotation decreased under the slipping model criteria resulting in 61˚ of retraction, 63˚ of supination, and 26˚ of pronation. For the manus, only maximum degrees of adduction (12˚) and abduction (28˚) remained unchanged from the crashing model criteria, while all other values decreased. These resulted in 34˚ of dorsiflexion, 32˚ of palmarflexion, 49˚ of supination, and 26˚ of pronation. These revised ranges of motion obtained using the slipping model criteria were selected for moment arm analysis.

4.3.2 Moment arm results

4.3.2.1 Moment arms through humeral protraction-retraction

For protraction moment arms in figures 44 to 47, a positive moment arm indicates a muscle functioning as a protractor of the humerus whereas a negative moment arm indicates a muscle functioning as a retractor of the humerus.

M. Pectoralis

As the humerus is retracted, the moment arms for protraction, adduction, and medial long axis rotation all plot in the negative quadrant (Fig. 46, 48). This indicates that for movement along the protraction-retraction axis, M. pectoralis functions as a retractor, abductor, and lateral rotator of the humerus. M. pectoralis also yields the highest moment arm values for retraction, abduction, and lateral rotation of the humerus for movement along the protraction-retraction axis. At full protraction (26˚ from vertical), M. pectoralis has a moment arm value of just over -0.25 m which remains constant until 60% humeral retraction, where the curve decreases slightly to a minimum of about -0.24 m. Overall, this suggests that M. pectoralis would transmit the greatest magnitude of retractive torque to the humerus during movement along the protraction-retraction axis than any other muscle of the shoulder. Though the initial moment arms for adduction and medial rotation begin somewhat small (-0.06 m and -0.12 m, respectively), they quickly increase to a peak of about -0.28 m halfway through retraction of the humerus, then decrease once again. This also yields the greatest moment arm values for adduction and medial retraction for this range of motion and suggests that M. pectoralis is largely responsible for much of these movements along the protraction-retraction axis. Oddly, the moment arm curve for rotation

abruptly increases at 90% humeral retraction and climbs past the zero-line indicating a shift from functioning as a medial to a lateral rotator at the maximum of retraction. However, at this point in the movement of the humerus, M. pectoralis comes into contact with a wrap object in SIMM and shifts position across the humeral shaft in an unnatural fashion. Therefore, this sudden shift in moment arm polarity will be dismissed as a limitation of the program.

M. Teres Major, M. deltoideus scapularis, M. subscapularis, M. scapulohumeralis posterior, and M. triceps (scapular head)

M. teres major, M. deltoideus scapularis, M. subscapularis, M. scapulohumeralis posterior, and M. triceps (scapular head) yielded very similar plot shapes with their moment arm magnitudes being the only remarkable difference between them (Fig. 46, 48). As this indicates similar function along the protraction-retraction range of motion, they will be discussed together.

Like M. pectoralis, M. teres major, M. deltoideus scapularis, M. subscapularis, M. scapulohumeralis posterior, and M. triceps (scapular head) plot entirely in the negative quadrant for the full range of motion in the protraction-retraction axis of the humerus. This suggests that like, M. pectoralis, these muscles all function as humeral retractors, abductors, and lateral rotators along this range of motion, though with approximately half the magnitude of M. pectoralis for the same movement. M. teres major, M. deltoideus scapularis, M. subscapularis, M. scapulohumeralis posterior, and M. triceps (scapular head) all display extremely similar curve trajectories for all three axes of movement (protraction, adduction, and medial rotation), with the rotation moment arm beginning small at full protraction then increasing steadily, whereas moment arm values for adduction and medial rotation display a less dramatic increase in value

but do still have a considerable slope to their curves. These curves all achieve peak moment arm lengths at 70% humeral retraction except for M. teres major which reaches a peak at 60% humeral retraction. At this point in the retraction cycle, the humerus is positioned in such a way that contraction of these muscles results in a posteriorly oriented pull on the humerus. Because of this, rotation moment arms values reach a peak then begin to decrease, while protraction and adduction moment arm values continue to increase slightly.

For the entire range of motion, M. teres major consistently has the greatest retractive, abductive, and lateral rotational moment arms other than M. pectoralis, indicating that M. teres major likely contributed to these movements significantly along the protraction-retraction axis, followed by M. triceps (scapular head), M. subscapularis, M. scapulohumeralis posterior, and finally M. deltoideus scapularis with the smallest moment arm values. The moment arm plot for M. deltoideus scapularis also displays a sudden shift in moment arm curve trajectory at 80% humeral retraction where the moment arm decreases suddenly from -0.1 m to -0.08 m. This shift was due to the muscle trajectory contacting a wrap object on the humeral head. This contact results in a sudden shifting of the muscle trajectory along the surface of the wrap object to the opposite side of the humeral head. As it is unlikely that a muscle would glide along the outer margin of the humeral head in a living, presumably quadrupedal animal, all moment arm results for M. deltoideus scapularis after 80% humeral retraction should be disregarded.

M. Deltoideus Clavicularis

For the complete range of protraction-retraction, M. deltoideus clavicularis moment arm values are low and positive (Fig. 46, 48), meaning that the torque potential of this muscle is the

lowest of the three muscles that act solely as extensors of the forelimb (including M. supracoracoideus and M. coracobrachialis). This makes sense given that the position of M. deltoideus clavicularis is restricted to the proximal-most humerus and the anterior-most scapula. Contraction of this muscle should only lead to protraction of the humerus with some abduction. Moment arm values decrease linearly with increasing retraction of the humerus, which fits well with this muscle functioning as an extensor of the humerus, since with greater retraction of the humerus, the moment arm increases, indicating a greater potential for this muscle to protract the brachium. This agrees with M. deltoideus clavicularis' muscular assessment in chapter 3 where its function was attributed mostly to protraction of the humerus.

While the forelimb is retracted, both the adduction and rotational moment arms of M. deltoideus clavicularis shift polarity indicating a shift in function. At maximum humeral protraction (26˚), M. deltoideus clavicularis yields negative moment arms suggesting that at until about 10% retraction, this muscle functions as an abductor of the humerus, then rapidly shift function to aid in adduction of the humerus. The angle of attachment on the humerus changes drastically with increasing retraction as it is placed very close to the humeral head medially, meaning that slight changes in elevation of the humerus will cause large changes in moment arm length. It is therefore reasonable to assume that this relatively short muscle would contribute mostly to stabilize the shoulder joint in resisting excess mediolateral movement of the proximal humerus and so the shift from functioning as a medial rotator and adductor to a lateral rotator and abductor with increased retraction would lend well to this stabilization.

M. Supracoracoideus and M. Coracobrachialis

Other than M. deltoideus clavicularis, M. supracoracoideus and M. Coracobrachialis are the only muscles to generate positive moment are results for protraction along the protraction-retraction movement, indicating function as a protractor of the humerus (Fig. 46, 48). These muscles are very close anatomically and show similar patterns in their moment arm plots, reflecting their similar function. M. supracoracoideus yielded the greatest moment arm values for humeral protraction remaining consistently about 0.02 m greater than M. coracobrachialis which has the second greatest moment arm values for humeral protraction. These muscles also both plot positively for rotation of the humerus, suggesting function as a medial rotator of the brachium along the protraction-retraction axis, with a decrease in rotational moment arm length after 60% humeral retraction. At 60% humeral retraction, both M. supracoracoideus and M. coracobrachialis shift from laying somewhat horizontally over the humeral head to being more vertically aligned as the humerus pulls the muscles ventrally. This results in M. supracoracoideus and M. coracobrachialis shifting from pulling posteriorly on the humerus to pulling dorsally which would explain this decrease to the moment arm lengths. These results agree with the earlier assessment of both M. supracoracoideus and M. coracobrachialis functioning as the primary protractors of the humerus.

Although M. coracobrachialis inserts onto the lateral humerus and M. supracoracoideus inserts onto the medial humerus, the adduction moment arm lengths generated through the protraction-retraction range of motion are quite similar (Fig. 46, 48). Both muscles plot in the negative at maximum protraction indicating they are functioning as abductors initially, then near 20% retraction both muscles abruptly shift in polarity to plot among the adductors, M. supracoracoideus being consistently greater on average by about 0.02 m. This is somewhat

counter-intuitive given their insertions on opposite sides of the humerus, but as the movement is limited to the axis of protraction-retraction (X axis in SIMM), and since their moment arms do plot with opposite polarity along the adduction-abduction axis (Z axis in SIMM), this strange curve geometry may be due to the close proximity of underlying wrap objects. In any case, one could assume from these results that the contribution of M. coracobrachialis and M. supracoracoideus to adduction or abduction while completing movement along the protraction-retraction axis is negligible.

4.3.2.2 Moment arms through humeral adduction-abduction

For adduction moment arms in figures 44 to 47, a positive moment arm indicates a muscle functioning as an adductor of the humerus whereas a negative moment arm indicates a muscle functioning as an abductor of the humerus.

M. Pectoralis

For movement along the adduction-abduction axis (z axis in SIMM), M. pectoralis yields the largest adduction and protraction moment arms, much like movement along the protraction-retraction axis (Fig. 47, 49). M. pectoralis consistently plots in the negative values for protraction, indicating function as a retractor for the full range of motion. Not only does this agree with earlier assessment based on muscular reconstruction, but also makes intuitive sense given that the muscle is anchored onto the central sternal plates and contraction of the muscle should consistently pull the humerus towards the body. These results reflect this and suggest that M. pectoralis provided the most protractive torque through the shoulder joint to the humerus of

any other shoulder muscles. Moment arms also reach a peak in protractive potential at 40% abduction where the humerus is completely vertical (0˚ adduction or abduction), then gradually decreases in moment arm length as the shoulder is further abducted.

M. pectoralis displays the most variable adduction moment arm lengths for movement along the adduction-abduction axis. At maximum adduction (26˚), M. pectoralis has a moment arm of -0.26 m indicating function as an abductor. This value deceases steadily until the humerus is once again resting vertically (0˚ protraction or retraction) where it crosses over the zero line, suggesting a shift from abductive potential to adductive potential where it once again yields the highest moment arm results of any other adductor. This result is anatomically sound since at full adduction, the origin of M. pectoralis on the sternum is lateral to the humerus, so contraction of M. pectoralis should result in lateral pulling of the humerus. The reverse is true for full abduction where the origin of M. pectoralis lies medially to its insertion on the humerus, meaning that contraction would result in medial pulling (adduction) of the humerus.

For rotational movement, M. pectoralis plots exclusively as a medial rotator with comparatively high rotational potential towards the extremes of adduction and abduction. At 0˚ of adduction or abduction, M. pectoralis remains negative, indicating potential for medial rotation, albeit of minimal magnitude. Therefore, it is likely that M. pectoralis contributed to medial rotation of the humerus while the forelimb was adducted or abducted but at resting position with the humerus oriented vertically M. pectoralis would not have been a particularly useful rotator.

M. Teres Major

For movement along the adduction-abduction axis (Z axis in SIMM), M. teres major yields the largest retractive moment arms, second only to M. pectoralis (Fig. 47, 49). This value remains steady at about -0.176 m for the entire range of motion which is unsurprising as the length of the muscle and the joint angle in the protractive-retractive axis if movement do not change as maximum adduction-abduction is completed. Rotational moment arm values for M. teres major also remain consistent at -0.027 m, making it the second largest lateral rotator in this plane of movement aside from M. deltoideus scapularis. M. teres major also plots as a minor abductor of the humerus, crossing the zero line toward maximum abduction. As this muscle inserts onto the lateral proximal humerus further dorsally than anteriorly, it seems realistic that this muscle would contribute minimally to humeral abduction and that the amount of abductive torque it would provide should decrease with increasing adduction, which is what can be observed on the moment arm plot. These findings agree with the assessment made in chapter 3 that M. teres major would function primarily as a retractor of the humerus.

M. Deltoideus Scapularis

All moment arm values for M. deltoideus scapularis along the adduction-abduction plane of movement generated negative results indicating that this muscle is functioning as a very minor retractor, a moderate abductor, and a comparatively strong lateral rotator (Fig. 47, 49). These results are consistent with our muscular assessment in chapter 3, however it is interesting to find such comparatively high moment arm values for rotational movement. M. deltoideus clavicularis wraps around a significant portion of the proximal humerus from its insertion on the medial

humerus, along the anterior edge, and much of the lateral humerus. It is almost certainly this high degree of muscular wrapping that accounts for the great rotational potential since contraction of this very long muscle would generate a very great lateral pull of the proximal humerus compared to the other muscles of the shoulder.

M. Deltoideus Clavicularis

For movement along the adduction-abduction plane (z axis in SIMM) M. deltoideus clavicularis consistently plotted as a protractor, abductor, and lateral rotator of the humerus (Fig. 47, 49). This is consistent with its assessment in chapter 3 to be a powerful protractor, however, for adduction-abduction movements M. deltoideus clavicularis has the smallest moment arm estimates (~0.01 m) than both other protractors of the humerus, M. supracoracoideus (~0.06 m) and M. coracobrachialis (~0.04 m). This is also true for movement in the protraction-retraction range of motion, though at maximum protraction M. deltoideus clavicularis does yield a slightly higher moment arm by about 0.01 m. Given its comparatively short muscle trajectory and its attachment site very close to the proximal edge of the humerus, these small moment arm values are to be expected, however it is interesting that M. deltoideus clavicularis has some of the greatest moment arm results for humeral abduction, M. triceps (scapular head) being the only muscle to yield a larger abduction moment arm. This suggests that M. deltoideus clavicularis may have contributed more to humeral abduction than was assumed during initial muscular reconstruction.

M. Subscapularis and M. Scapulohumeralis Posterior

M. subscapularis and M. scapulohumeralis posterior yielded very similar moment arm results for movement along the adduction-abduction axis (Fig. 47, 49). These muscles consistently plotted as retractors, abductors, and medial rotators of the humerus. Given their close attachment sites this is expected. Moment arm values for retraction are moderate comparatively, indicating they were likely not heavily involved in protraction but were able to assist in provided protractive torque through both protraction-retraction and adduction-abduction movements. Abduction moment arms were small, and suggest only minimal involvement in this movement of the humerus. For rotational movement, however, M. subscapularis and M. scapulohumeralis yielded the highest medial rotation moment arms of any other muscles other than M. pectoralis at maximum adduction (31˚), and maximum protraction (26˚). This suggests that M. subscapularis and M. scapulohumeralis were not only stabilizers of the shoulder, but were the primary medial rotators.

M. Triceps (scapular head)

M. triceps (scapular head) plotted similarly to M. subscapularis and M. scapulohumeralis for humeral retraction and abduction, though M. triceps has a greater abduction moment arm even than that of M. deltoideus clavicularis while the humerus is adducted even slightly (Fig. 47, 49). Given that M. triceps attached on the posterior lateral humeral shaft it is in a good position to draw the humerus medially, and these results are consistent with M. triceps' assignment as a major humeral adductor. M. triceps also shows the second lowest lateral rotation moment arm

results in this plane of movement, indicating it could have assisted in lateral rotation of the humerus but was likely not a primary function of this muscle.

M. Supracoracoideus

For the range of humeral adduction-abduction, M. supracoracoideus yields the largest moment arm results for humeral protraction, remaining steady at approximately 0.06 m for the entire range of motion (Fig. 47, 49). It also had consistent values (~0.01 m) for humeral adduction, being the only muscle to plot as an adductor while the humerus is adducted even slightly. For rotational movement, M. supracoracoideus has fairly low moment arm values for medial rotation of the humerus (<0.01 m). This agrees with our initial muscular assessment since its contribution to rotational movement was likely negligible, and its primary function was probably as one of the main protractors of the humerus. This muscle originates on the lateral coracoid which, when articulated with the forelimb, is oriented diagonally so that the origin of M. supracoracoideus is directly anterior to the scapula on the coracoid. Its insertion on the anterior deltopectoral crest makes this muscle's trajectory nearly vertical dorsoventrally, and would presumably allow for a good amount of protractional torque about the shoulder joint.

M. Coracobrachialis

M. coracobrachialis has an interesting trajectory as it originates on the lateral coracoid then wraps around the proximal humerus to insert on the lateral deltopectoral crest (Fig. 44, 45). From this geometry one would expect this muscle to be involved in protraction and medial rotation of the humerus, which is consistent with moment arm results in the adduction-abduction

plane of movement. M. coracobrachialis has minimal moment arm values for medial rotation of the humerus but does increase slightly when the humerus is abducted (Fig. 47, 49). This suggests that during adduction, the contribution of M. coracobrachialis to medial rotation of the humerus is negligible, but when abducted it may lend some assistance in medial rotation as a secondary function to its primary role as a protractor of the humerus. M. coracobrachialis has the second highest protractive moment arm results (about 0.04 m), and has small (~0.05 m) moment arms for humeral abduction which decreases with increased abduction.

4.3.2.3. Axial rotation moment arms

For long axis rotation moment arms in figures 44 to 47, a positive moment arm indicates a muscle functioning as a medial rotator of the humerus whereas a negative moment arm indicates a muscle functioning as a lateral rotator of the humerus.

Lateral Rotators

Axial rotation was not assessed as an individual movement like protraction-retraction and adduction-abduction, as this type of movement is typically utilized in conjunction with other movements and not completely on its own. Nonetheless, medial and lateral rotational moment arms were assessed as part of the protraction-retraction and adduction-abduction movements (Fig. 46 – 49). For both planes of movement (X and Z axis), four muscles consistently plot within the negative quadrant indicating function as lateral rotators. These, in order from highest moment arms to lowest were: M. deltoideus scapularis, M. teres major, M. triceps (scapular head), and M. deltoideus scapularis. M. teres major and M. deltoideus scapularis maintained consistent moment arm values (0.035 m and 0.06 m, respectively), and yielded the largest

moment arm values of the lateral rotators. M. deltoideus clavicularis and M. triceps (scapular head), showed very slight fluctuation in moment arm values during humeral adduction / abduction (~0.01 m and ~0.015 m). However, during humeral protraction / retraction, M. deltoideus clavicularis and M. triceps begin with moderately large moment arms at full humeral protraction (26˚, 0.027 m and 0.03 m, respectively), then decrease linearly with increasing humeral retraction. At full retraction, these muscles yield comparatively small moment arms, both less than 0.01 m. One other muscle, M. coracobrachialis, plots within the range of lateral humeral rotators (~0.01 m), however this value decreases linearly with increasing retraction and at rest (0˚ protraction / retraction), it crosses the zero line indicating a shift to functioning as a medial rotator. Given that this muscle wraps over the proximal humerus, as discussed above, this shift is not surprising as the orientation of the humerus will drastically change the orientation of muscle pulling on the lateral humerus. During humeral adduction / abduction, M. coracobrachialis begins on the zero line at full adduction (31˚), and does increase in moment arm length during abduction but even at its maximum (~0.006 m) still has the smallest medial rotator moment arms than any other muscle.

Medial Rotators

As discussed above, M. scapulohumeralis posterior and M. subscapularis yield the largest consistent moment arm values, especially during humeral adduction and abduction (Fig. 46 – 49). During these movements both muscles' moment arm values remain steady at about 0.042 m. At full protraction (26˚), moment arms for both M. scapulohumeralis posterior and M. subscapularis initially yield moment arms of about 0.03 m, then increase linearly to about 0.05 m at full retraction (13˚), which is likely due to the angle of the humerus relative to the scapula

decreasing, functionally lowering the sites of attachment of these muscles on the humerus and increasing the moment.

As mentioned above, M. coracobrachialis plots as a medial rotator at full abduction (31˚), but only minimally (~0.006 m). M. supracoracoideus also yields moment arm results within the medial rotator range (positive quadrant), remaining stable during adduction / abduction (~0.008 m), but fluctuating during humeral protraction / retraction. At maximum protraction (26˚), M. supracoracoideus has a moment arm values of ~0.015 m and decreases steadily until maximum retraction (13˚) where it reaches a minimum moment arm of ~0.005 m). Similar to M. coracobrachialis, this is likely due to a degree of muscle wrapping along the anterior humerus during high protraction, and elongation of the muscle during retraction.

M. pectoralis also plots as a medial rotator except for at 80% to 100% retraction where it crosses the zero line to function as a comparatively low valued lateral rotator. As discussed above, this seems improbable for M. pectoralis given its origin on the anterior sternum and insertion on the medial humerus. It is possible that this result was caused by interaction with a wrap object on the posterior humeral shaft, shifting M. pectoralis' position to the lateral side of the humerus which would, clearly, not have been the case in a living animal. In any case, M. pectoralis yielded comparatively very large moment arms for humeral retraction and adduction so function as a medial rotator was likely secondary to those primary functions, but would have been particularly efficient at transmitting medial rotational torque about the shoulder joint when the humerus is protracted or at high degrees of adduction or abduction.

4.4 Discussion

Plausibility of Range of Motion

The ranges of motion observed in this analysis help to constrain the degrees of movement possible for much of the forelimb of TMP2015.044.0036 (Table 4). As discussed above, under the crashing model criteria several ranges of motion obtained were unrealistically high (Table 3). Specifically, these were humeral protraction (224˚), abduction (279˚), and medial rotation (242˚), antebrachium medial (148˚) and lateral (122˚) rotation, and manus medial rotation (145˚). This is unsurprising given that the model used here for range of motion could not account for soft tissues (muscles, tendons, ligaments), aside from a hypothetical cartilaginous cap on the proximal humerus. In living animals, the influence of soft tissues on the joint range of motion is variable and seems to be dependent on the type of joint, specifically hinge / ball and socket or gliding (Hutson and Hutson 2014), and the nature of the movement being performed (flexion, adduction, or rotation) (Safran et al. 2013; Han et al. 2020). Within the extant phylogenetic bracket of dinosaurs specifically, soft tissues have been shown to limit ranges of motion that are otherwise much larger when the soft tissue is removed from the bone (Hutson and Hutson 2014; Han et al. 2020). However, it has also been shown that the addition of soft tissues, cartilage in particular, to the extant archosaurian elbow and shoulder repeatedly yields a larger range of motion than "bare-bones" models (Lipkin and Carpenter 2008; Hutson and Hutson 2012; Hutson and Hutson 2013; Senter and Sullivan 2019), suggesting that range of motion analyses on the elbow and shoulder of extinct archosaurs are typically underrepresenting the range of motion *in vivo*. However, it is important to note that these models are presumably based on the criterion of slipping as opposed to crashing. Further study in this area will be required to understand to what

degree this occurs across Archosauria before limitations can be confidently applied to extinct representatives.

Although soft tissues were also not considered for range of motion analysis under the "slipping model" criteria, range of motion estimates were much more reasonable, and comparative studies with extant archosaurs generally agree that this sort of analysis constrained by articular surfaces losing contact with one another in "bare-bones" models do give a realistic estimate of joint range of motion in specimens for which soft tissues cannot be recreated (Hutson and Hutson 2012; Hutson and Hutson 2013; Senter and Sullivan 2019), though additional cartilaginous surfaces may increase this range. Under the slipping model criteria, humeral movements were limited to 57˚ total of mediolateral swing (adduction-abduction), 39˚ total of antero-posterior swing (protraction-retraction), and 97˚ total of rotational movement (Fig. 35 – 39). Antebrachial (radius and ulna) movements were evaluated at 93˚ total of antero-posterior swing (protraction-retraction), 54˚ of mediolateral swing (adduction-abduction), and 87˚ of rotational movement (Fig. 40, 41). Of these, only adduction of the ulna and radius seem somewhat unrealistic. This may be due to the olecranon process, which is small in comparison with other hadrosaurid ulnae, indicating that the olecranon may constrain the limits of motion further. It is also possible that the olecranon is simply underdeveloped in TMP2015.044.0036 as it is presumably a juvenile to sub-adult individual. In any case, muscular assessment (chapter 3) shows that the musculature of the antebrachium and manus was not particularly robust and would be accompanied by long tendons and ligaments that would span the lateral and medial elbow (specifically those of M. triceps, M. biceps brachii, and M. brachialis) thereby limiting this range drastically. Finally, the manual range of motion was found to have a total of 66˚ of antero-posterior swing (protraction-retraction), 54˚ of antero-medial swing (adduction-

abduction), and 87˚ of rotational movement (Fig. 42, 43). Of course, the possibility of cartilaginous carpals in the wrist could change this assessment but as no credible carpal material, ossified or otherwise, has been recovered for hadrosaurids (see discussion in chapter 2), this is speculative at best.

Though range of motion analyses for hadrosaurid forelimbs are rare, range of motion results obtained here are somewhat similar to results obtained by Carpenter and Wilson (2008) for *Camptosaurus.* However, TMP2015.044.0036 shows a greater range of humeral protraction-retraction than *Camptosaurus* and a much smaller range of antebrachial protraction. Degrees of manual rotation in TMP2015.044.0036 is consistent with that of *Camptosaurus.* The reconstructed posture of *Camptosaurus* is interpreted by the authors as necessarily quadrupedal like that of TMP2015.044.0036, though differs from TMP2015.044.0036 by having a partially sprawling gait and a manus that is necessarily supinated (Carpenter and Wilson 2008). These variations are to be expected since *Camptosaurus* is an early ornithopod, showing an anatomical arrangement of the forelimb that appears almost transitionary from the basal iguanodontian form to that of hadrosaurids proper.

Senter and Sullivan (2019) suggest that a limited range of motion for the elbow and shoulder are plesiomorphic for Dinosauria as this condition is seen in non-coelurosaurian theropods (Carpenter 2002; Carpenter and Robins 2005; Senter and Sullivan 2019), basal sauropodomorphs (Bonnan and Senter 2007; Langer et al. 2007), and basal ceratopsians (Senter 2007), while greater ranges of motion can be observed for the elbow in later coelurosaurs (Gishlick 2001; Carpenter 2002; Senter 2006b) and at least one quadrupedal ceratopsian (Senter 2007), and a larger range of humeral protraction observed in dromaeosaurids (Senter 2006b), and humeral elevation seen in paravians (Senter 2006), ornithomimids (Senter 2006c), and

quadrupedal ceratopsians (Senter 2007). The condition seen in TMP2015.044.0036 agrees with the assessment of Senter and Sullivan (2019) as it represents a Late Cretaceous hadrosaurid whose elbow and shoulder range of motion is greater than that observed in these earlier archosaurs, especially for humeral protraction. However, Senter and Sullivan (2019) attribute this greater range of humeral motion to a laterally oriented glenoid and argue that the sprawling gait of crocodilians and lizards reflects this plesiomorphic condition. This makes sense for sprawling animals like crocodilians or bipedal, potentially flapping animals like paravians, but does not account for those organisms for which the glenoid is ventrally oriented and adopt a quadrupedal stance as is the case for most, if not all, hadrosaurids. I therefore agree that TMP2015.044.0036's greater ability to protract the humerus and extend the elbow is reflective of a derived condition but via a separate evolutionary mechanism where the glenoid remains oriented ventrally and the simple act of straightening the forelimb (as opposed to a laterally oriented glenoid) allows for a much larger range of motion of the shoulder and elbow simply because there is less bony material restricting movement.

Implications of Moment Arm Estimates for Lambeosaurine Shoulder Musculature

Moment arm estimates for the shoulder musculature of TMP2015.044.0036 presented here (Fig.46 – 49) largely agrees with the muscle functions hypothesized in chapter 3. This not only lends support to the proposed muscular arrangement for TMP2015.044.0036, but also reinforces the idea that carefully created biomechanical models can provide an accurate approximation of the musculoskeletal arrangement of extinct animals. Although high or low moment arm values do not necessarily imply low or high strength of a muscle (Bates et al. 2012), moment arm values can be a useful guide to what a particular part of the musculoskeletal system

is well-adapted to do, as they provide an estimate of the magnitude of torque that could be transmitted across a joint. Moment arm estimates for TMP 2015.044.0036 using inferred musculature from chapter 3 yield a very reasonable model for the shoulder mechanics of a large, quadrupedal animal. During forward locomotion, the forelimb must be raised off the ground and swung forward. Then, as the opposing limb is swung forward, the original limb must bear the weight of the body while simultaneously propelling this mass forward. It then follows that the musculature involved in protracting the forelimb would not necessarily require the same degree of strength or rotational torque as would be required for muscles that retract the forelimb. This is reflected in the comparatively low moment arm lengths of the muscles that plot as protractors of the forelimb. In fact, the muscle with the highest retractive moment arm values, M. pectoralis, has a moment arm length on average of five times greater than that of the muscle with the largest protractive moment arm, M. supracoracoideus, over the course of a complete stride cycle (Fig. 46, 48). M. pectoralis clearly plays a crucial role in the step cycle as reconstructed for TMP2015.044.0036, yielding high moment arm lengths for retraction, medial rotation, and both adduction and abduction of the humerus. Comparison with the extant phylogenetic bracket (chapter 3) suggests that M. pectoralis functions as a primary retractor and adductor of the humerus. These findings agree with this assessment, though the high abductive moment arms values generated while the humerus is adducted suggests that M. pectoralis acts as a stabilizer for the humerus in counteracting excessive mediolateral movement rather than functioning only as an adductor. Though cross-sectional area of these muscles cannot be estimated with any amount precision, it is likely that M. pectoralis would have been one of the largest muscles of the shoulder of TMP2015.044.0036 and certainly the most powerful of the humeral retractors. With M. pectoralis providing much of the retractive force to propel the body forward, moment arm

analysis suggests that M. teres major, M. triceps (scapular head), M. subscapularis, M. scapulohumeralis posterior, and M. deltoideus scapularis would also have assisted in humeral retraction rather significantly (Fig. 46, 48), M. teres major in particular having the largest retractive moment arms of these. Humeral protraction would then be achieved primarily via contraction of M. supracoracoideus with assistance from M. coracobrachialis and to a lesser extent, M. deltoideus clavicularis.

As mentioned previously, M. pectoralis yields the highest moment arm lengths for humeral adduction and abduction for movement in the adduction-abduction range of motion (Fig. 47, 49). It is unclear if this muscle was primarily responsible for these movements, but given its clear role in retraction and medial rotation of the humerus, it is likely that M. pectoralis functioned in stabilization of the shoulder as a secondary function only. Nonetheless, phylogenetic bracketing suggests that M. pectoralis would significantly assist in humeral adduction and the high moment arm values seem to agree. Furthermore, the only other muscle to plot as a humeral adductor is M. supracoracoideus which has consistently very low moment arm lengths (Fig. 47, 49). Muscles that plot within the range of humeral abductors (M. triceps, M. deltoideus clavicularis, M. scpulohumeralis posterior, M. coracobrachialis, M. deltoideus scapularis, M. subscapularis, and M. teres major) all maintain low moment arm lengths (<0.05 m) (Fig. 47, 49). Of these, only M. deltoideus scapularis was hypothesized to contribute to humeral abduction during muscular reconstruction. It is possible that as a quadrupedal animal, there may not be a need for much humeral adduction or abduction so this musculature may simply remain undeveloped in lambeosaurines.

Of the muscles associated with rotation of the humerus, M. subscapularis and M, scapulohumeralis posterior consistently generate the largest moment arm values for medial

rotation with M. supracoracoideus and M. coracobrachialis yielding minimal medial rotator moment arm length (Fig. 46 – 49). M. pectoralis also seems to be capable of some degree of medial rotation of the humerus. M. supracoracoideus and M. coracobrachialis plot as clear primary protractors of the humerus so any involvement in medial rotation is likely secondary or negligible. For lateral rotation, M. deltoideus scapularis and M. teres major yield the largest moment arm lengths while M. deltoideus clavicularis and M. triceps also plot as lateral rotators. However, given that these muscles yield the largest moment arms for humeral abduction, any role they play in humeral rotation is likely minimal.

Postural Implications for Lambeosaurinae

The range of motion and moment arm estimates found for the forelimb and shoulder of TMP2015.044.0036 would be well suited to a facultatively bipedal animal. Ranges of humeral protraction and retraction limit the orientation of the humerus to just above sub-vertical with an inability to protract or retract the humerus above this level. A moderately greater range of motion was found for the elbow of TMP2015.044.0036 (Table 4; Fig. 40, 41), extending the reach of the forelimb which would result in long forward oriented strides that are supported by robust shoulder musculature, particularly M. pectoralis providing powerful retractive force and M. supracoracoideus and M. coracobrachialis providing humeral protraction. Range of motion and moment arm estimates suggest that humeral adduction and abduction would have been severely limited by both osteological interruption and a lack of particularly well-developed muscles associated with these movements. This further supports the hypothesis that forelimb movements in hadrosaurid dinosaurs would be limited to mostly anterior-posterior swing of the arm.

The osteology of the manus of TMP2015.044.0036 suggests limited mobility of the hand in hadrosaurids. The metacarpals are arranged in a column-like structure, with metacarpal III sitting above metacarpals II and IV (Fig. 34). The bones of the digits rest against one another and this pillar-like structure of the manus as a whole in addition to the distal phalanges being modified into hooves suggests that the manus was not particularly useful as anything other than a weight bearing structure and would certainly not have had the flexibility to perform even the most basic grasping movements. The manus of TMP2015.044.0036 shows a range of 66˚ degrees total of dorsiflexion and palmarflexion (Fig. 43), which raises the possibility that the manus may have had the potential to be used for scratching or digging at the ground, or perhaps for leaning against surfaces when the animal reared onto its hindlimbs. However, without further comparison to extant animals that display these behaviours or more extensive modelling of the range of motion and force capabilities of the manus itself this is entirely speculation.

The forelimbs of hadrosaurids are much smaller than the hindlimbs in both length and robustness. This has been largely attributed to their putative secondarily bipedal condition (Carrano 2001; Maidment and Barrett 2012; Maidment and Barrett 2014). Nevertheless, these comparatively small forelimbs present a potentially stressful biomechanical condition on the forelimbs in that they must bear a potentially disproportionate amount of body mass on the forelimbs, seemingly implying that these animals might have possessed at least some degree of bipedalism. However, I would argue that the very robust and massive tail that is common for all hadrosaurids would have acted as a counterbalance to reduce the amount of mass distributed to the forelimbs, as suggested for *Camptosaurus*, a non-hadrosaurid hadrosauroid, by Gilmore (1909) and corroborated by Carpenter and Wilson (2008). Therefore, though this study cannot confidently assign TMP2015.044.0036 as entirely quadrupedal, it suggests that a quadrupedal

stance would have easily been supported by the skeletal framework and proposed muscular arrangement, and that adopting a bipedal stance regularly would not have been incredibly beneficial for anything other than potentially rearing up to gain a height advantage which may have been useful in niche partitioning.

Table 2. List of skeletal elements laser scanned from TMP2015.044.0036 with Flexscan 3D (copyright © 2019 Polyga). Digital retrodeformation was done in ZBrush (copyright © 2020 Pixologic Inc).

Element	side scanned	digitally retrodeformed
Scapula	right	yes
Coracoid	right	yes
Sternal Plates	both	no
Humerus	left	yes
Radius	right	no
Ulna	right	no
Metacarpal II	left	no
Metacarpal III	right	no
Metacarpal IV	right	no
Metacarpal V	left	no
Digit II Phalanx I	left	no
Digit II Phalanx II	left	no
Digit II Phalanx III	left	no
Digit III Phalanx I	left	no
Digit III Phalanx II	right	no
Digit III Phalanx III	right	no
Digit IV Phalanx I	left	no
Digit IV Phalanx II	left	no
Digit IV Phalanx III	left	no
Digit V Phalanx I	left	no
Digit V Phalanx II	left	no
Digit V Phalanx III	left	no

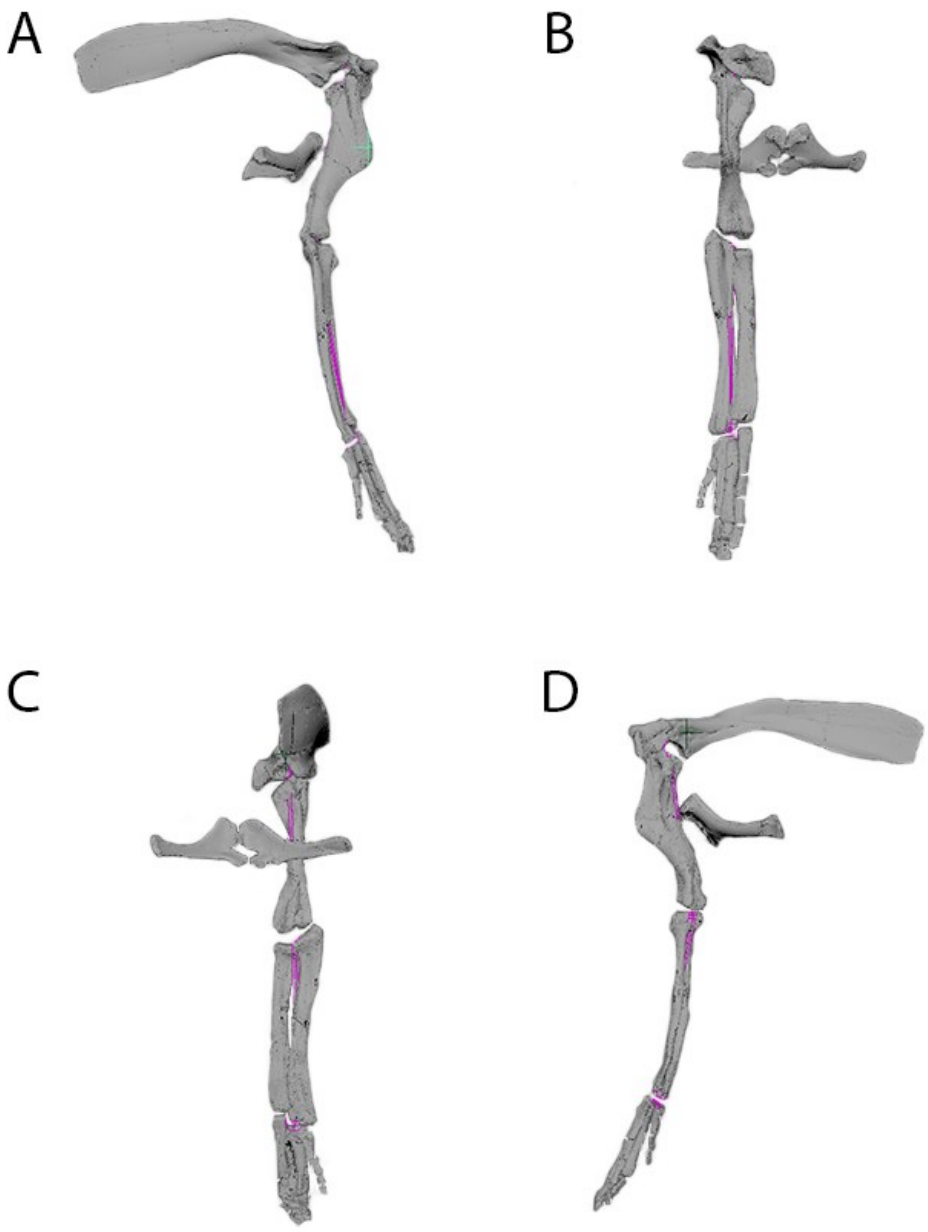

Figure 34. Three-dimensional reconstruction of the right forelimb and shoulder girdle of TMP2015.044.0036 in resting position in Maya (© Copyright 2020 Autodesk Inc) in (A) lateral, (B) anterior, (C) posterior, and (D) medial views. Purple lines represent the hierarchy of Maya joints.

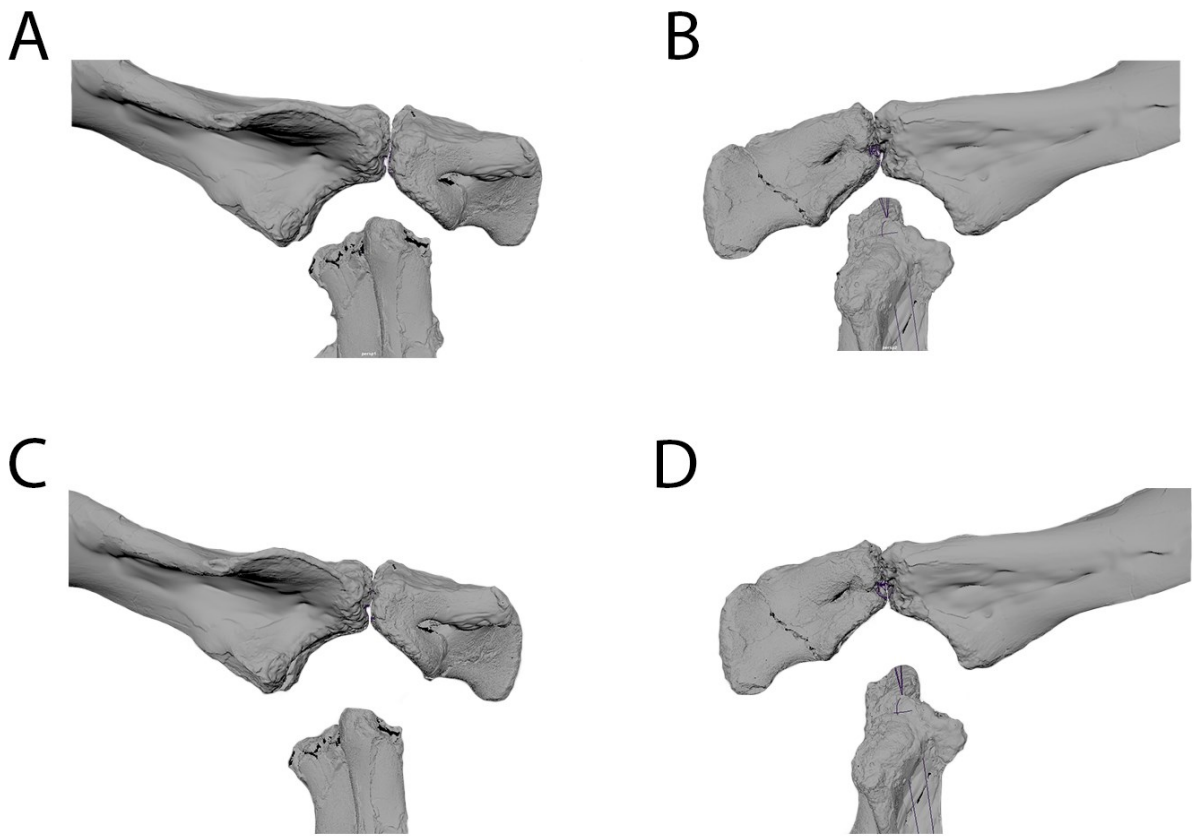

Figure 35. Three-dimensional reconstruction of the right shoulder joint of TMP2015.044.0036 in Maya (© Copyright 2020 Autodesk Inc) at a vertical distance of 77.34 mm (**A**, **B**) and 119.22 mm (**C**, **D**) from the centre of the contact between the scapula and coracoid in lateral (**A**, **C**) and medial (**B**, **D**) views.

Table 3. Maximum degrees of rotation found for the right forelimb joints of TMP2015.044.0036 in Maya (© Copyright 2020 Autodesk Inc) before collision with adjacent bones. An asterisk denotes values that are unrealistically large, theoretically resulting in joint failure (dislocation). Abbreviations: **LAR**, long axis rotation.

	Shoulder (77.34 mm vertical distance)	**Shoulder (119.22 mm vertical distance)**	**Elbow**	**Wrist**
moving element(s)	Humerus	Humerus	Radius and Ulna	Manus
Protraction / Dorsiflexion	26	224*	32	42
Retraction / Palmarflexion	13	34	92	79
Adduction	31	66	41	12
Abduction	40	279*	13	28
Medial LAR / Supination	34	242*	148*	145*
Lateral LAR / Pronation	63	91	122*	55

Table 4. Maximum degrees of rotation found for the right forelimb joints of TMP2015.044.0036 in Maya (© Copyright 2020 Autodesk Inc) before slipping out of realistic contact with articulated elements. Abbreviations: **LAR**, long axis rotation.

	Shoulder (77.34 mm vertical distance)	**Shoulder (119.22 mm vertical distance)**	**Elbow**	**Wrist**
moving element(s)	Humerus	Humerus	Radius and Ulna	Manus
Protraction / Dorsiflexion	26	44	32	34
Retraction / Palmarflexion	13	10	61	32
Adduction	31	44	41	12
Abduction	26	41	13	28
Medial LAR / Supination	34	64	63	49
Lateral LAR / Pronation	63	91	24	26

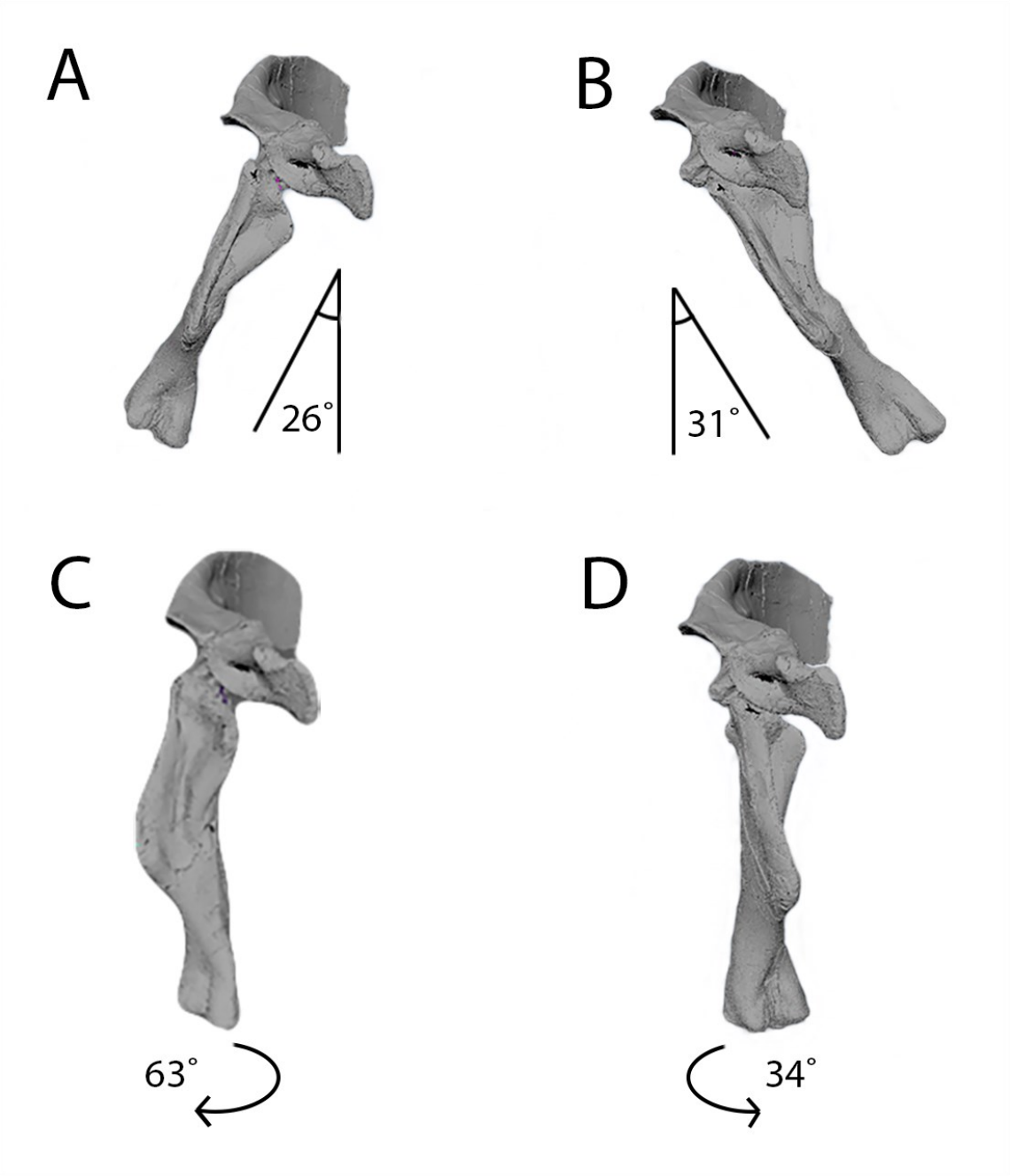

Figure 36. Anterior view showing estimated ranges of abduction/adduction and long-axis rotation for the right shoulder joint of TMP2015.044.0036 at a vertical distance of 77.34 mm from the centre of the contact between the scapula and coracoid. Measured in Maya (© Copyright 2020 Autodesk Inc). (**A**) 40˚ abduction, (**B**) 76˚ adduction, (**C**) 44˚ long axis rotation laterally, and (**D**) 70˚ long axis rotation medially.

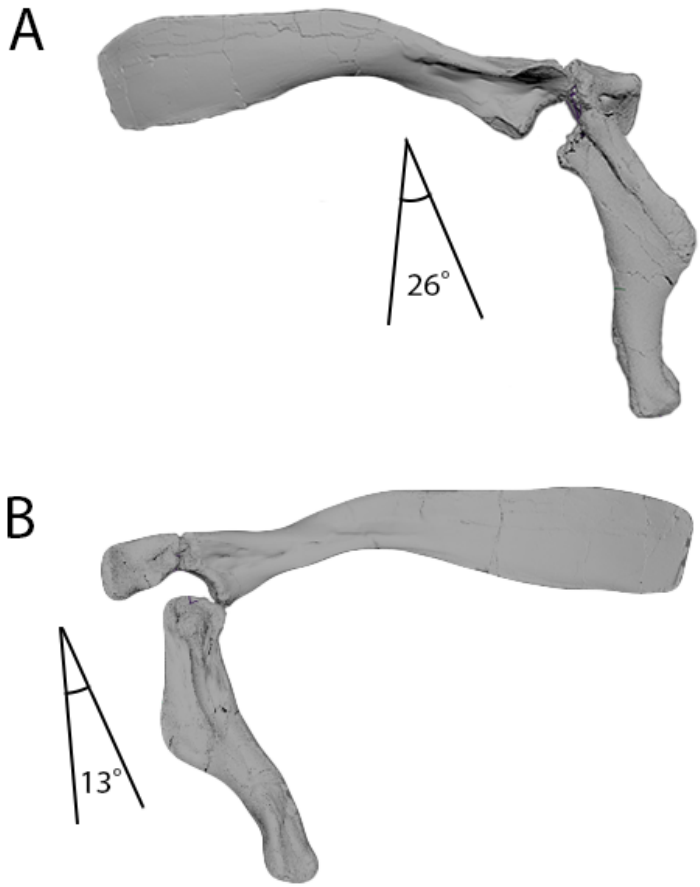

Figure 37. Maximum estimated ranges of protraction/retraction for the right shoulder joint of TMP2015.044.0036 at a vertical distance of 77.34 mm from the centre of the contact between the scapula and coracoid. Measured in Maya (© Copyright 2020 Autodesk Inc). (**A**) 26˚ protraction in lateral view, and (**B**) 13˚ retraction in medial view.

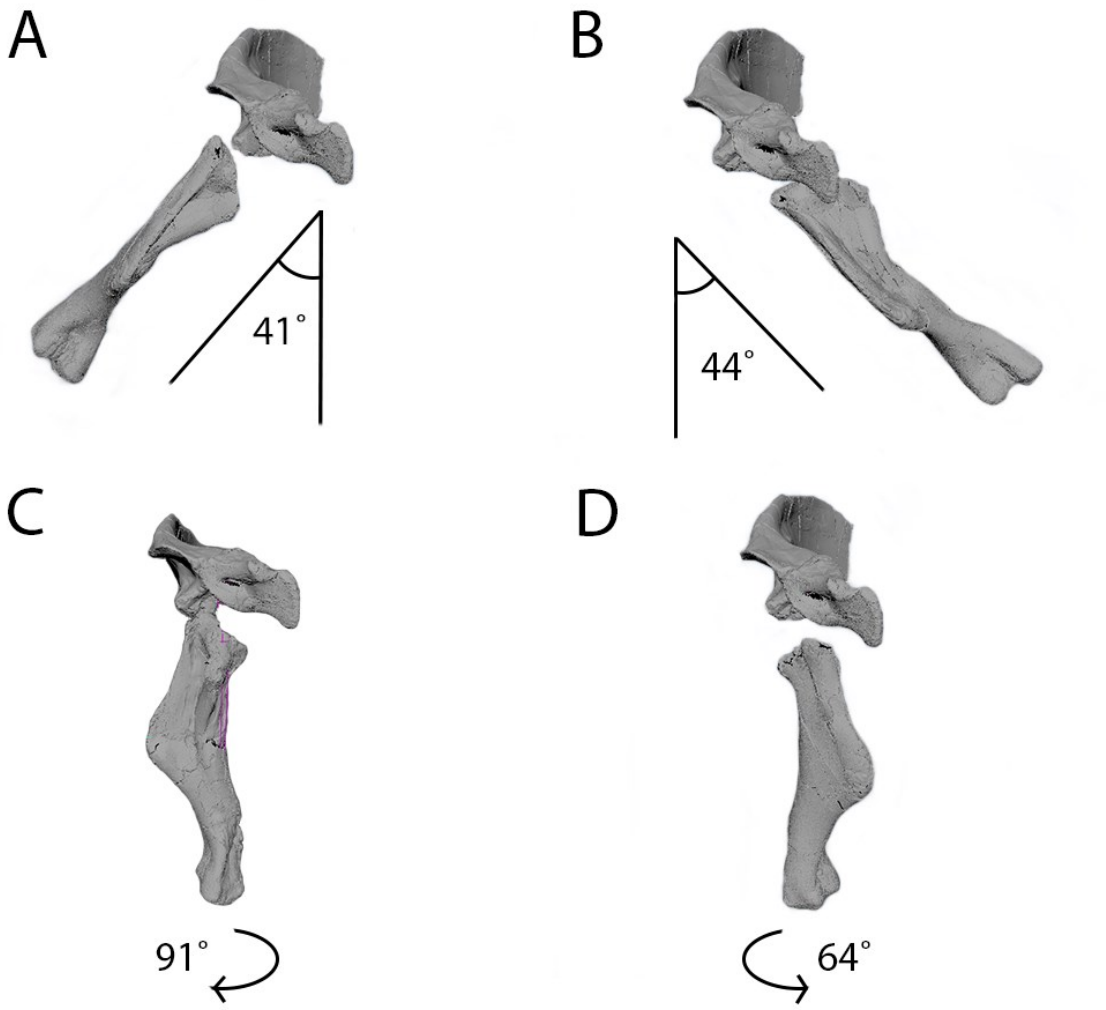

Figure 38. Anterior view showing estimated ranges of abduction/adduction and long-axis rotation for the right shoulder joint of TMP2015.044.0036 at a vertical distance of 119.22 mm from the centre of the contact between the scapula and coracoid. Measured in Maya (© Copyright 2020 Autodesk Inc). (**A**) 50˚ abduction, (**B**) 66˚ adduction, (**C**) 91˚ long axis rotation laterally, and (**D**) 242˚ long axis rotation medially.

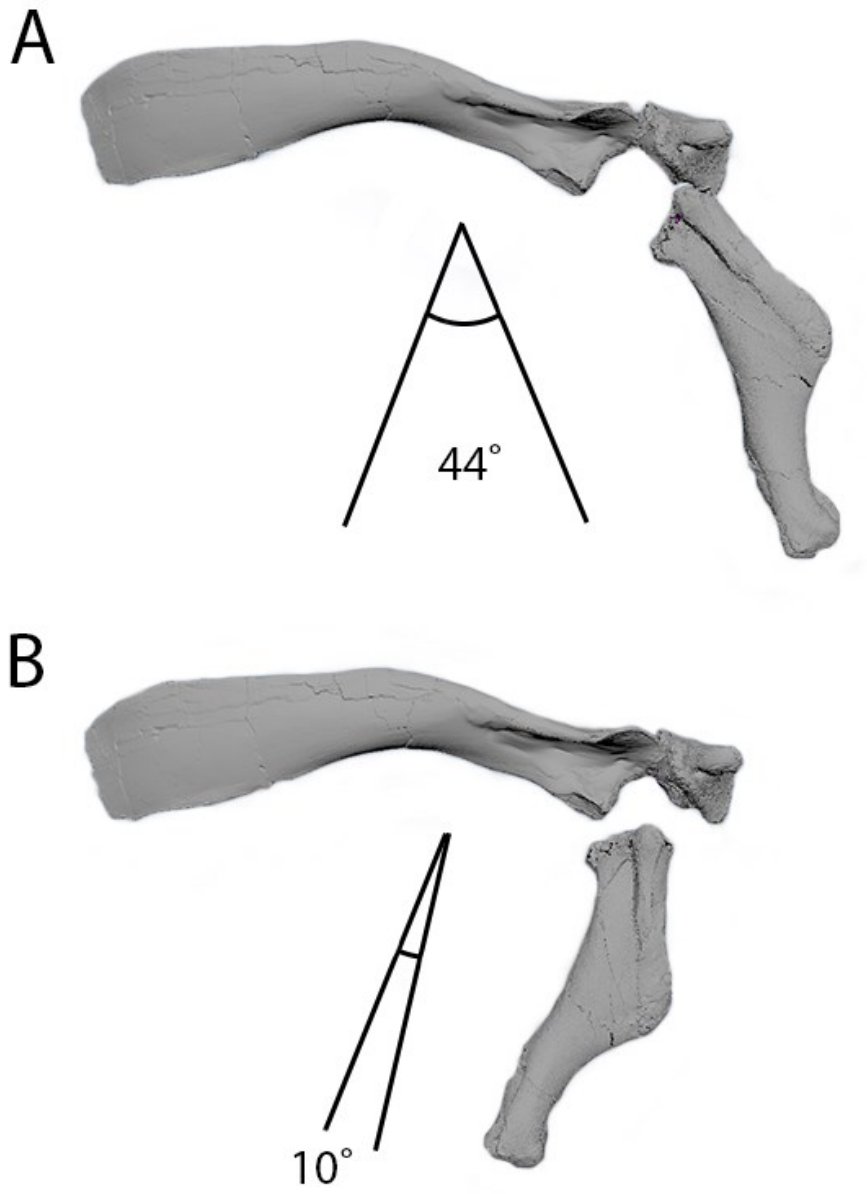

Figure 39. Maximum estimated ranges of protraction/retraction for the right shoulder joint of TMP2015.044.0036 at a vertical distance of 119.22 mm from the centre of the contact between the scapula and coracoid. Measured in Maya (© Copyright 2020 Autodesk Inc). (**A**) 40˚ protraction in lateral view, and (**B**) 34˚ retraction in lateral view.

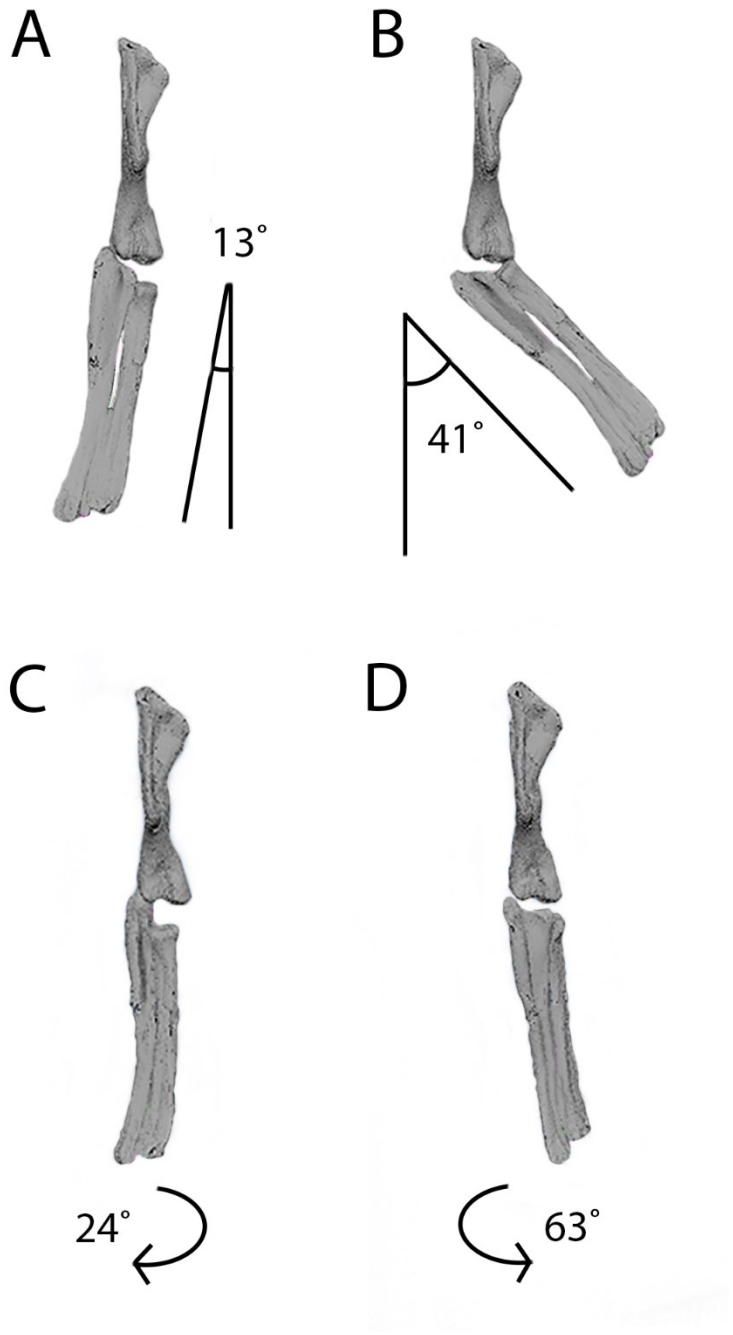

Figure 40. Anterior view showing estimated ranges of abduction/adduction and long-axis rotation for the right elbow joint of TMP2015.044.0036. Measured in Maya (© Copyright 2020 Autodesk Inc). (**A**) 13˚ abduction, (**B**) 41˚ adduction, (**C**) 122˚ long axis rotation laterally, and (**D**) 148˚ long axis rotation medially.

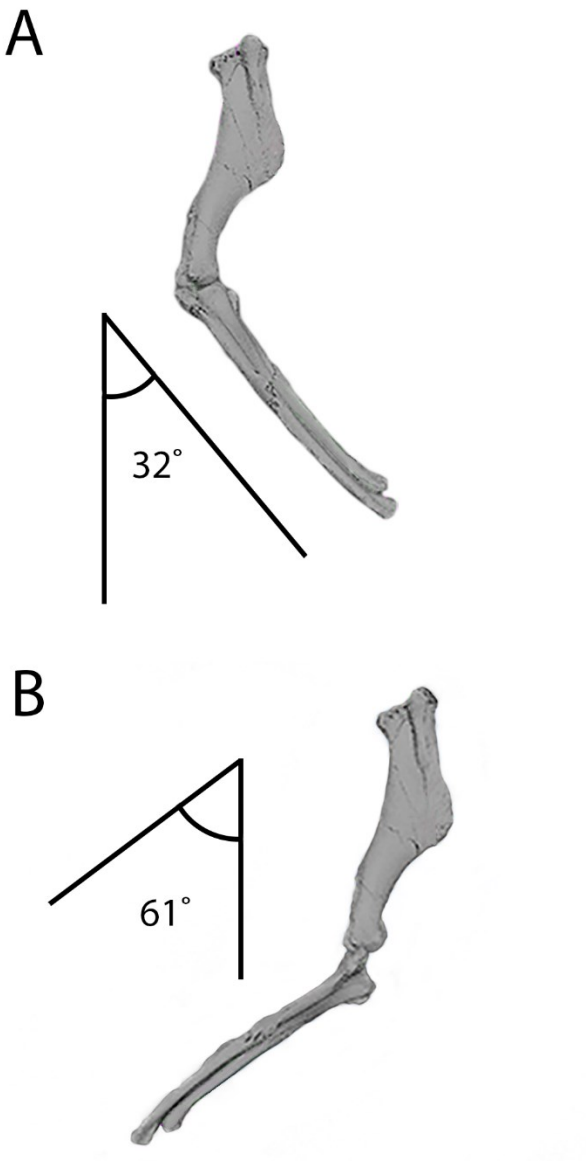

Figure 41. Maximum estimated ranges of protraction/retraction for the right elbow joint of TMP2015.044.0036. Measured in Maya (© Copyright 2020 Autodesk Inc). (**A**) 32˚ protraction in lateral view, and (**B**) 92˚ retraction in lateral view.

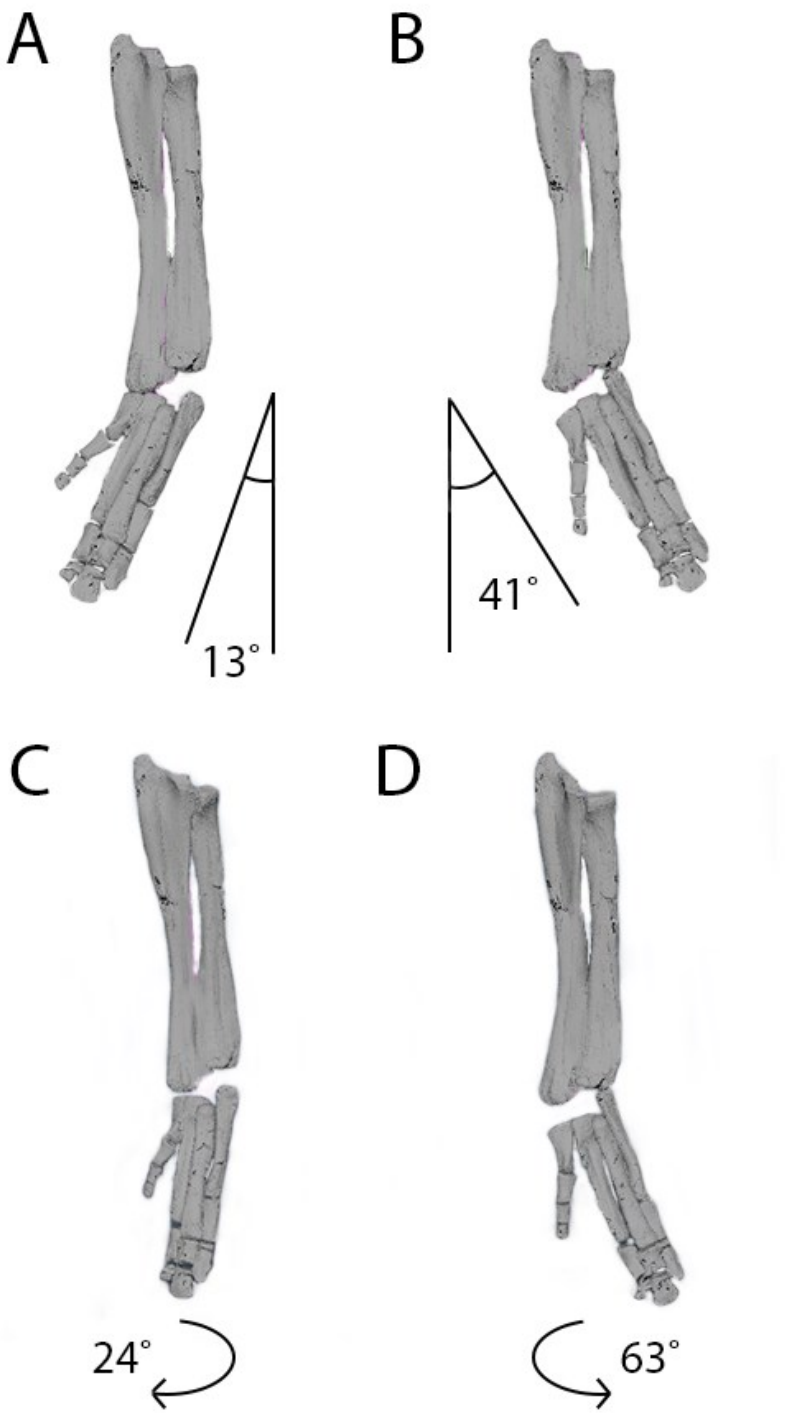

Figure 42. Anterior view showing estimated ranges of abduction/adduction and long-axis rotation for the right wrist joint of TMP2015.044.0036. Measured in Maya (© Copyright 2020 Autodesk Inc). (**A**) 28˚ abduction, (**B**) 12˚ adduction, (**C**) 55˚ long axis rotation laterally, and (**D**) 145˚ long axis rotation medially.

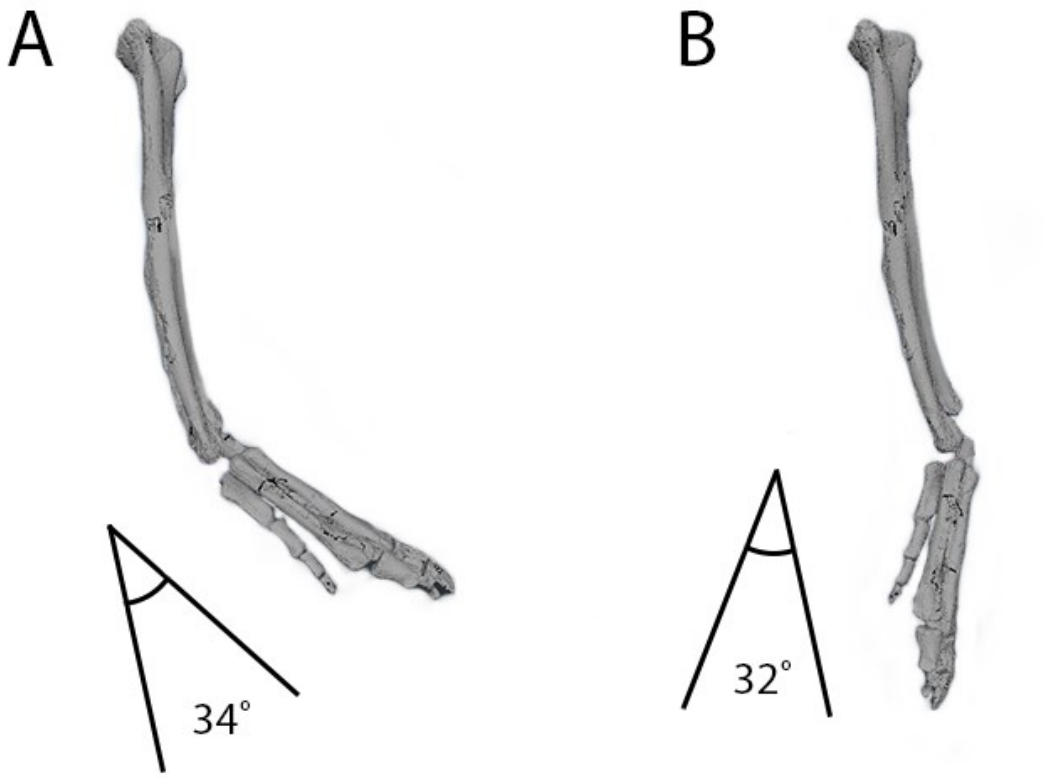

Figure 43. Maximum estimated ranges of protraction/retraction for the right wrist joint of TMP2015.044.0036. Measured in Maya (© Copyright 2020 Autodesk Inc). (**A**) 42˚ protraction in lateral view, and (**B**) 79˚ palmarflexion in lateral view.

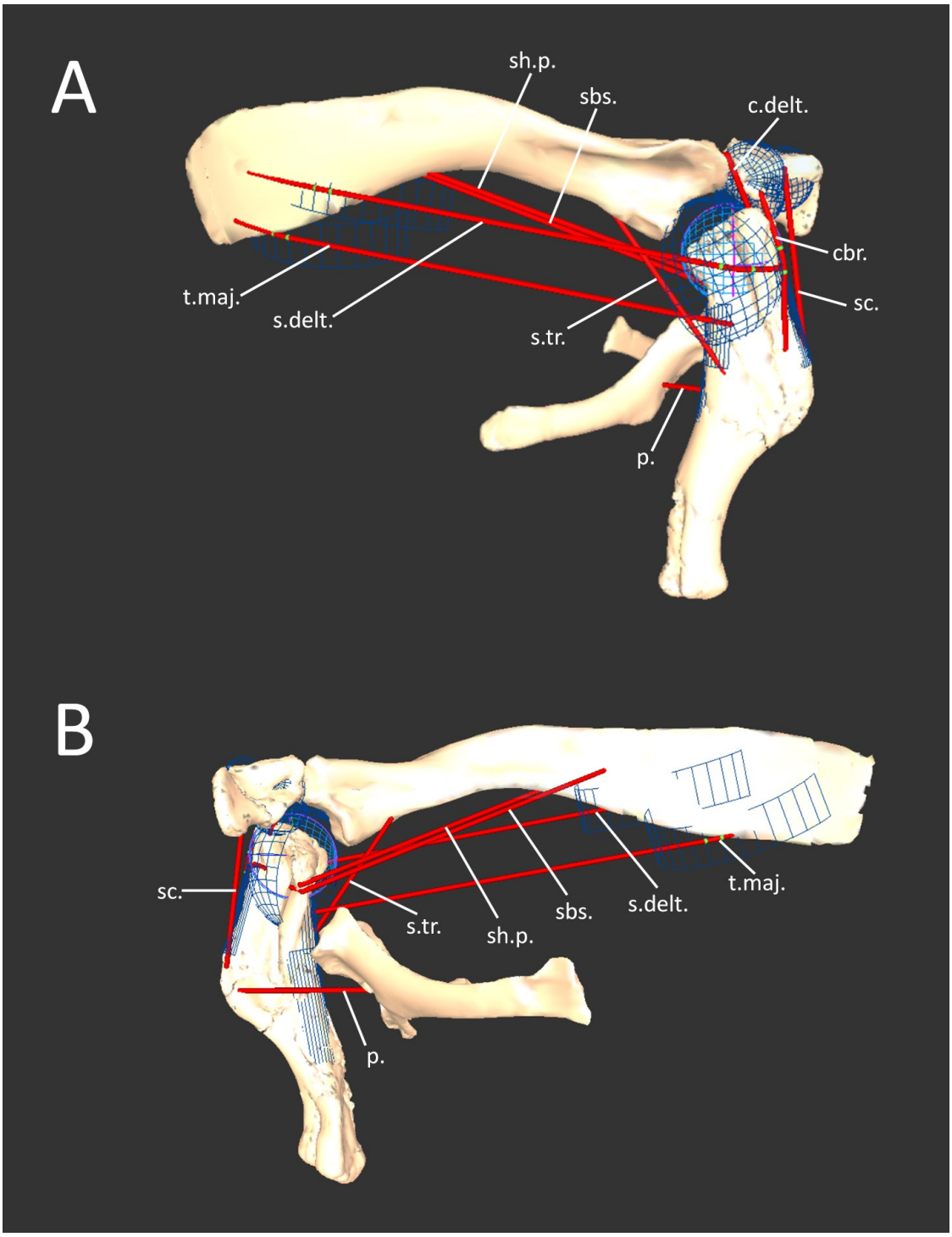

Figure 44. Right shoulder and corresponding pectoral musculature reconstructed in SIMM for TMP2015.044.0036. (**A**) Lateral and (**B**) medial views of the scapula, coracoid, humerus, sternal plates and reconstructed muscle trajectories with blue wrap objects visible. Abbreviations: **cbr.**, M. coracobrachialis; **c.delt.**, M. deltoideus clavicularis; **p.**, M. pectoralis; **s.delt.**, M. deltoideus scapularis; **s.tr.**,M. triceps (scapular head); **sbs.**, M. subscapularis; **sc.**, M. supracoracoideus; **sh.p.**, M. scapulohumeralis posterior; **t.maj.**, M. teres major.

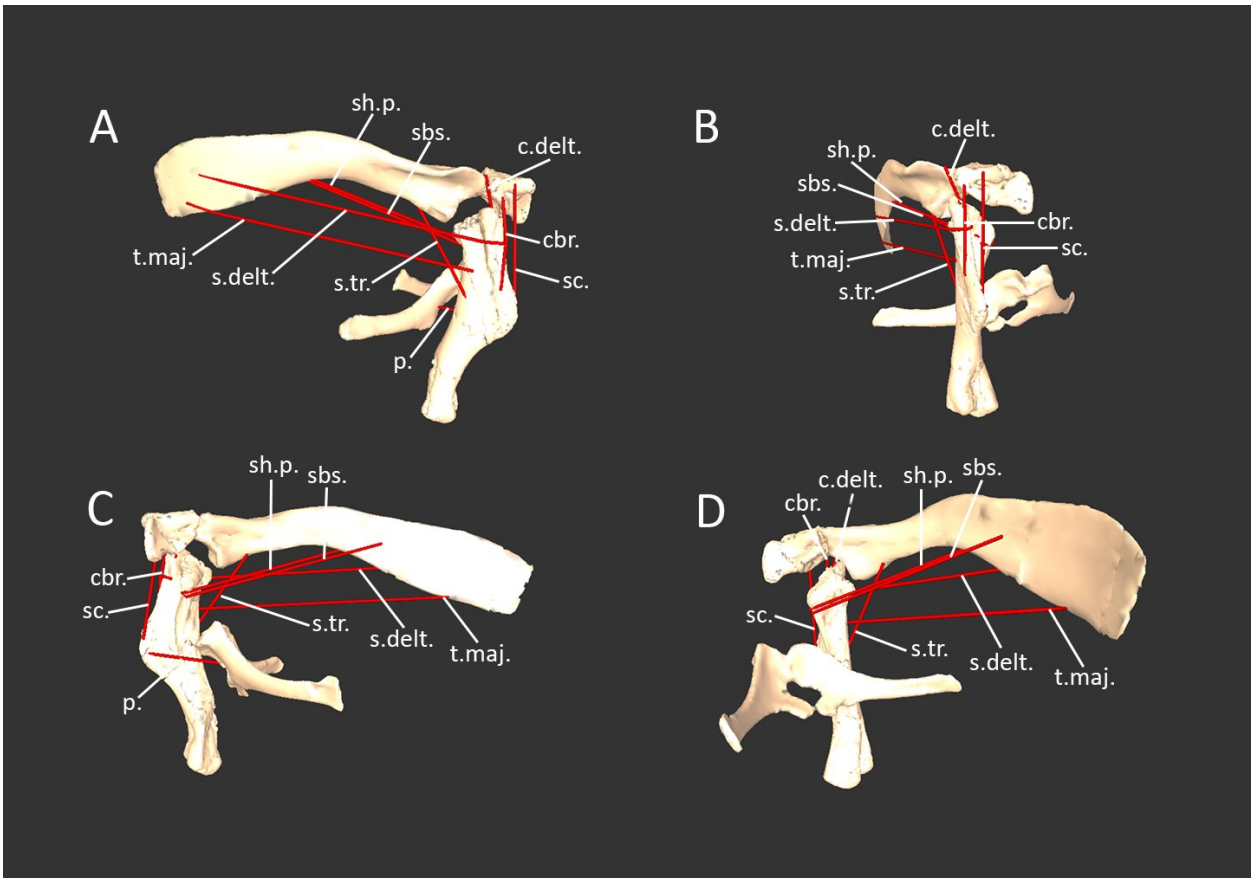

Figure 45. Right shoulder and corresponding pectoral musculature reconstructed in SIMM for TMP2015.044.0036. (**A**) Lateral, (**B**) anterolateral, (**C**) medial, and (**D**) posteromedial views of the scapula, coracoid, humerus, sternal plates and reconstructed muscle trajectories. Abbreviations: **cbr.**, M. coracobrachialis; **c.delt.**, M. deltoideus clavicularis; **p.**, M. pectoralis; s.delt., M. deltoideus scapularis; s.tr.,M. triceps (scapular head); sbs., M. subscapularis; **sc.**, M. supracoracoideus; **sh.p.**, M. scapulohumeralis posterior**; t.maj.**, M. teres major.

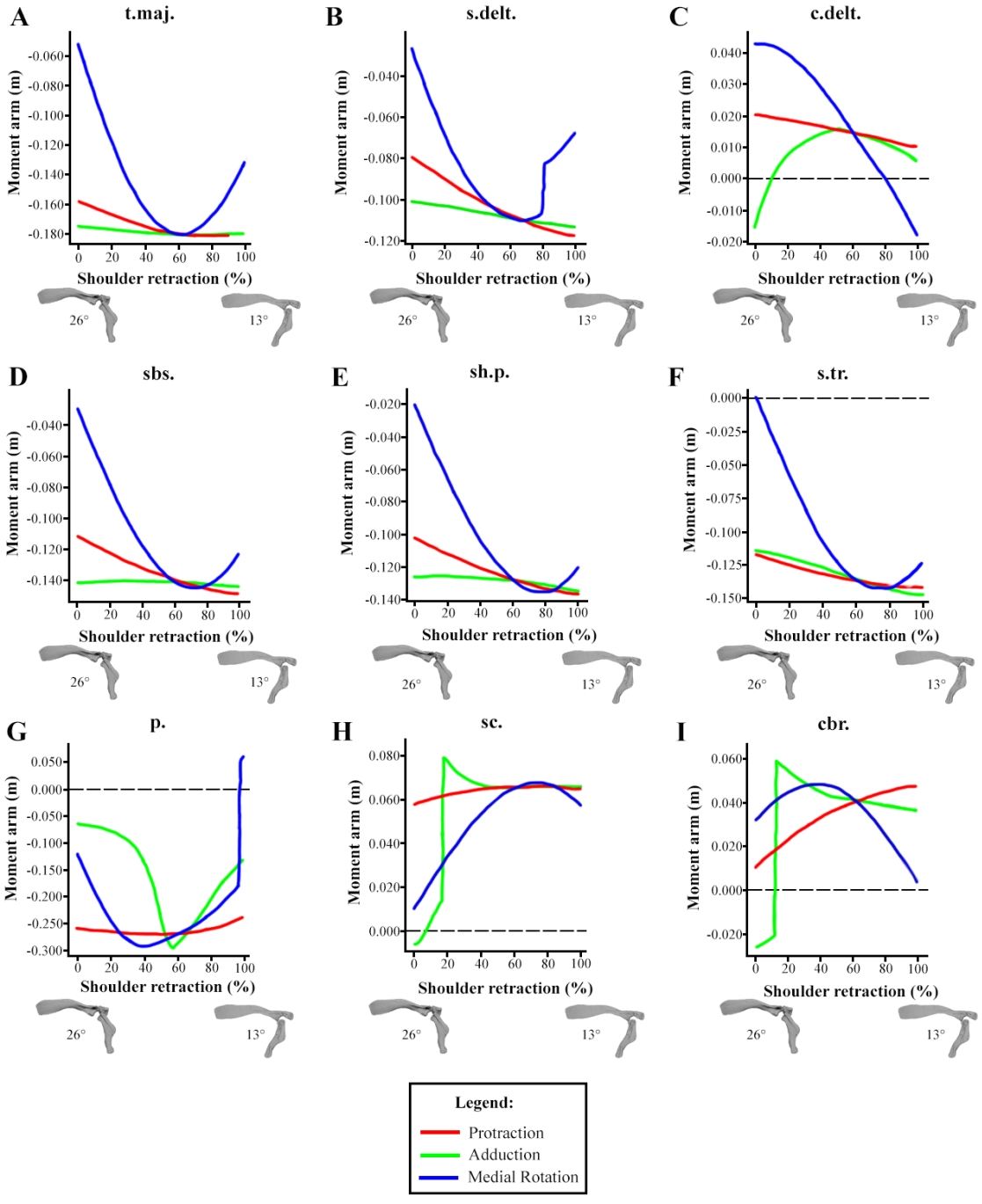

Figure 46. Shoulder muscle moment arm plots for the predicted maximum range of humeral protraction / retraction in TMP2015.044.0036. (**A**) M. teres major, (**B**) M. deltoideus scapularis, (**C**) M. deltoideus clavicularis, (**D**) M. subscapularis, (**E**) M. scapulohumeralis posterior, (**F**) M. triceps (scapular head), (**G**) M. pectoralis, (**H**) M. supracoracoideus, and (**I**) M. coracobrachialis. Positive moment arm values indicate humeral protraction, adduction, and medial rotation while negative moment arm values indicate humeral retraction, abduction, and lateral rotation.

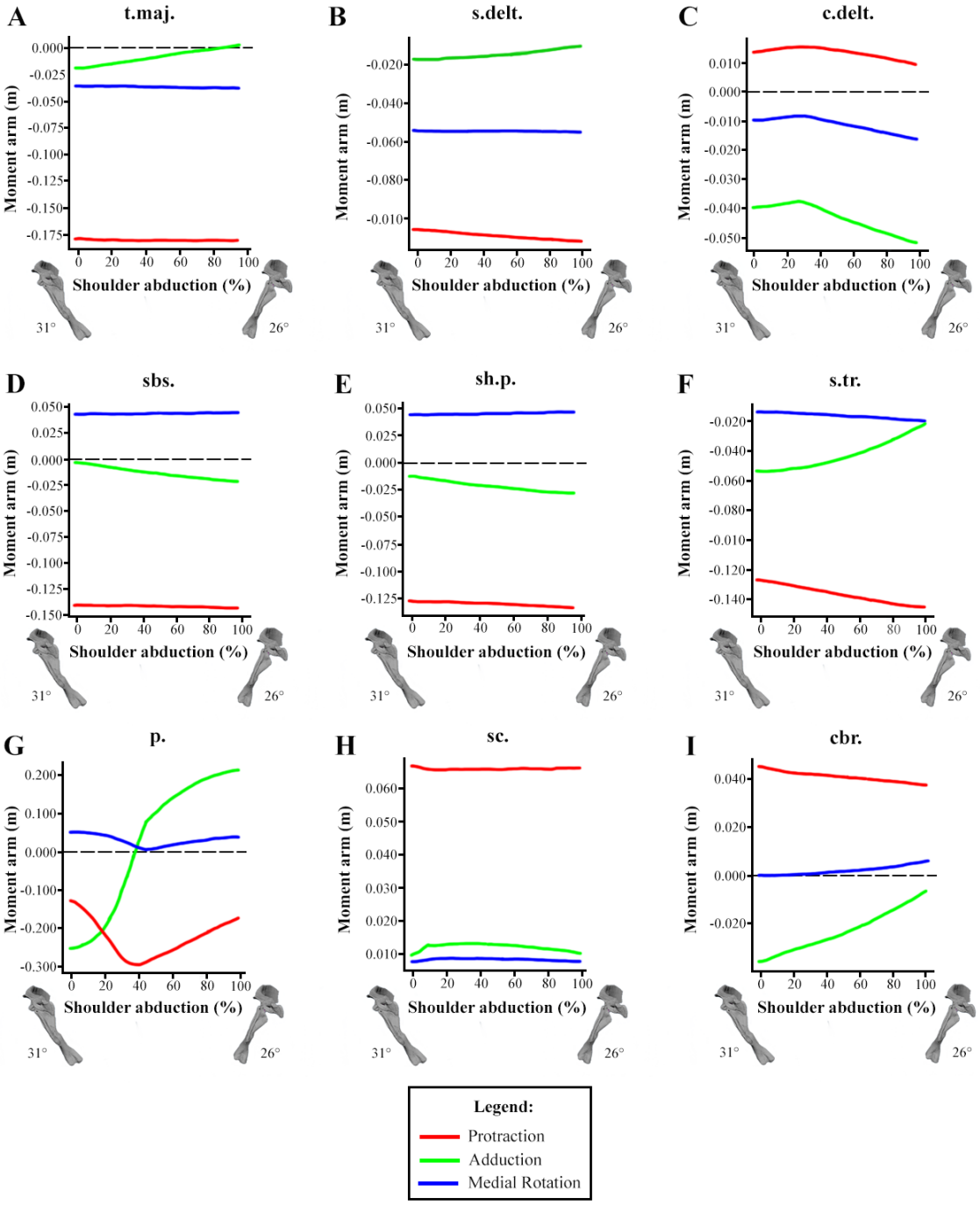

Figure 47. Shoulder muscle moment arm plots for the predicted maximum range of humeral adduction / abduction in TMP2015.044.0036. (**A**) M. teres major, (**B**) M. deltoideus scapularis, (**C**) M. deltoideus clavicularis, (**D**) M. subscapularis, (**E**) M. scapulohumeralis posterior, (**F**) M. triceps (scapular head), (**G**) M. pectoralis, (**H**) M. supracoracoideus, and (**I**) M. coracobrachialis. Positive moment arm values indicate humeral protraction, adduction, and medial rotation while negative moment arm values indicate humeral retraction, abduction, and lateral rotation.

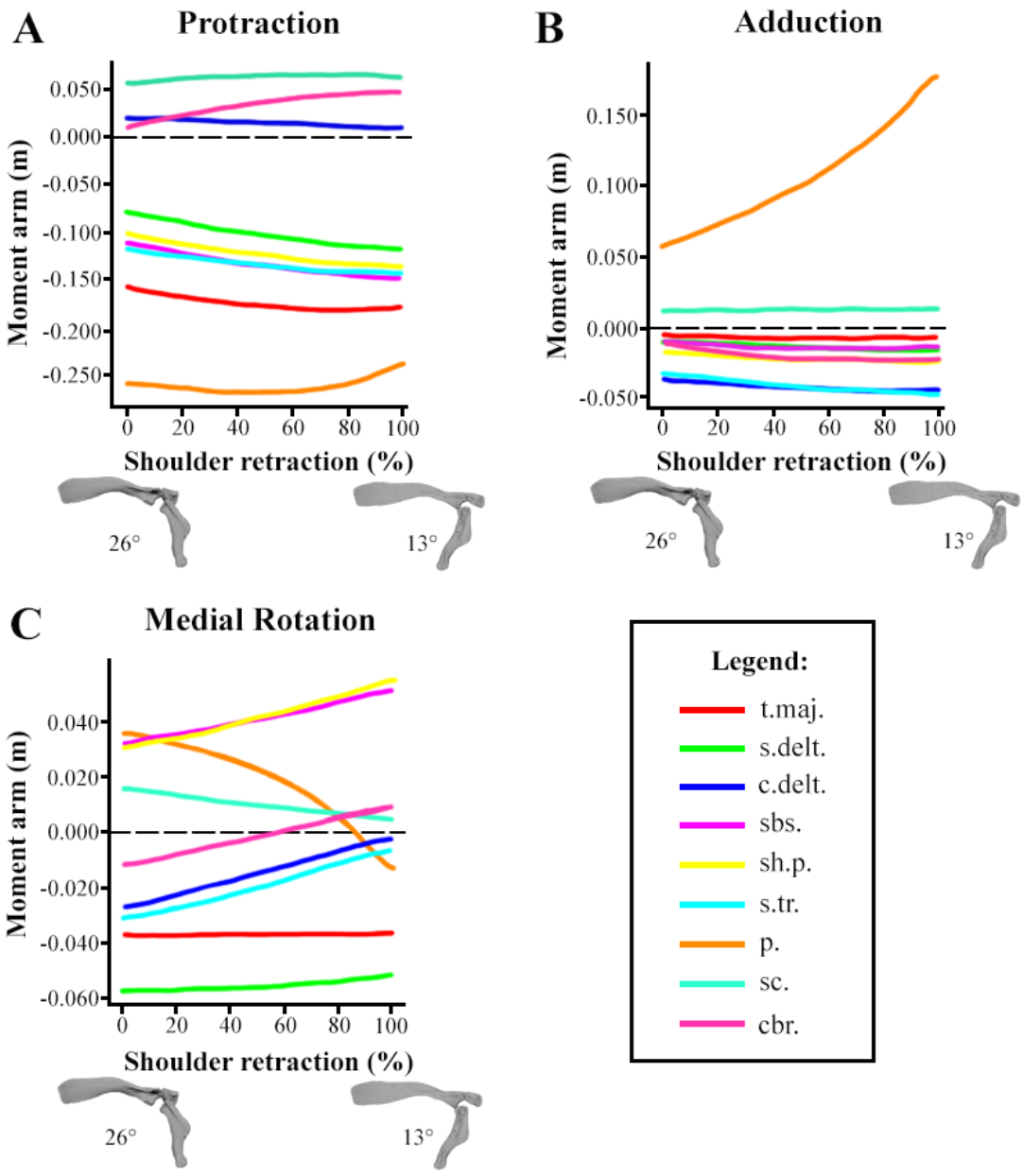

Figure 48. Comparative shoulder muscle moment arm plots for directional movement for the predicted maximum range of humeral protraction / retraction in TMP2015.044.0036. (**A**) Flexion, (**B**) Adduction, and (**C**) Rotation. **Abbreviations: cbr.**, M. coracobrachialis; **c.delt.**, M. deltoideus clavicularis; **p.**, M. pectoralis; **s.delt.**, M. deltoideus scapularis; **s.tr.**,M. triceps (scapular head); **sbs.**, M. subscapularis; **sc.**, M. supracoracoideus; **sh.p.**, M. scapulohumeralis posterior; **t.maj.**, M. teres major. Positive moment arm values indicate humeral protraction, adduction, and medial rotation while negative moment arm values indicate humeral retraction, abduction, and lateral rotation.

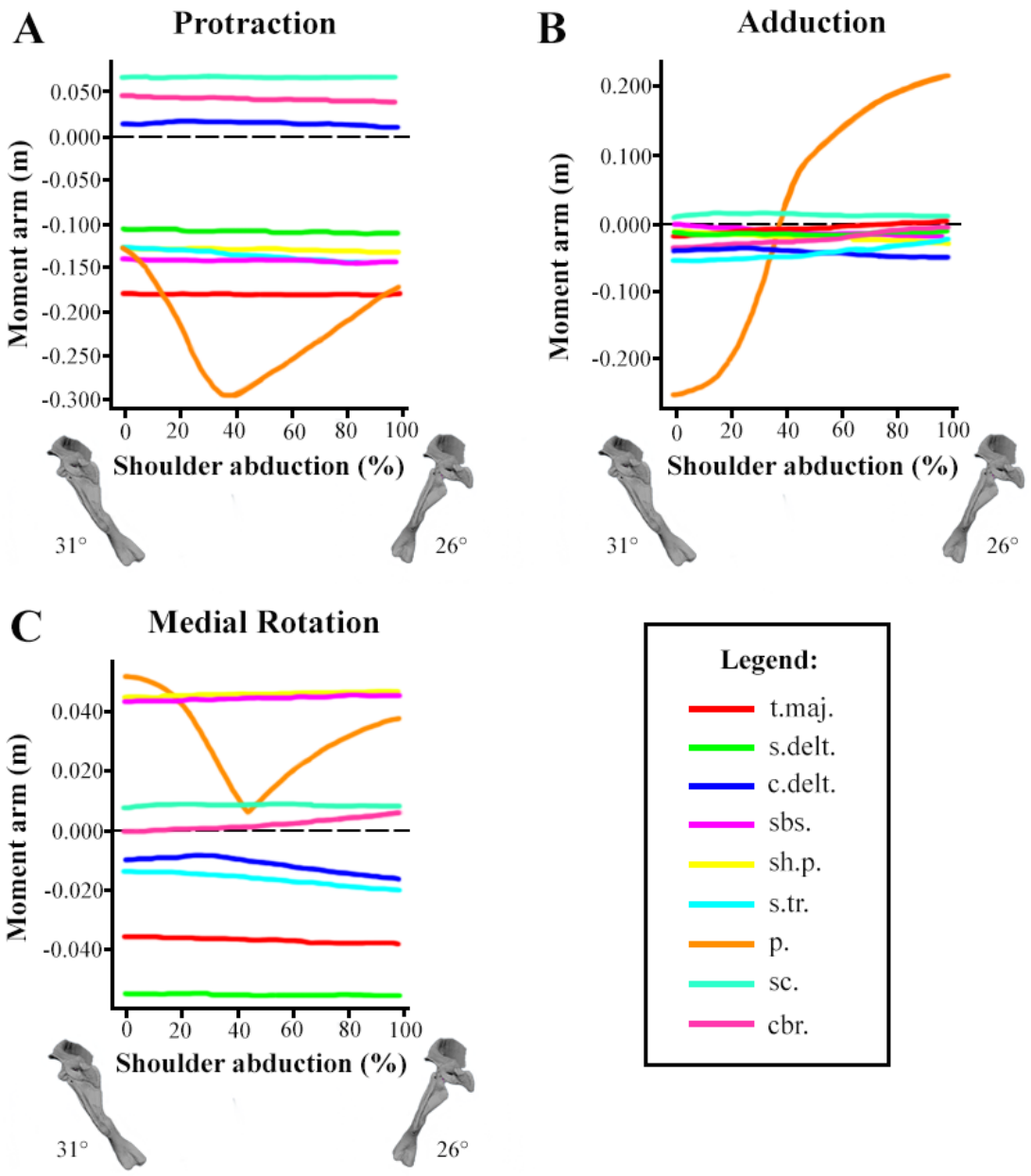

Figure 49. Comparative shoulder muscle moment arm plots for directional movement for the predicted maximum range of humeral adduction / abduction in TMP2015.044.0036. (**A**) Flexion, (**B**) Adduction, and (**C**) Rotation. **Abbreviations: cbr.**, M. coracobrachialis; **c.delt.**, M. deltoideus clavicularis; **p.**, M. pectoralis; **s.delt.**, M. deltoideus scapularis; **s.tr.**,M. triceps (scapular head); **sbs.**, M. subscapularis; **sc.**, M. supracoracoideus; **sh.p.**, M. scapulohumeralis posterior; **t.maj.**, M. teres major. Positive moment arm values indicate humeral protraction, adduction, and medial rotation while negative moment arm values indicate humeral retraction, abduction, and lateral rotation.

Chapter 5. Conclusions

Hadrosaurid dinosaurs present an interesting case in the exploration of postural shift through evolution, given their apparent change from bipedal ancestors to secondary quadrupedalism (Dodson et al. 2004; Horner et al. 2004; Norman et al. 2004; Maidment and Barrett 2012; Maidment et al. 2014b), and the possibility of facultative quadrupedality appearing separately several times after this initial shift in posture (Norman 1980; Wright 1999; Carpenter and Wilson 2008; Maidment and Barrett, 2014). Here I have presented the comparative osteology, myology, range of motion, and moment arm estimates for the pectoral girdle, sternum, forelimb, and manus of a recently recovered lambeosaurine hadrosaurid (TMP2015.044.0036) in hopes of gauging the degree of involvement of the forelimbs in locomotion. Results obtained here largely support the hypothesis that TMP2015.044.0036 represents at least a facultatively bipedal animal that would have predominantly adopted a quadrupedal stance.

Chapter 2 and 4 present osteological evidence for quadrupedalism in TMP2015.044.0036. A downward facing glenoid suggests that the forelimb of TMP2015.044.0036 was held vertically, which combined with a limited range of protractive-retractive range of motion of the humerus implies that even if TMP2015.044.0036 adopted a bipedal stance with the trunk held mostly vertically, the forelimbs would consistently protrude anteriorly and not be capable of resting against the body. TMP2015.044.0036, and indeed many hadrosaurids (e.g. Brown 1916; Brett-Surman and Wagner 2007; Prieto-Márquez 2008; Campione 2014), also display a stacked arrangement of their metacarpals II, III, and IV in which metacarpal III lies anteriorly to metacarpals II and IV and in close association with one another. This would effectively create a pillar-like structure that would be particularly advantageous for weight bearing since the mechanical load of the body's mass is transmitted to compressional

force that is spread over a greater combined cross-sectional area than any one metacarpal on its own. This would be particularly effective in the configuration seen in TMP2015.044.0036 considering the close proximity of these elements suggest there was a negligible amount of movement that could occur between adjacent metacarpals, given their close proximity to each other, resulting in a mechanical bracing effect in the manus. Indeed, the presumably cartilaginous carpals resting just below these metacarpals would result in an effective cushion to dissipate these compressional forces from bearing the weight of the body. Given that most other dinosaur taxa possess well-developed ossified carpals, cartilaginous carpals in hadrosaurids are likely a response to the increased mechanical strain on the forelimbs which are comparatively much smaller than the hindlimbs, especially if this is coupled with a reversion to quadrupedalism from a previously bipedal lineage. The typically massive tails of hadrosaurids may also assist with this transition in acting as a particularly effective counterbalance which would relieve much of the strain of the body's weight from the forelimbs and shift it proportionally onto the pelvis and hindlimbs. Furthermore, the fact that hadrosaurids consistently possess distal manual phalanges in the form of hoof-like unguals suggest that the forelimbs were habitually in contact with the ground.

Range of motion estimates for the elbow of TMP2015.044.0036 indicate a reasonably large reach of the forelimb, permitting large strides that are supported by robust shoulder musculature, particularly M. pectoralis providing powerful retractive force and M. supracoracoideus and M. coracobrachialis providing humeral protraction. Range of motion and moment arm estimates suggest that humeral adduction and abduction would have been severely limited by both osteological interruption and a lack of particularly well-developed muscles associated with these movements. This further supports the hypothesis that forelimb movements

in hadrosaurid dinosaurs would be limited to mostly anterior-posterior swing of the arm. Furthermore, the very close proximity of the bones comprising the shoulder creating a rigid pectoral region, coupled with muscles dedicated to stabilization of the shoulder, and a partially ossified sternum with very long ossified anterolateral processes limit the movement of the thoracic and pectoral region of TMP2015.044.0036 by resisting independent movement of the pectoral girdle and adding an aspect of rigidity to the chest, all of which could constitute a mechanical load-bearing response in the anterior portion of the body. Although these results seem to indicate a facultatively bipedal mode of locomotion for TMP2015.044.0036, carefully constrained biomechanical models for other hadrosaurids will be required to draw meaningful conclusions about the postural states that exist within Hadrosauria.

Bibliography

Baier DB, Garrity BM, Moritz S, Carney RM. 2018. *Alligator mississippiensis* sternal and shoulder girdle mobility increase stride length during high walks. J Exp Biol. 221: jeb186791

Baier DB, Gatesy SM. 2013. Three-dimensional skeletal kinematics of the shoulder girdle and forelimb in walking *Alligator*. J Anat. 223: 462 – 473.

Bates KT, Schachner ER. 2012. Disparity and convergence in bipedal archosaur locomotion. J R Soc Interface. 9: 1339 – 1353.

Bates KT, Maidment SCR, Allen V, Barrett PM. 2012. Computational modelling of locomotor muscle moment arms in the basal dinosaur *Lesothosaurus diagnosticus*: assessing convergence between birds and basal ornithiscians. J Anat. 220: 212 – 232.

Bates K, Maidment SCR, Schachner ER, Barrett PM. 2015. Comments and corrections on 3D modeling studies of locomotor muscle moment arms in archosaurs. PeerJ. 16p.

Baumel JJ, King AS, Lucas AM, Breazile JE, Evans HE, Vanden Berge JC. 1993. Handbook of avian anatomy: nomina anatomica avium, 2nd edn. Cambridge: Nuttall Ornithological Club.

Bishop PJ, Cuff AR, Hutchinson JR. 2021. How to build a dinosaur: Musculoskeletal modeling and simulation of locomotor biomechanics in extinct animals. Paleobiology. 47(1): 1 – 38.

Böhmer C, Fabre AC, Taverne M, Herbin M, Peigné S, Herrel A. 2019. Functional relationship between myology and ecology in carnivores: do forelimb muscles reflect adaptations to prehension? Biol J Linn Soc. 127(3): 661 – 680.

Bonnan MF, Senter P. 2007. Were the basal sauropodomorph dinosaurs *Plateosaurus* and *Massospondylus* habitual quadrupeds? Spec Pap Palaeontol. 77: 139 – 155.

Bramble K, Currie PJ, Tanke DH, Torices A. 2017. Reuniting the "head hunted" *Corythosaurus excavatus* (Dinosauria: Hadrosauridae) holotype skull with its dentary and postcranium. Cret Res. 76: 7 – 18.

Brett-Surman MK. 1989. A Revision of the Hadrosauridea (Reptilia: Ornithischia) And Their Evolution During the Campanian and Maastrichtian [Dissertation]. George Washington University Graduate School of Arts and Sciences. 214p.

Brett-Surman MK, Wagner JR. 2007. Discussion of character analysis of the appendicular anatomy in Campanian and Maastrichtian North American hadrosaurids- variation and ontogeny. In K. Carpenter (ed.), horns and beaks: ceratopsian and ornithopod dinosaurs. Indiana University Press, Bloomington. Pp. 135 – 169.

Brink KS, Zelenitsky DK, Evans DC, Therrien F, Horner JR. 2011. A sub-adult skull of *Hypacrosaurus stebingeri* (Ornithischia: Lambeosaurinae): anatomy and comparison. Hist Biol. 23(1): 63 – 72.

Brown B. 1916. *Corythosaurus casuarius*: skeleton, musculature, and epidermis. B Am Mus Nat Hist. 35, article 38.

Bultynck P. 1992. An assessment of posture and gait in *Iguanodon bernissartensis*. Bull Inst R Sci Nat Belg Sciences de la Terre. 63: 5 – 11.

Burch SH. 2014. Complete forelimb myology of the basal theropod dinosaur *Tawa hallae* based on a novel robust muscle reconstruction method. J Anat. 225: 271 – 197.

Burch SH. 2017. Myology of the forelimb of *Majungasaurus crenatissimus* (Theropoda, Abelisauridae) and the morphological consequences of extreme limb reduction. J Anat. 231(4): 515 – 531.

Butler RJ, Upchurch P, Norman DB. 2008. The phylogeny of the ornithischian dinosaurs. J Syst Palaeontol. 6: 1 – 40.

Calmaestra RG, Moreno E. 2005. Forelimb muscles and migration: finding ecomorphological patterns using a phylogenetically-based method. Ardeola. 52(2): 253 – 268.

Campione NE. 2014. Postcranial anatomy of *Edmontosaurus regalis* (Hadrosauridae) from the Horseshoe Canyon Formation, Alberta, Canada. Pp. 208 – 244 in D. A. Eberth and D. C. Evans (eds.), Hadrosaurs. Indiana University Press, Bloomington, Indiana.

Carpenter K. 2002. Forelimb biomechanics of nonavian theropod dinosuars in predation. Senckenbergiana Lethaea. 82: 59 – 76.

Carpenter K, Wilson Y. 2008. A new species of *Camptosaurus* (Ornithopoda: Dinosauria) from the Morrison Formation (Upper Jurassic) of Dinosaur National Monument, Utah, and a biomechanical analysis of its forelimb. BioOne. 76(4): 227 – 263.

Carrano MT. 2001. Implications of limb bone scaling, curvature and eccentricity in mammals and non-avian dinosaurs. J Zool Lond. 254: 41 – 55.

Carrano MT, Hutchinson JR. 2002. Pelvic and Hindlimb musculature of *Tyrannosaurus rex* (Dinosauria: Theropoda). J Morphol. 253: 207 – 228.

Carrier DR. 2011. The Advantage of Standing Up to Fight and the Evolution of Habitual Bipedalism in Hominins. Plos One. 6(5): e19630.

Codd JR. 2004. The Uncinate Processes in Birds and their Implications for the Breathing Mechanics of Maniraptoran Dinosaurs [Dissertation]. Rheinische Friedrich-Wilhelms-Universität Bonn. 167p.

Codd JR. 2010. Uncinate processes in birds: Morphology, physiology and function. Comp Biochem Physiol A. 156: 303 – 308.

Colbert EH. 1951. Environment and adaptations of certain dinosaurs. Biol Rev. 26: 265 – 284.

Cong L, Hou L, Wu X-C, Hou J. 1998, The gross anatomy of *Alligator sinensis Fauvel.* Beijing: Science Press.

Cope ED. 1883. On the characters of the skull in the Hadrosauridae. Proc R Ac Nat Sci Phil. 35: 97 – 107.

Cullen TM, Evans DC. 2016. Palaeoenvironmental drivers of vertebrate community composition in the Belly River Group (Campanian) of Alberta, Canada, with implications for dinosaur biogeography. BMC Ecol. 16(52): 35 pp.

Currie PJ. 1983. Hadrosaur trackways from the Lower Cretaceous of Canada. Palaeontologica. 28(1-2): 62 – 73.

Currie PJ, Russell DA. 2005. The Geographic and Stratigraphic Distribution of Articulated and Associated Dinosaur Remains. In: Currie PJ, Kopplehus EB (editors), Dinosaur Provincial Park: A Spectacular Ancient Ecosystem Revealed. Indiana University Press, Bloomington, p. 537 – 569.

Currie PJ, Zhao X-J. 1993. A new carnosaur (Dinosauria, Theropoda) from the Jurassic of Xinjiang, People's Republic of China. Can J Earth Soc. 30: 2037 – 2081.

Cuthbertson RS, Holmes RB. 2010. The first complete description of the holotype of *Brachylophosaurus canadensis* Sternberg, 1953 (Dinosauria: Hadrosauridae) with comments on intraspecific variation. Zool J Linn Soc-Lond. 159: 373 – 397.

Dilkes DW. 2000. Appendicular myology of the hadrosaurian dinosaur *Maiasaura peeblesorum* from the Late Cretaceous (Campanian) of Montana. T Roy Soc Edin Earth. 90: 87 – 125.

Dilkes DW. 2001. An ontogenetic perspective on locomotion in the Late Cretaceous dinosaur *Maiasaura peeblesorum* (Ornithischia: Hadrosauridae). Can J Earth Sci. 38: 1205 – 1227.

Dodson P, Madsen Jr. JH. 1981. On the Sternum of Camptosaurus. J Paleontol. 55(1): 109 – 112.

Dodson P, Forster CA, Sampson SD. 2004. Ceratopsidae. In: Weishampel DB, Dodson P, Osmólska H (editors). The Dinosauria. Second Edition. University of California Press, Berkeley. pp. 494 – 516.

Eberth DA. 2005. The Geology. In: Currie PJ, Kopplehus EB, editors. Dinosaur Provincial Park: a spectacular ancient ecosystem revealed. Bloomington: Indiana University Press; 2005. P 54 – 200.

Eberth DA, Hamblin AP. 1993. Tectonic, stratigraphic, and sedimentologic significance of a regional discontinuity in the upper Judith River Group (Belly River wedge) of southern Alberta, Saskatchewan, and northern Montana. Can J Earth Sci. 30(1): 174 – 200.

Egi N, Weishampel DB. 2002. Morphometric analyses of humeral shapes in hadrosaurids (Ornithopoda, Dinosauria). Senck Lethaea. 82(1): 43 – 58.

Evans DC. 2007. Ontogeny and Evolution of Lambeosaurine Dinosaurs (Ornithischia: Hadrosauridae). PhD dissertation. University of Toronto, Department of Ecology and Evolutionary Biology. Toronto, Ontario.

Evans DC, Bavington R, Campione NE. 2009. An unusual hadrosaurid braincase from the Dinosaur Park Formation and the biostratigraphy of *Parasaurolophus* (Ornithischia: Lambeosaurinae) from southern Alberta. Can J Earth Sci. 46: 791 – 800.

Evans DC, Reisz RR. 2007. Anatomy and relationships of *Lambeosaurus magnicristatus*, a crested hadrosaurid dinosaur (Ornithischia) form the Dinosaur Park Formation, Alberta. J Vertebr Paleontol. 27(2): 373 – 393.

Farmer CG. 2015. Similarity of Crocodilian and Avian Lungs Indicates Unidirectional Flow is Ancestral for Archosaurs. Integr Comp Biol. 55(6): 962 – 971.

Forster CA. 1990. The postcranial skeleton of the ornithopod dinosaur *Tenontosaurus tilletti*. J Vertebr Paleontol. 10(3): 273 – 294.

Fowler DW. 2017. Revised geochronology, correlation, and dinosaur stratigraphic ranges of the Santonian-Maastrichtian (Late Cretaceous) fromations of the Western Interior of North America. Plos One. 12(11): e0188426.

Galton PM. 1970. The Posture of Hadrosaurian Dinosaurs. J Paleontol. 44(3): 464 – 473.

Gates TA, Evans DC, Sertich JJW. 2021. Description and rediagnosis of the crested hadrosaurid (Ornithopoda) dinosaur *Parasaurolophus cyrtocristatus* on the basis of new cranial remains. Peer J. 9: e10669.

Gatesy SM, Bäker M, Hutchinson JR. 2009. Constraint-based exclusion of limb poses for reconstructing theropod dinosaur locomotion. J Vertebr Paleontol. 29(2): 535 – 544.

Gatesy SM, Middleton KM. 1997. Bipedalism, flight, and the evolution of theropod locomotor diversity. J Vertebr Paleontol. 17(2): 308 – 329.

Gilmore CW. 1909. Osteology of the Jurassic reptile *Camptosaurus*, with a revision of the species of the genus, and description of two new species. Proc U.S. Nat Mus. 36: 197 – 332.

Gishlick AD. 2001. The function of the manus and forelimb of *Deinonychus antirrhopus* and its importance for the origin of avian flight. In: Gauthier J, Gall LF (editors). New Perspectives on the Origin and Early Evolution of Birds. Yale Peabody Museum, New Haven. p. 301 – 318.

Grand TI. 1997. How muscle mass is part of the fabric of behavioural ecology in East African bovids. Anat Embryol. 195: 375 – 386.

Han S, Owens VL, Patel RV, Ismaily SK, Harrington MA, Incavo SJ, Noble PC. 2020. The continuum of hip range of motion: From soft-tissue restriction to bony impingement. J Orthop Res. 38: 1779 – 1786.

Holliday CM, Ridgely RC, Sedlmayr JC, Witmer LM. 2010. Cartilaginous epiphyses in extant archosaurs and their implications for reconstructing limb function in dinosaurs. Plos One. 5(1): 1 – 16.

Horner JR, Currie PJ. 1994. Embryonic and neonatal morphology and ontogeny of a new species of *Hypacrosaurus* (Ornithischia, Lambeosauridae) from Montana and Alberta. Pp. 312 – 334. In: Carpenter K, Hirsch KF, Horner JR (editors). Dinosaur Eggs and Babies. Cambridge University Press. Cambridge, Massachusetts.

Horner JR, Weishampel DB, Forster CA. 2004. Hadrosauridae. In: Weishampel DB, Dodson P, Osmólska H (editors), The Dinosauria. University of California Press, Berkeley. pp. 438 – 463.

Howell B. 1936. Morphogenesis of the shoulder architecture. Part IV. Reptilia. Quarterly Review of Biology. 11: 183 – 208.

Howell B. 1937. Morphogenesis of the shoulder architecture: Aves. Auk. 54: 364 – 375.

Hu Cheng-chih. 1973. A new Hadrosaur from the Cretaceous of Chucheng, Shantung. Acta Geologica Sinica. 2: 179 – 206.

Hudson GE, Schreiweis DO, Wang SC, Lancaster DA. 1972. A numerical study of the wing and leg muscles of tinamous (Tinamidae). Northwest Sci. 46: 207 – 255.

Hutchinson JR, Allen V. 2009. The evolutionary continuum of limb function from early theropods to birds. Naturwissenschaften. 96: 423 – 448.

Hutchinson JR, Bates KT, Molnar J, Allen V, Makovicky PJ. 2011. A computational analysis of limb and body dimensions in *Tyrannosaurus rex* with implications for locomotion, ontogeny, and growth. Plos One. 6(10): 1 – 20.

Hutson JD, Hutson KN. 2012. A test of the validity of range of motion studies of fossil archosaur elbow mobility using repeated-measures analysis and the extant phylogenetic bracket. J Exp Biol. 215: 2030 – 2038.

Hutson JD, Hutson KN. 2013. Using the American Alligator and a repeated-measures design to place constraints on *in vivo* shoulder joint range of motion in dinosaurs and other fossil archosaurs. J Exp Biol. 216: 275 – 284.

Hutson JD, Hutson KN. 2014. A Repeated-Measures Analysis of the Effects of Soft Tissues on Wrist Range of Motion in the Extant Phylogenetic Bracket of Dinosaurs: Implications for the Functional Origins of an Automatic Wrist Folding Mechanism in Crocodilia. Anat Rec. 297: 1228 – 1249.

Jasinoski SC, Russell AP, Currie PJ. 2006. An integrative phylogenetic and extrapolatory approach to the reconstruction of dromaeosaur (Theropoda: Eumaniraptora) shoulder musculature. Zool J Linn Soc-Lond. 146: 301 – 344.

Jenkins FAJ. 1993. The evolution of the avian shoulder joint. Am J Sci. 293a: 253 – 267.

Kälin JA. 1929. Über Den Brustschulterapparat Der Krokodile. Acta Zoologica. 23: 343 – 399.

Klinkhamer AJ, Wilhite DR, White MA, Wroe S. 2017. Digital dissection and three-dimensional interactive models of limb musculature in the Australian estuarine crocodile (*Crocodylus porosus*). Plos One. 12(4): e0175079

Koizumi M. 2021. Comparative anatomy of the subscapularis, teres major, and latissimus dorsi muscles from salamanders to mammals with special reference to their innervations from the brachial plexus. Anat Sci Int. p. 1 – 14.

Langer MC, França MAG, Gabriel S. 2007. The pectoral girdle and forelimb anatomy of the stem-sauropodomorph *Saturnalia tupiniquim* (Upper Triassic, Brazil). Spec Pap Palaeontol. 77: 113 – 137.

Leidy J. 1858. *Hadrosaurus foulkii,* a new saurian from the Cretaceous of New Jersey. Proc R Ac Nat Sci Phil. 27: 145 – 218.

Lipkin C, Carpenter K. 2008. Looking again at the forelimb of *Tyrannosaurus rex*. In: Larson P, Carpenter K (editors). *Tyrannosaurus rex: The Tyrant King.* Indiana University Press. Bloomington, Indiana. pp. 166 – 190.

Lockley MG, Wright JL. 2001. Trackways of large quadrupedal ornithopods from the Cretaceous: a review. In: Tanke DH, Carpenter K (editors). Mesozoic Vertebrate Life. Indiana University Press, Bloomington, Indiana. pp. 428 – 442.

Lockley MG, Young BH, Carpenter K. 1983. Hadrosaur locomotion and herding behaviour: evidence from footprints in the Mesaverde Formation Grand Mesa coal field, Colorado. Rocky Mt Assoc Geol. 20(1): 5 – 14.

Lull RS, Wright NE. 1942. Hadrosaurian dinosaurs of North America. Geol Soc Am Spec Pap. 40: 1 – 242.

Maidment SCR, Bates KT, Barrett PM. 2014a. Three-dimensional computational modeling of pelvic locomotor muscle moment arms in *Edmontosaurus* (Dinosauria, Hadrosauridae) and comparisons with other archosaurs. In: Eberth DA, Evans DC, eds. *Hadrosaurs*. Bloomington: Indiana University Press.

Maidment SCR, Bates KT, Falkingham PL, VanBuren C, Arbour V, Barrett PM. 2014b. Locomotion in ornithiscian dinosaurs: an assessment using three-dimensional computational modelling. Biological Reviews. 89: 588 – 617.

Maidment SCR, Barrett PM. 2011.The locomotor musculature of basal ornithischian dinosaurs. J Vertebr Palaeontol. 31(6): 1265 – 1291

Maidment SCR, Barrett PM. 2012. Does morphological convergence imply functional similarity? A test using the evolution of quadrupedalism in ornithiscian dinosaurs. Proceedings of the Royal Society of London B: Biological Sciences. 279: 3765 – 3771.

Maidment SCR, Barrett PM. 2014. Osteological correlates for quadrupedality in ornthischian dinosaurs. Acta Palaeontol Pol. 59(1): 53 – 70.

Mallon JC, Evans DC, Ryan MJ, Anderson JS. 2012. Megaherbivorous dinosaur turnover in the Dinosaur Park Formation (upper Campanian) of Alberta, Canada. Palaeogeogr Palaeocl. 350 – 352: 124 – 138.

Mariańska T and Osmólska Halszka.1984. Postcranial anatomy of *Saurolophus angustirostris* with comments on other hadrosaurs. Palaeontologia Polonica. 46: 119-141.

Maxwell EE, Larsson HCE. 2009. Comparative ossification sequence and skeletal development of the postcranium of palaeognathous birds (Aves: Palaeognathae). Zool J Linn Soc-Lond. 157: 169 – 196.

Meers MB. 2003. Crocodylian forelimb musculature and its relevance to Archosauria. Anat Rec Part A. 274A: 891 – 916.

Meso JG, Qin Z, Pittman M, Canale JI, Salgado L, Díaz VD. 2021. Tail anatomy of the Alvarezsauria (Theropoda, Coelurosauria), and its functional and behavioural implications. Cretaceous Res. 124: 104830.

Nicholls EL, Russell AP. 1985. Structure and function of the pectoral girdle and forelimb of *Struthiomimus altus* (Theropoda: Ornithomimidae). Palaeontology. 28: 643 – 677.

Norman DB. 1980. On the ornithischian dinosaur *Iguanodon bernissartensis* form the lower Cretaceous of Bernissart (Belgium). Mem I R Sci Nat Bel. 178: pp. 106.

Norman DB. 1986. On the anatomy of *Iguanodon atherfieldensis* (Ornithischia: Ornithopoda). Bull Inst R Sci Nat Belg Sciences de la Terre. 56: 281 – 372.

Norman DB. 2002. On Asian ornithopods (Dinosauria: Ornithischia). 4. *Probactrosaurus* Rozhdestvensky, 1996. Zool J Linn Soc-Lond. 136: 113 – 144.

Norman DB, Weishampel DM. 1990. Iguanodontidae and related Ornithopoda. In: Weishampel DB, Dodson P, Osmólska H (editors), The Dinosauria. University of California Press, Berkeley. pp. 510 – 533.

Norman DB, Witmer LM, Weishampel DB. 2004. Basal Thyreophora. In: Weishampel DB, Dodson P, Osmólska H (editors), The Dinosauria. University of California Press, Berkeley. pp. 335 – 342.

Osborn HF. 1912. Integument of the iguanodont dinosaur *Trachodon*. Mem Am Mus Nat Hist. 1: 33 – 54.

Ostrom JH. 1963. *Parasaurolophus cyrtocristatus*, a crested Hadrosaurian dinosaur from New Mexico. Fieldiana: Geology. 14(8): 168 p.

Ostrom JH. 1964. A reconsideration of the paleoecology of hadrosaurian dinosaurs. Am J Sci. 262: 975 – 997.

Otero A, Allen V, Pol D, Hutchinson JR. 2017. Forelimb muscle and joint actions in Archosauria: insights from Crocodylus johnstoni (Pseudosuchia) and *Mussaurus* patagonicus (Sauropodomorpha). PeerJ. 5: e3976.

Otero A. 2018. Forelimb musculature and osteological correlates in Sauropodomorpha (Dinosauria, Saurischia). Plos One. 13(7): e0198988.

Paul GS, Christiansen P. 2000. Forelimb posture in neoceratopsian dinosaurs: implications for gait and locomotion. Paleobiology. 26: 450 – 465.

Persons WS, Currie PJ. 2017. The functional origin of dinosaur bipedalism: Cumulative evidence of bipedally inclined reptiles and disinclined mammals. J Theor Biol. 420(2017): 1 – 7.

Poole KE. 2015. Phylogeny and Biogeography of Iguanodontian Dinosaurs, with Implications from Ontogeny and an Examination of the Function of the Fused Carpal-Digit I Complex. PhD dissertation. George Washington University. Washington, D.C., United States.

Prieto-Márquez A. 2008. Phylogeny and historical biogeography of hadrosaurid dinosaurs (Dissertation). Florida State University. Tallahassee, Florida. 937 p.

Prieto-Márquez A. 2010. Global Phylogeny of Hadrosauridae (Dinosaurs: Ornithopoda) using parsimony and Bayesian Methods. Zool J Linn Soc. 159: 435 – 502.

Prieto-Márquez A. 2014. A juvenile *Edmontosaurus* from the late Maastrichtian (Cretaceous) of North America: Implications for ontogeny and phylogenetic inference in saurolophine dinosaurs. Cretaceous Res. 50: 282 – 303.

Prieto-Márquez A, Norell MA. 2010. Anatomy and relationships of *Gilmoreosaurus mongoliensis* (dinosauria: Hadrosauroidea) from the Late Cretaceous of Central Asia. American Museum Novitates. 3694: 1 – 49.

Rasmussen ME. 1998a. Notes on the morphology and the orientation of the forelimb of *Ouranosaurus Nigeriensis.* Oryctos. 1: 127 – 130.

Rasmussen ME. 1998b. The Hadrosaurian Forelimb Morphology, Function, and Inferred Phylogeny (MSc thesis). University of Copenhagen. Copenhagen, Denmark.

Ravey M. 1978. Bipedalism: An early Warning System for Miocene Hominoids. Science. 199(4327): pp. 372.

Rhodes MM, Funston GF, Currie PJ. 2020. New material reveals the pelvic morphology of Caenagnahidae (Theropoda, Oviraptorosauria). Cretaceous Res. 114: 104521.

Romer AS. 1922. The locomotor apparatus of certain primitive and mammal-like reptiles. Bull Am Mus Nat Hist. 46: 517 – 606.

Romer AS. 1944. The development of the tetrapod limb musculature- the shoulder girdle of *Lacerta*. J Morphol. 74: 1 – 41.

Rosser BWC, George JC. 1985. An exceptionally high density of muscle spindles in a slow-tonic pigeon muscle. Anat Rec. 212: 118 – 122.

Ryan MJ, Evans DC. 2005. Ornithischian Dinosaurs. In: Currie PJ, Koppelhus EB (editors). 2005. Dinosaurs Provincial Park: a spectacular ancient ecosystem revealed. Indiana University Press, Bloomington. Ind., pp. 312 – 348.

Safran MR, Lopomo N, Zaffagnini S, Signorelli C, Vaughn ZD, Lindsey DP, Gold G, Giordano G, Marcacci M. 2013. In vitro analysis of peri-articular soft tissues passive constraining effect on hip kinematics and joint stability. Knee Surg Sports Traumatol Arthrosc. 21(7): 1655 – 1663.

Sanders RK, Farmer CG. 2012. The Pulmonary Anatomy of *Alligator mississippiensis* and its Similarity to the Avian Respiratory System. Anat Rec. 295: 699 – 714.

Schachner ER, Lyson TR, Dodson P. 2009. Evolution of the Respiratory System in Nonavian Theropods: Evidence from Rib and Vertebral Morphology. Anat Rec. 292: 1501 – 1513.

Sellers WI, Manning PL, Lyson T, Stevens K, Margetts L. 2009. Virtual palaeontology: gait reconstruction of extinct vertebrates using high performance computing. Palaeontol Electron. 12(3)11A: 26p.

Senter P. 2006a. Comparison of forelimb function between *Deinonychus* and *Bambiraptor* (Theropoda: Dromaeosauridae). J Vertebr Paleontol. 26: 897 – 906.

Senter P. 2006b. Scapular orientation in theropods and basal birds, and the origin of flapping flight. Acta Palaeontologica Polonica. 51: 305 – 313.

Senter P. 2007. Analysis of forelimb function in basal ceratopsians. J Zool (Lond). 273: 305 – 314.

Senter P. 2012. Forearm orientation in Hadrosauridae (Dinosauria: Ornithopoda) and implications for museum mounts. Palaeontologia Electronica. 15(3): 10 p.

Senter P, Robins JH. 2005. Range of motion in the forelimb of the theropod dinosaur *Acrocanthosaurus atokensis*, and implications for predatory behaviour. J Zool (Lond). 266: 307 – 318.

Senter PJ, Sullivan C. 2019. Forelimbs of the theropod dinosaur *Dilophosaurus wetherilli*: Range of motion, influence of paleopathology and soft tissues, and description of a distal carpal bone. Palaeontol Electron. 22.2 (30A): 1 – 19.

Sereno PC. 1986. Phylogeny of the bird-hipped dinosaurs (Order Ornithischia). Natl Geogr Res. 2: 234 – 256.

Smith DK. 2021. Forelimb musculature and function in the therizinosaur *Nothronychus* (Maniraptora, Theropoda). J Anat. 239(2): 307 – 335.

Snively E, Russell AP. 2007. Functional morphology of the neck musculature in the Tyrannosauridae (Dinosauria, Theropoda) as determined via a hierarchical inferential approach. Zool J Linn Soc-Lond. 151(4): 759 – 808.

Sternberg CM. 1935. Hooded hadrosaurs of the Belly River Series of the Upper Cretaceous: a comparison, with descriptions of new species, Canada, Dept. of Mines, Nat Mus Bull. 77, Geol ser. 52: 1 – 37.

Sullivan CS. 2007. Function and Evolution of the Hind Limb in Triassic Archosaurian Reptiles. PhD Dissertation. Harvard University, Cambridge, Massachusetts.

Sullivan RM, Williamson TE. 1999. A new skull of *Parasaurolophus* (Dinosauria: Hadrosauridae) from the Kirtland Formation of New Mexico and a revision of the genus. New Mex Mus Nat Hist Sci Bull. 15: 1 – 41.

Verdú FJ, Godefroit P, Royo-Torres R, Cobos A, Alcalá L. 2017. Individual Variation in the postcranial skeleton of the Early Cretaceous *Iguanodon bernissartensis* (Dinosauria: Ornithopoda). Cretaceous Research. 74: 65 – 86.

Wang X, Pan R, Butler RJ, Barrett PM. 2011. The postcranial skeleton of the iguanodontian ornithopod *Jinzhousaurus yangi* from the Lower Cretaceous Yixian Formation of western Liaoning, China. Earth Env Sci T R So. 101: 135 – 159.

Weishampel DB. Jensen JA. 1979. Parasaurolophus (Reptilia: Hadrosauridae) from Utah. J Paleontol. 53(6): 1422 – 1427.

Wheeler PE. 1991. The thermoregulatory advantages of hominid bipedalism in open equatorial environments: the contribution of increased convective heat loss and cutaneous evaporative cooling. J Hum Evol. 21: 107 – 115.

White MA, Bell PR, Cook AG, Barnes DG, Tischler TR, Bassam BJ, Elliott DA. 2015. Forearm Range of Motion in *Australovenator wintonensis* (Theropoda, Megaraptoridae). Plos One. 10(9): e0137709.

Wright JL. 1999. Ichnological evidence for the use of the forelimb in iguanodontid locomotion. Special Papers in Palaeontology. 60: 209 – 219.

APPENDIX A. Procedures for Creating a Biomechanical model in Autodesk Maya for Range of Motion Analysis

1. **Import 3D mesh into Maya**
    a. After importing you may be required to zoom out to see the object

2. **Establish the centre of rotation of the object**. This will ensure the point of rotation is in centre of object, not the centre of the axis or some other arbitrary origin, as usually occurs when a new object is first imported. This centre of rotation is called the "pivot". To see where the pivot of your object is located in the coordinate system:
    a. ***select the object → select attribute editor*** (on panel on the right) **→** ***select the pivots drop down***

    To centre the pivot in the middle of the object:

    b. ***Select Modify → Select center pivot***

    The mesh should now rotate around center of the object.

    Note: If this does not work, you can place your own custom pivot by using the "D" key.

3. **Scale your mesh to reasonable dimensions**. Your mesh should sit comfortably within the coordinate plane in Maya. If you cannot see the coordinate plane, the object is likely far away from the centre. Zoom out to find your mesh. The mesh might also be very large, in which case it will need to be scaled down. When scaling an object (e.g. a bone), you must also scale all other objects (bones) by the same scaling factor, so that their size relative to each other is preserved. (For example, if you scale a humerus by 0.2, you must scale every other bone that pertains to that model by 0.2 as well).

    To Scale:

    a. **Select Edit (right panel) → Select channel box/ layer editor → type in your scaling factor** (e.g. 0.02) for all
    b. Position bones along the X axis. This zero position will be used to specify the position of all body components in the world space.
    c. Set position to zero at axis.

4. **Note:** if you can not see some/all meshes, they may be hidden. To hide or reveal elements:
    a. **Windows → general editors → hypergraph hierarchy → right click to edit visibility**

5. **Place the object in the center of the grid in Maya**. When imported, objects are positioned randomly. To have accurate measurements for body position and range of motion, your elements should start by being centred at the origin, so that their final position in the coordinate system is some distance or angle from the origin. Important: do

not move the object before doing this, it will not place it in the centre. To place your objects in the centre of the coordinate system:

a. **Attribute editor** (on right panel) → **pivots** (a drop down) this will show where the pivots of elements are located in world space (ie the coordinate plane)
b. go to the first drop-down **transform attributes** and enter the negative of the number shown in **pivots** for each section. This will correct the distance from the origin, essentially translating the element back to the true origin in maya)
c. once your object is centered, freeze transformations: **modify → click box to the right of "freeze" → select freeze all**
d. Repeat for each element. Your objects should now be centered with their pivots at the origin.
e. Use rotation tools (on the left panel) to align your elements along the x axis. The long axes of bones should point along the positive or negative x axis.

Note: Maya update- pivots is now located under modelling toolkit → move settings → set to world, use the negative of those x, y, z values.

6. **Choose your view**. Orthographic view is best for biomechanical analyses because the size of the object is fixed. If you zoom in on it, the size of the object is maintained (does not get bigger).

7. **Place joints to control body elements**. You are creating a system (or series) of joints that control the body or model that you are creating. Consider all planes of motion that an object can move along in a coordinate system: yaw (side to side), pitch (up / down), and roll. Think about the order of this movement. As an object yaws, its pitch axis will change in response. However, no matter how much the object pitches, the yaw axis will always be vertical. For this reason, the order of the movements must be: 1. Yaw; 2. Pitch; 3. Roll. This means that the pitch is "subordinate" to the yaw. Roll is "subordinate" to pitch and yaw. If a higher order movement occurs, it will also affect those below (or subordinate to) it. In maya, this hierarchy uses the terms "daughter" (for subordinate objects) and "parent" (for superior, or higher placed objects in the series). Each bone (or element) that you have must have a joint placed on its pivot to be able to control and quantify the position of that element. Therefore, on the pivot of each object, you will place three joints.
    a. **Select rigging → create joints → Place with mouse** (3 per joints per joint)
    b. Name joints:
    (e.g. Scapula yaw→ Scap_yaw) **y axis**
    (e.g. Scapula pitch → scap_pitch) **z axis**
    (e.g. Scapula roll → Scap_roll) **X axis**

8. **Consider all planes of motion that constitute a joint**: yaw (side to side), pitch (up / down), and roll. Therefore, like the joints created to control the position of bones or

elements, each joint is made up of three joints. Add joints on the articular surfaces of bones. Note: Joint orient needs to be set to zero. If not, it changes the axis of rotation.

a. **Select rigging → create joints → Place with mouse** (3 per joints per joint)
b. Name joints. (e,g. Shoulder protraction/ retraction → Sh_Pro_Ret) **Z axis**
(e,g. Shoulder Adduction / Abduction → Sh_Add_Abd) **y axis**
(e,g. Shoulder long axis rotation → Sh_LAR) **x axis**

9. **Note the Gimble effect:** Yaw affects pitch. Yaw and pitch both affect roll. At high angles of pitch, the yaw and roll axes can become parallel. When this occurs it becomes impossible to move them independently. E.g: if pitch is straight down, yaw basically becomes roll since their axes of rotation become the same. The yaw axis of rotation does not ever change, however, because it is at the top of the joint hierarchy.

10. **Hierarchy of movement**. You now must indicate the hierarchy of joints and objects in your model. This involves telling the program what order things need to move in. For example, if the entire body rolls, the arm will roll with it. However, the arm can pivot on its own without the body moving on any axis. In this case the arm is a "daughter" of the body, which is the "parent". If a parent moves, the daughter objects and joints must move with it. A daughter can move independently of the parent.
    a. **Select Windows → hypergraph hierarchy → use centre button on mouse to drag daughter items below parent items**

    e.g. the scapula (lowest in hierarchy) is a daughter of the yaw, pitch, and roll of the shoulder joint. The shoulder joints are daughters of the body (highest in hierarchy).

    b. Hierarchy of joints: 1. Flexion / Extension (Protraction / Retraction)

    2. Adduction / Abduction

    3. Long axis rotation (pronation / supination)

11. **Add a locator to control joints**. A locator is essentially a point in space, but it has attributes associated with it. You will use these attributes to control your system of objects and joints. You will use the controller panel to move objects along joints, while obtaining angles for each movement.
    a. Will show as "**locator 1**" in channel box. Rename to "**Controller 1**".
    b. **Select modify → add attribute → "Body_Yaw" → Add** do this for as many elements and joints you have at this point.
    c. **Windows → animation editors → expression editor →** write in Expression: **"Scap_yaw.ry = |Controller1.Body_Yaw;" → Create** This creates a controller for rotation about the y-axis. (The expression you write tells the program that your attribute controls your joint via rotation (r) or translation (t) about a certain axis).
    d. Repeat from (b) to add attributes and expressions for shoulder rotation (ry, rx, rz) and translation (ty, tx, tz). Many lines can be added at once.

12. **Use the model.** The controller can now be used to change positions and angles of elements and joints. The values of displacement are relative to the "zero" starting position. This model can now be used to evaluate range of motion, body positions, create animations, or can be imported into another 3D modelling program.

Figure A1. Hypergraph hierarchy created in Autodesk Maya for for the biomechanical model of TMP2015.044.0036 (Step 10).

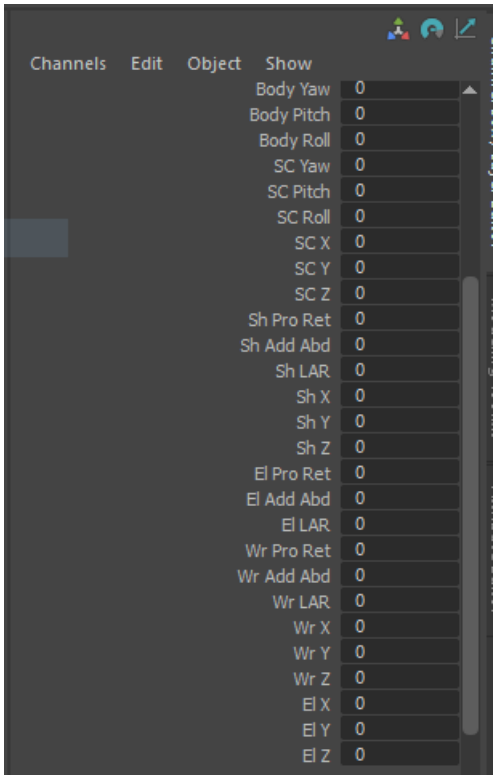

Figure A2. List of attributes created in Autodesk Maya for the biomechanical model of TMP2015.044.0036 (Step 11 b).

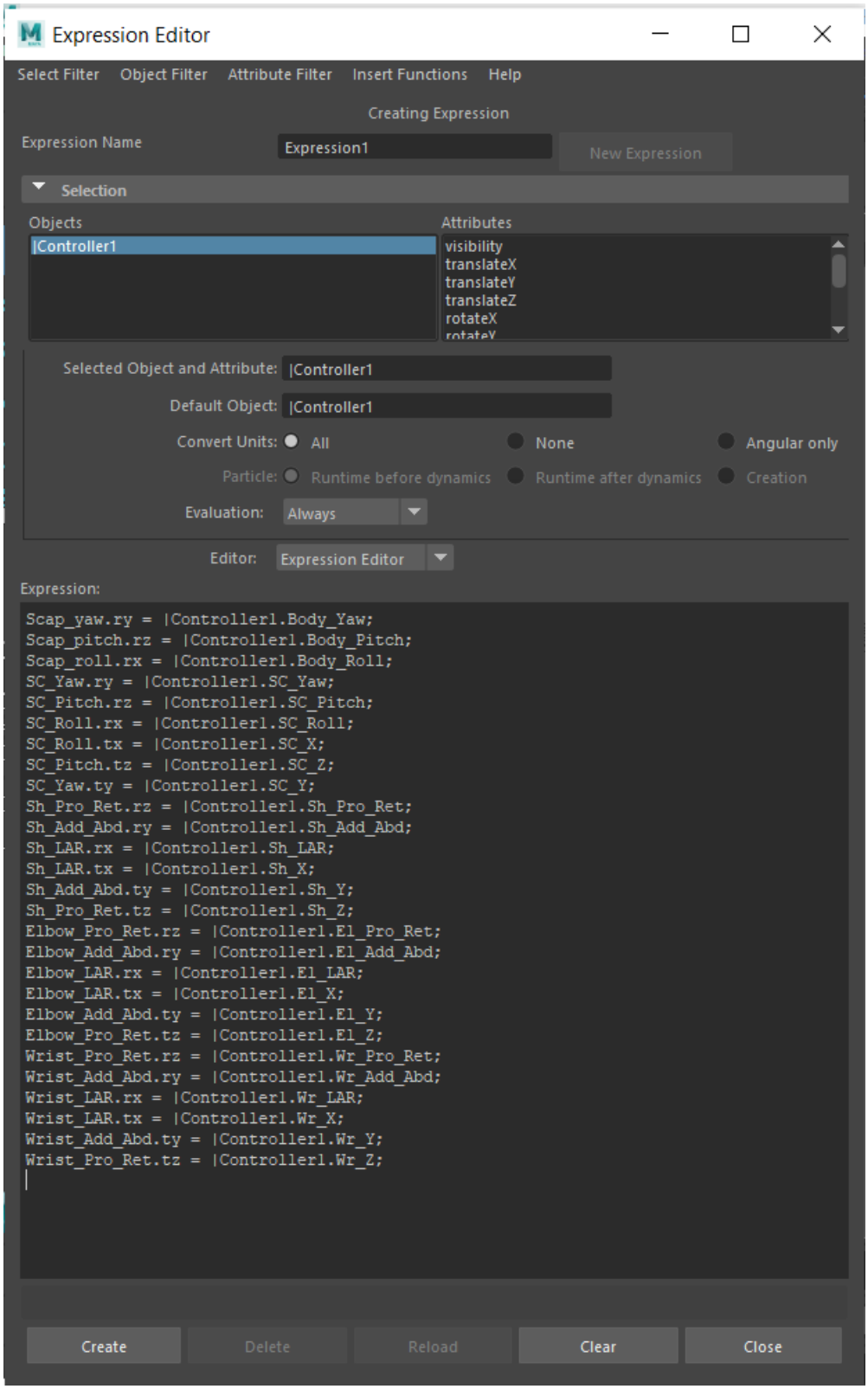

Figure A3. Expression1 created in Autodesk Maya for the biomechanical model of TMP20157.044.0036 (Step 11 c).

APPENDIX B. Procedures for creating a biomechanical model in SIMM for Muscle Moment Arm Extrapolation

1. **Prepare 3D meshes**.
    a. SIMM does not accept 3D model files that are larger than 2 MB. 3D meshes can be decimated (made smaller) in programs such as ZBrush or Blender. Note that if using blender for multiple meshes simultaneously, the meshes may be exported all as one object. Check your models before adding to your SIMM file.
        i. If needed, decimate 3D models
            1. in ZBrush using the "decimation master" plugin under ZPlugins)
            2. in Blender: Select mesh, switch to Edit Mode, select "Mesh" > "Clean up" > "Decimate Geometry". In Decimation window input percentage of existing polygons to keep.
    b. The SIMM window is made to accommodate very small bone models (much less than a meter in length). ZBrush or Blender can be used to re-size 3D meshes before importing into SIMM.

2. **Set up folder** and create a joint (.jnt) file. This is a text file you can create in notepad and save as a joint file. This file will contain information on what 3D model files will be in your model, what joints will appear in your model, and how these elements will move. You cannot simply import 3D models into SIMM, you must create a jnt file to create your model in SIMM.
    a. Create a folder with the name of your model. E.g.: "Test Model"
    b. Create a folder titled "bones" within this folder. Import your individual bone meshes in a compatible format (e.g., .obj) into this folder. The elements can be no larger than a couple MBs each.
    c. Create a .jnt file to go into your "Test Model" folder.

3. **Write your jnt file script**. Begin by adding bone elements (segments) (See example script below)
    a. Use "name" to name your model.
    b. Use "bone_path" to tell SIMM where your bone meshes are located
    c. Use "beginsegment" to name and begin a segment (each skeletal element is one segment). Use "endsegment" to conclude each segment

4. **Create joints**. You can open a jnt file at this point if you only have one bone. If you have more than one bone you need to tell SIMM the relationships between them (ie the joints). These must be written into your jnt file as well.
    a. Use "beginjoint" to name your joint.
    b. Use "Segments" to identify which segments the joint is between.
    c. Use "order" to give the order of movements in your joint
    d. Axes, translations, and rotations must also be defined (see example text below)
    e. Use "endjoint" to finalize the joint

f. Repeat for as many joints as you need. Note that all 3D files (ie bone elements) need to be attached to something vis a joint or else the model will not open.

5. **Adding muscles**. You should now be able to open your joint file in SIMM.
   a. add muscles to your model following the methods outlined in the SIMM7.0 user guide (Musculographics Inc.).
   b. Save your muscles as a muscle file (.msl) in the same folder as your .jnt file.
   c. In your .jnt file, you can add a line below "bone_path bones" that will indicate the muscle file you wish to be associated with your model (ie your .msl file). For example, if your muscle file is titled "muscles.msl", you would write "muscle_file muscles.msl". Adding this line will automatically generate your muscles along with your bones when you open your .jnt file in SIMM.

6. **Generating movement in SIMM**. If you are not using motion capture data, as will be the case for most fossil vertebrates, you must create a motion file (.mot) to define the movements of your model. This involves defining the limits of movement in your .jnt file and writing a .mot file to define where this movement will take place in 3D space. You cannot manipulate movement of your bones in the SIMM window without both of these lines of script, and the .mot file designated within your .jnt file.
   a. In your .jnt file, create a gencoord and a function for each movement (e.g. shoulder flexion). The gencoord defines the range of motion and the function defines how the movement will take place. For example, if we were writing a gencoord and function to define shoulder flexion, where the movement can range from 26 degrees extension to 13 degrees flexion, and the "h" key and left mouse button toggle the motion, they would be written as follows:
      i. Gencoord:

```
begingencoord Shoulder_flexion
range 26.0 -13.0
keys h_key leftmouse_button
endgencoord
```

      ii. Function:

```
beginfunction f1
(-360.0, -360.0)
(360.0,   360.0)
endfunction
```

   b. Now you must write a .mot file that defines the movement of your element. Your .mot file must begin by stating its name, the number of data columns in the file, and the number of rows (ie the range). The first data column will be time in seconds, the second will be the position of your element relative to the coordinate system, and the third is degree of rotation of the joint. See figure B3 below for a .mot file script for humeral flexion. Note that this image used percent time instead of time in seconds. This is because SIMM has a "normalize time" function that

makes any motion into a percent of that motion. This is useful for comparing movements graphically that do not take the same amount of time in seconds. It is good practice, once you have written a .mot file, to open it in simm, and save it as a normalized motion in another .mot file.

c. Once you have both written your .mot file and defined your gencoord and function in your .jnt file, add your selected motion file into your .jnt file as we did with the muscle file.
    i. Below "muscle_file muscles.msl" write (supplemented with your .mot file name):

    motion_file motion1.mot

d. Repeat the above steps for all movements you wish to produce in SIMM.

7. You should now be able to open your .jnt file and see your bones with muscles attached. You can go into the motion reporter or motion editor to view your motions. Once this is all working properly, you can generate data plots for moment arms or whatever your desired variable using the graph editor in SIMM. Instructions for this can be found in the SIMM7.0 user guide. Note that models may need to be scaled down to fit in the functional space in SIMM. If this has been done, a scaling factor must be applied when generating plots to compensate for this.

```
name DeadDogModel3
bone_path bones
muscle_file muscles.msl
motion_file DeadDogModelProRet2.mot
motion_file DeadDogModelAddAbd2.mot
motion_file DeadDogModelLAR2.mot

length_units m
force_units N

beginmaterial my_bone
ambient 0.65 0.65 0.65
specular 0.7 0.55 0.4
diffuse 0.55 0.4 0.35
shininess 10
endmaterial

beginsegment ScapulaCoracoid
bone ScapulaCoracoid.obj
endsegment

beginsegment SternalPlates
bone SternalPlates.obj
endsegment

beginsegment Humerus
bone Humerus.obj
endsegment

begingencoord Shoulder_flexion   /* 26 deg. extension to 13 deg. flexion */
range 26.0  -13.0
keys h_key leftmouse_button
endgencoord

begingencoord Shoulder_adduction    /* 40 deg. abduction to 76 deg. adduction */
range -40.0  76.0
keys h_key middlemouse_button
endgencoord

begingencoord Shoulder_rotation    /* 70 deg. hip internal to 44 deg. external rotation */
range -70.0  44.0
keys h_key rightmouse_button
endgencoord
```

Figure B1. Part 1/2 of the .jnt script file created for TMP2015.044.0036 for muscle moment arm analysis in SIMM.

```
beginjoint Shoulder
segments ScapulaCoracoid Humerus
order t r1 r2 r3
axis1 1.000000 0.000000 0.000000
axis2 0.000000 1.000000 0.000000
axis3 0.000000 0.000000 1.000000
tx constant 0.0000
ty constant 0.0000
tz constant 0.0000
r3 function f1(Shoulder_flexion)
r1 function f2(Shoulder_adduction)
r2 function f3(Shoulder_rotation)
endjoint

beginjoint Sternocoracoid
segments SternalPlates ScapulaCoracoid
order t r1 r2 r3
axis1 1.000000 0.000000 0.000000
axis2 0.000000 1.000000 0.000000
axis3 0.000000 0.000000 1.000000
tx constant 0.000000
ty constant 0.000000
tz constant 0.000000
r1 constant 0.000000
r2 constant 0.000000
r3 constant 0.000000
endjoint

beginfunction f1        /* Shoulder flexion (+) and extension (-) */
/* (Shoulder flexion angle (radians), rotation about axis 3 (radians) */
(-360.0, -360.0)
( 360.0,  360.0)
endfunction

beginfunction f2        /* Shoulder addduction (+) and abduction (-) */
/* (Shoulder adduction angle, rotation about axis 1) */
(-360.0, -360.0)
( 360.0,  360.0)
endfunction

beginfunction f3        /* Shoulder internal (+) and external rotation (-) */
/* (Shoulder rotation angle, rotation about axis 2) */
(-360.0, -360.0)
( 360.0,  360.0)
endfunction
```

Figure B2. Part 2/2 of the joint (.jnt) script file created for TMP2015.044.0036 for muscle moment arm analysis in SIMM.

```
# Motion file made by SIMM 7.0
# D:\Sam\SIMM\DeadDogModel3\DeadDogModelProRet2.mot

name DeadDogModelProRet
datacolumns 4
datarows 101
x_column 1
wrap
enforce_loops yes
enforce_constraints yes
show_markers yes
show_marker_trail_lines no
show_marker_trail_points no
show_force_trails no
show_force_plates yes
show_foot_prints yes
show_gencoord_moments no
show_other_objects yes
show_external_forces yes
show_body_forces no
show_joint_reaction_forces yes
show_joint_reaction_forces_as_arrows yes
show_joint_reaction_torques no
show_joint_reaction_torques_as_arrows yes
show_contact_forces no
show_spring_forces no
event_color 1.000000 0.000000 1.000000
endheader

percent time    Humerus_tx      Shoulder_flexion
0.0000000000000000      0.0000000000000000      0.0000000000000000      26.0000000000000000
1.0000000000000000      0.0020000000000000      0.0041866686405135      25.5999999999968640
2.0000000000000000      0.0040000000000000      0.0068880029607702      25.1999999999952950
3.0000000000000000      0.0060000000000000      0.0082960029607702      24.7999999999952930
4.0000000000000000      0.0080000000000000      0.0086026686405135      24.3999999999968620
5.0000000000000000      0.0100000000000000      0.0080000000000000      24.0000000000000000
6.0000000000000000      0.0120000000000000      0.0066954639032811      23.6000000000043930
7.0000000000000000      0.0140000000000000      0.0049583946706136      23.2000000000084690
8.0000000000000000      0.0160000000000000      0.0030735934863055      22.8000000000103530
9.0000000000000000      0.0180000000000000      0.0013258615346650      22.4000000000081560
10.0000000000000000     0.0200000000000000      -0.0000000000000000     22.0000000000000000
11.0000000000000000     0.0220000000000000      -0.0006965242536380     21.5999999999855700
```

Figure B3. The motion (.mot) script file created to define the shoulder flexion of TMP2015.044.0036 in SIMM. Only the first 12 of 101 lines of data are shown.